Final Report

on research carried out under

NIOSH-CDC Grant No. 5 R01 OH 002984

entitled

WORKPLACE AEROSOL SAMPLING AT REALISTIC LOW WINDSPEEDS

by

James H. Vincent, Ph.D., D.Sc., FRSC (Principal Investigator)

Darrah K. Sleeth, Ph.D. (Graduate Student Research Assistant)

Yi-Hsuan Wu (Research Fellow)

(Project started: 09/01/2004; Project ended: 08/31/2009)

Project awarded to:
University of Michigan
Department of Research Development and Administration
3003 South State Street, Room 1040
Ann Arbor, MI 48109

Communicating author:
Professor Emeritus James H. Vincent, Ph.D., D.Sc., FRSC
Department of Environmental Health Sciences
School of Public Health
University of Michigan
109 S. Observatory
Ann Arbor, MI 48109
Phone: (734) 604-0919
e-mail: jhv@umich.edu

Revised version submitted April 2010

Acknowledgements

The authors of this report wish to thank the National Institute of Occupational Safety and Health for its support not only of the work described here but also for its support over many years of the large body of related work which preceded it. In the same regard we also wish to thank the Department of Environmental Health Sciences and the School of Public Health at the University of Michigan for their support and encouragement. Finally we wish to thank the many colleagues – graduate students, research students and faculty members – that participated in the long body of work leading up to this project. Finally, and not least, we wish to thank our colleagues on the administrative staff of the Department, School and University for their day-to-day support and efforts in making sure that management of the project was as efficient as possible.

Table of contents

Title page

Acknowledgements

Table of contents

List of terms and abbreviations

Abstract 1

SECTION 1

1. Highlights and significant findings 2

2. Translation of findings 3

3. Outcomes, relevance and impact 3

SECTION 2: TECHNICAL REPORT

1. Introduction 4

2. Development of experimental facilities 8

3. Visualization of the air flow around the heated breathing mannequin 32

4. Aspiration efficiency of the breathing mannequin 43

5. Personal sampler performance 65

6. Integration and implications 89

7. Conclusions from the research 103

References 105

List of terms and abbreviations

There follows a list of the primary terms and abbreviations used in this Report:-

A	sampler aspiration efficiency
d_{ae}	particle aerodynamic diameter
Fr	Froude number, referring to the relative influence of gravity on particle motion
I	inhalability, the aspiration efficiency of the human head during breathing
$MMAD$	mass median aerodynamic diameter
Q	sampling flowrate
R	ratio of windspeed to sampler inlet velocity
R_c	ratio of particle settling velocity to sampler inlet velocity
St	Stokes number referred to windspeed and tube diameter
St_c	Stokes number referred to sampler inlet velocoity and tube diameter
U	windspeed
U_s	sampler inlet velocity
σ_g	geometric standard deviation (for particle size)

ABSTRACT

This Report describes a large body of research that involved the development of facilities never previously seen and their application in the exploration of human inhalability in relation to aerosol exposures under realistic windspeed conditions. The specific objective was to acquire experimental data on the efficiency with which humans inhale particles in the range of particle aerodynamic diameter up to about 90 μm and on a range of personal sampling instruments aimed at making representative measurements of the inhalable fraction. The new facility consisted of a novel ultra-lowspeed wind tunnel capable of providing windspeeds in the range from about 0.05 to 0.5 m/s representing realistic conditions in most actual workplaces, and a mannequin capable of simulating breathing parameters and body temperature representative of people at work. The experimental research program began with flow visualizations to examine the nature of the patterns of air movement around the heated, breathing, followed by studies of human inhalability and personal sampler performance. The flow visualizations provided striking visual information about the roles of windspeed and breathing flowrate, as well as body heat, clothing, etc., on the nature of the flow, in turn enabling to qualitative assessment of the potential influences on aerosol transport and hence human aspiration efficiency. At combinations of low windspeed and high breathing rate, and especially for breathing through the mouth, it was seen that large and persistent disturbances in the approaching air flow were generated. It was postulated that such disturbances will have a significant influence on aerosol transport near the mannequin, and so on inhalability and personal sampler performance. This was borne out in the sets of data that were obtained for both aerosol inhalability and personal sampler performance. These showed that both human inhalability and personal sampler performance were significantly dependent on windspeed, both being the highest at the lowest windspeed. In particular they revealed that inhalability at ultra-low windspeeds was much greater than the currently-accepted criterion based on data obtained at higher windspeeds. This was shown to be true also for the personal samplers tested, namely the IOM, Button and GSP inhalable aerosol samplers and the closed-face cassette sampler (CFC) widely used by industrial hygienist in the United States. While the IOM, Button and GSP samplers were shown to provided adequate measures of what was inhaled by the mannequin, the CFC sampler did not. We next examined the possibility (and implications) of modifying existing inhalability criteria to better estimate workplace exposures at the ultra-low windspeeds of interest. It was concluded that the existing criterion (e.g., as recommended by ACGIH and other standards-setting bodies) is still relevant to workplace environments where windspeeds exceed about 0.25 m/s. However a modified criterion is needed for lower windspeeds in the ultra-low range of the order of 0.10 m/s and below. A criterion for (nominally) calm air has already been recommended by researchers in Europe, and this is currently on the table for discussion by several major standards setting bodies. Our results are broadly consistent with that suggested new criterion, and so we support its inclusion in revised standards. Overall, the large body of research carried out under this project has provided important new findings relevant to occupational aerosol exposure assessment, and should therefore be of interest to industrial hygienists, occupational epidemiologists and standards setting bodies. At its core, the work has focused on issues underlying the fundamental principles of aerosol science and industrial hygiene. It is fair to say that the new wind tunnel and mannequin system have enabled the generation of data that will be highly significant in how we think in the future about inhalable aerosol in workplaces, providing a basis for improved standards and exposure assessment methodology.

SECTION 1

1. Highlights and significant findings

This Report describes a large body of innovative research involving the development of facilities never previously seen and their application in the exploration of human inhalability in relation to aerosol exposures and personal samplers aimed at providing representative measures of such exposures. The first, and very difficult, part of the work, involved the development of a novel set of facilities, consisting of an ultra-lowspeed wind tunnel and a heated, breathing mannequin and associated auxiliary equipment, all of which capable of operating under the realistic very-low windspeed conditions relevant to most workplaces. In order to successfully perform experiments at windspeeds in the range upwards of just a few centimeters per second, it was necessary to overcome severe difficulties well known to be inherent in conducting aerosol sampler research in such environments. We developed a system that incorporated the characteristics of both moving-air wind tunnels and calm air chambers that have (separately) been used in previous work. This system may be referred to as 'hybrid', allowing for the influence of gravitational settling to be accounted for while maintaining a spatially uniform distribution of aerosols, both in terms of aerosol concentration and particle size distribution. This part of the project represented a major achievement in itself, providing the basis of an experimental program under ultra-low windspeed conditions previously widely considered to be too difficult to achieve in the laboratory.

Flow visualization studies were carried out to provide a large library of very informative digital flow visualization videos from which publishable-quality still pictures could also be obtained. From these it was possible to catalog air flow patterns around the heated, breathing mannequin over the whole range of experimental conditions we set out to study. Assessment of those pictorial records provided striking visual information about the roles of factors such as windspeed and breathing flowrate, as well as body heat, clothing, etc., on the nature of the flow, in turn enabling qualitative assessment of potential influences on human aspiration efficiency. At combinations of low windspeed and high breathing rate, and especially for breathing through the mouth, it was seen that large and persistent disturbances in the approaching air flow were generated. It is highly likely that such disturbances will have a profound effect on aerosol transport near the mannequin, and in turn on inhalability and personal sampler performance.

Quantitative data were obtained, for both aerosol inhalability and personal sampler performance. These showed that both human inhalability and sampling efficiency were significantly dependent on windspeed, both being the highest at the lowest windspeed. In addition, it was revealed that inhalability at ultra-low windspeeds was much greater than the currently-accepted criterion based on data obtained at higher windspeeds. Taken as a whole, the results and analyses performed here supported the initial hypothesis, which stated that previous measures of inhalability at high windspeeds had under-estimated aerosol exposures at ultra-low windspeeds. This was shown to be true for both the human aspiration process – as assessed by the mannequin – as well as for the personal samplers tested. In the case of the personal samplers, rudimentary correction factors of 0.73, 0.78 and 0.83 were estimated for the IOM, Button and GSP samplers, respectively, for use at ultra-low windspeeds to better estimate the inhalable aerosol fraction. The CFC sampler, despite being one of the most commonly used devices by industrial hygienists, was confirmed as being inadequate for measuring the inhalable aerosol fraction at all ultra-low windspeeds, in

addition to – as has been shown elsewhere – to higher windspeeds. It is has now clear that the CFC sampler cannot be recommended for collecting the health-related inhalable fraction.

2. Translation of findings

An overarching objective was to examine the possibility – and practical implications – of modifying existing particle size-selective aerosol sampling criteria to better estimate workplace exposures at the ultra-low windspeeds of interest. Taking into account the practical need to maintain simplicity, it was concluded that the existing standard for inhalability is still relevant to workplace environments where windspeeds exceed about 0.25 m/s. However we have decided that a modified criterion is clearly needed for lower windspeeds in the ultra-low range of the order of 0.10 m/s and below. A criterion for (nominally) calm air had already been recommended by Aitken *et al.* (1999) based on their studies in a calm air chamber, and this is currently on the table for discussion by several major standards setting bodies. Our results are broadly consistent with that suggested criterion, and so we support its inclusion in revised aerosol exposure standards. In turn, the new knowledge about the performances of selected personal aerosol samplers provides professional industrial hygienists with the basis for making informed choices of sampling instruments to be used in practical situations. In this way, the setting of standards and their application in the real world will provide better protection of workers everywhere.

3. Outcomes, relevance and impact

Respiratory ill-health remains a significant occupational health concern, as reflected for many years in the list of priorities in the NIOSH National Occupational Research Agenda (NORA). Many such conditions may be directly linked with exposures to aerosols, so that aerosol-related health effects have continued to be of great concern to occupational health professionals. The new particle size-selective criteria for aerosol exposure assessment and the emerging corresponding occupational exposure limits (OELs) are important in making exposure assessment more directly relevant to the health effects of interest. But prior to the research described in this Report, there had remained important gaps in our knowledge about the particle size-selectivity of sampling instruments under realistic workplace conditions, notably for the largest inhalable particles and at the low environmental windspeeds pertaining to many industrial locations. Therefore, we still could not fully rationalize the large biases that are found when different sampling instruments, nominally intended for collecting the same aerosol fraction, are used in actual workers' exposure assessment. This has persisted as a significant problem for both standards-setting bodies and industry. The two central issues were concerned with (a) human inhalability, and (b) sampler physical performance characteristics under realistic workplace environmental conditions, specifically very low windspeed. Occupational health standards can only be truly effective if exposure assessment is scientifically matched with what happens during actual human inhalation, and when the most appropriate personal sampling instruments are identified (and, coinversely, unsatisfactory ones revealed). The project described in this Report addresses all of these, and has been successful in closing the previous gaps in our knowledge. In the process, therefore, it has made significant new contributions to the establishment of rational, science-based criteria and methods for occupational aerosol exposure assessment and standards setting, putting occupational aerosol exposure assessment on a still more realistic footing that will meet the needs of future occupational health research and practice.

SECTION 2
TECHNICAL REPORT

1. Introduction

Background

Industrial hygienists have long been concerned with human exposure to aerosols in the workplace. In fact, aerosol science was one of the driving forces of this field in its formative years, due in large part to significant airborne hazards present in the mining and nuclear industries. Today, interest in aerosol exposure has expanded to include a much wider range of workplaces and contaminants, including minerals, metals, combustion-related products, pesticides, bioaerosols and nanomaterials. Obtaining a thorough understanding of aerosol behavior is vital for accurate exposure assessment and control, sampler development, standards setting, and epidemiological research. Another primary interest is understanding adverse health outcomes that result from either intermittent or continuous exposure to aerosols, which can result in both short and long term health complications, including pneumoconiosis, cancer, COPB, occupational asthma, and chronic bronchitis, among others. The basis for establishing links between exposure to airborne materials and such health effects requires precise knowledge of the efficiency with which the human respiratory system inhales such contaminants.

It has been known since the early twentieth century that only the smallest inhaled particles eventually reach the deepest part of the lung, the alveolar region (McCrea, 1913). Based on this knowledge, experiments were conducted to quantify the particle size dependency of the penetration of inhaled aerosol particles into the respiratory tract, typically involving human volunteer subjects. However, an additional consideration is the efficiency with which particles are inhaled in the first place. Since the 1970s, the relationship between particle size and the efficiency of human inhalation through the nose and/or mouth has been officially accepted as a physical definition of 'inhalability' (ACGIH, 1999; CEN; 1992; ISO, 1992). This curvilinear relationship, commonly known as the 'inhalability curve,' has typically been studied inside wind tunnels using life-sized models of the human head and torso. In principle, this curve is intended to provide the basis for the desired particle size dependency of aerosol samplers so that those devices accurately reflect what humans inhale (ACGIH, 2004). That relationship has also become very important around the world in the development of criteria for setting occupational exposure standards based on the inhalable aerosol fraction.

Notably, finer aerosol sub-fractions also exist, such as the thoracic and respirable fractions, which each represent a particular subset of the inhalable fraction. While these are similarly important in relation to specific aerosol-related diseases, the current research is focused on the coarser particles that encompass the full range of the inhalable aerosol fraction. It should also be noted that these finer size fractions all describe *penetration* of inhaled particles into the various regions of the respiratory system. In other words, the portion of inhaled particles that might be exhaled back into the ambient air is included in typical aspiration efficiency estimates.

Most of the previous wind tunnel experiments reported in the literature have been conducted at windspeeds above 0.5 m/s. This was due in part to the practical difficulty inherent in generating

well-defined test aerosols in low windspeeds, but also because of the important original application of much of this earlier research to strongly-ventilated coal mines. There has also been some focus on aerosol behavior at essentially zero windspeed using calm air aerosol chambers. Recently, however, it has been shown that typical workplaces actually have windspeeds that lie somewhere between these extreme scenarios, in the range from about 0.05 to 0.5 m/s (Baldwin and Maynard, 1998; Berry and Froude, 1989). This represents an important gap in our scientific knowledge, since both human inhalability and personal samplers have not been fully characterized in that environment. Findings in calm air indicate that inhalability under those conditions is substantially different than that for faster moving air, suggesting that current standards for inhalable aerosols may be based on criteria that are not entirely appropriate.

As mentioned, the technical difficulty involved in creating well-controlled experiments at the lower windspeeds typical of most actual workplaces has so far constrained the ability to generate data for inhalability in such environments. Taking this into consideration, one important objective of this research was to develop experimental methods with which to make more accurate estimates of the inhalability of coarse aerosols at the lower windspeeds of interest. This involved the design and development of brand new facilities, including a novel ultra-lowspeed wind tunnel and a physical model of a living, breathing human. Ultimately, this research hopes to provide further knowledge about aerosol behavior that is more directly relevant to today's workplaces, with possible application to the development of improved occupational health standards and sampling methodologies.

Aims of the research

The goals of the research were modified only slightly from the original ones as the work progressed, based on the shifting priorities dictated by emerging new views of the problem that was being addressed and the technical challenges that were encountered along the way. The primary broad objective remained the same, namely:-

- To develop means to sample aerosols in a way that enables reliable, relevant measurement of workers' exposures in settings under realistic conditions of workplace air.

The specific objectives were:-

- Design of a new ultra-lowspeed wind tunnel for studies to be conducted at windspeeds between 0.05 and 0.5 m/s;
- Design of a new heated, breathing mannequin system for inhalability experiments at ultra-low windspeeds;
- Characterization of airflow patterns around the mannequin during inhalation, exhalation, and while heated;
- Development of experimental methods to assess the inhalability of aerosols at ultra-low windspeeds;
- Identification of other factors that may influence inhalability and establish their effects, including: nose versus mouth breathing, breathing flowrate, body temperature, clothing, personal protective equipment, and orientation;

- Development of experimental methods to assess personal sampler performance at ultra-low windspeeds; and
- Comparison and integration of data for mannequin inhalability and personal sampler performance in relation to existing standards and/or sampling methodologies.

These objectives are very close to the ones that were originally proposed long before the work actually began. They were slightly modified as the work progressed in the light of emerging new inputs and priorities, most notably from standards-setting bodies, along with new scientific insights gained along the way. The objectives listed therefore include a range of goals, increased to include: (a) an extended study of the physical factors that might influence the performances of aerosol samplers mounted on the body of a simulated worker, including breathing (by the mannequin) and body heat; and (b) discussion of the impact of what was learned on the existing (and potentially new) standards for workplace aerosol exposure assessment. The latter in particular was developed through discussion over the whole duration of the project with leading standards organizations, specifically the International Standards Organisation (ISO) and the Comité Européen de Normalisation (CEN).

Research approach

It was the central hypothesis of this research that previous measures of inhalability and personal sampler performance for coarse aerosols, based on high-speed wind tunnel experiments, had underestimated the inhalable fraction of aerosols in low windspeed environments. It was believed that reliable experiments for measuring human inhalability and personal sampler performance could be performed at low windspeeds, but that they must take into account the effects of body heat, breathing parameters and other physical factors that may become more important as external air velocity decreases. In order to achieve the above stated objectives, the research described here employed a novel ultra-low speed wind tunnel and a mechanically-breathing, heated mannequin, both designed specifically for this project. After commissioning of the experimental system, which included initial airflow visualizations inside the working section of the wind tunnel, experiments were performed to assess human inhalability and personal sampler performance under simulated realistic workplace conditions.

Primary facilities

The new facilities will be described in detail below. For the present a short summary will suffice. The ultra-low speed wind tunnel designed and built within this project was capable of producing continuously-variable windspeeds in the test section of between 0.05 and 0.5 m/s. It combined the principles and modes of operation of both a conventional aerosol wind tunnel and a calm air aerosol chamber, both of which have been widely used in other research, including in our own laboratory, albeit separately. In this way, the new facility may be thought of as a 'hybrid' aerosol test system. It allowed for the generation of very low windspeeds while, after considerable post-construction development work, maintaining a uniform particle size distribution and uniform aerosol concentration. It was large enough to accommodate a full-sized mannequin torso, comprising a life-sized (and life-like) head and torso, including upper arms. The mannequin itself comprised an external mechanical breathing apparatus whose operating parameters were controlled through a computer, providing the ability to simulate a representative range of

respiratory rates, both in terms of breath frequency and tidal volume. It could be heated to provide a representative range of body surface temperatures, involving the zonal heating of five separate areas. Any combination of nose and mouth breathing could be simulated (e.g., inspiration through the nose and expiration through the mouth, and all other combinations) with inspiration and expiration taking place along separate pathways (for reasons that will become evident shortly). A filter holder was situated along the inspiration pathway for the collection of inhaled particles.

As part of the facility commissioning, it was important to understand the airflow inside the wind tunnel working section and to ensure that no confounding air movements existed. This was achieved by digitally visualizing the airflow around the heated, breathing mannequin using smoke lines, from which a library of videos was created showing air patterns around the mannequin under various conditions.

Experimental program

The main experimental program involved examination of the inhalability of the human head and the performances of various personal sampling devices typically used by industrial hygienists. Inhalability was measured for the mannequin for various particle sizes at different windspeeds, with the inhaled particulate matter for each test aerosol – both collected on the filter and deposited on the inside walls along the inhalation pathway – analyzed gravimetrically. The personal samplers were placed on the mannequin body in the so-called 'breathing zone' (in the manner of sampling carried out by practicing professional occupational hygienists) to collect samples simultaneously, and these samples were analyzed in the same manner. Reference samples were taken upstream of the mannequin using thin-walled cylindrical sampling probes operating isokinetically. The concentration of aerosols inhaled by the mannequin and collected by the samplers was compared to the measured reference sampler concentration to calculate human inhalability and personal sampler collection efficiency, respectively. Analyses were performed in order to not only directly compare the inhalability and personal sampler data that were obtained but also to examine the results in light of existing standards and criteria. Finally the impact of parameters such as windspeed, breathing flowrate, and mode of breathing were examined, involving both statistical and physical analyses based on what we already know about aerosol behavior and the aspiration process.

2. Development of experimental facilities

As mentioned before, it has long been recognized among aerosol scientists that it is very difficult to generate a laboratory test environment that is uniform in terms of the spatial distributions of air velocity, aerosol concentration and particle size respectively in the ultra-low windspeed range of interest. Previous studies of aerosol inhalability and related personal samplers have been performed almost exclusively in either higher-speed wind tunnels (windspeeds exceeding 0.5 m/s) or in (nominally) calm air chambers, in each of which the principles underlying the nature of aerosol exposure and measurement are distinctly different. A central aspect of this research program was therefore the development of appropriate facilities in which to perform the necessary experiments, taking into account such differences. We therefore now describe the theoretical and practical aspects of a novel ultra-lowspeed wind tunnel and a heated, breathing mannequin. Both systems were custom-designed and built specifically primarily for this project.

The new ultra-low speed wind tunnel

The following sections describe the basic principles underlying the new wind tunnel and its initial design and construction. Also described are some modifications that were subsequently made in response to results obtained in the initial experiments that were carried out. There being no off-the-shelf equipment of this type available, the new facility was purpose-designed and built completely from scratch for the very purpose of this research. Following description of the new apparatus, there follows a description of experiments to evaluate the uniformity of the air flow over the working cross-section of the new facility and to characterize the test aerosols that were generated.

Principle of design:

For conventional wind tunnels of the type that have been used for much of the aerosol research reported in the literature, the horizontal air movement is sufficient for the vertical motion of particles associated with gravitational settling to be negligible in comparison to the horizontal motion, to an extent determined by the particle size. Under such conditions, for practical purposes the test aerosol is brought into the region of the apparatus being tested entirely by the horizontal air flow. By contrast, calm air aerosol chambers rely on gravitational settling to bring aerosols into contact with the apparatus being studied. Here it is customary that test aerosols are introduced from overhead and fall into the working section under the influence of gravitational settling only, there now being no external air movement, horizontal or otherwise, beyond that resulting from the aspirating action of the apparatus being studied or from the influence of any forced air involved in the generation and dispersion of the test aerosols. The two systems just described represent two extreme possibilities. However, for ultra-low windspeeds, where particle settling velocities may be of the same order of magnitude as – or even greater than – the velocities associated with horizontal air movement, we are drawn towards consideration of a system that represents a transitional region between the two extremes. This presents a unique experimental challenge. With this in mind, the design of the new wind tunnel for the research described in this Report was based on a combination of the principles of both of the generic aerosol systems described above, leading to what might be referred to as a 'hybrid' system.

Starting from this insight, a design evolved that enabled aerosols to be injected both upstream of and directly above the working section. In this new system, it was postulated that large particles from upstream that settled out before reaching the working section of the wind tunnel system would be compensated for by corresponding large particles falling into the working section from an overhead mixing chamber. Conversely, small particles entering from overhead would be carried downstream by convection and barely enter the working section, but would be compensated for by corresponding small particles entering horizontally from the upstream mixing chamber. If we allow simultaneous injection of the same test aerosols into the working section from both the upstream and overhead mixing chambers, and assume minimal losses of particles during entry, it may be shown trivially that the losses of particles are perfectly offset by the gains, resulting in a spatially uniform distribution of aerosols throughout the working section, in terms of both concentration and particle size distribution. A conceptual sketch of the idealized ultra-low windspeed facility based on these principles is shown in Figure 2.1.

Construction and modification:

On the basis of the preceding considerations, a new, ultra-low windspeed wind tunnel was built. For this we worked with Engineering Laboratory Design, Inc. (Lake City, MN, USA), a company that had previously built a number of purpose-designed aerosol test facilities for the PI's laboratories. The new facility was designed to be capable of: (a) containing a life-size human mannequin, consisting of a full life-sized torso above the waist; (b) providing acceptably uniform, smooth air flow at velocities continuously variable between 0.05 and 0.50 m/s; and (c) enabling the injection of acceptably spatially-uniform test aerosols with well-defined particle size distributions having mass median aerodynamic diameter (MMAD) in the range up to about 100 μm. The resultant facility measured 1.22 m x 1.22 m in cross-section and approximately 6 m in overall length, with the actual working section 3 m in length. Two mixing chambers, one upstream of and one directly above the working section, were used for injection and mixing of the test aerosols. Each of these mixing chambers was separated from the working section by a metal honeycomb screen that served to straighten and smooth the air flow entering the working section (in the case of the upstream screen) and to minimize the penetration of turbulent motions generated from the forced introduction of the test aerosol. (As will be described below, some modification of the upstream screen was later required.)

The wind tunnel described was of the 'open-cycle' type. That is, air from the laboratory entered the system through a pre-filter, passing through the upstream mixing chamber and the metal honeycomb screen, and entering into the working section, finally discharging back into the laboratory through a system of pre- and high-efficiency particulate air (HEPA) filters, situated just in front of the four fans. These four downstream fans were regulated and synchronized by means of a frequency inverter, enabling easy manipulation of the windspeed in the working section. A photograph of the new ultra-low windspeed facility is shown in Figure 2.2. As will be described in more detail later, initial attempts at aerosol injection and system calibration demonstrated that uniform distribution of aerosols in the upper particle size range tested, between about 30 and 90 μm, was not achievable using the wind tunnel configuration in its initial form. Specifically, it was observed that the upstream honeycomb

section at the entrance to the working section collected a large fraction of the injected particles by elutriation, the more so for the coarser aerosols and lower windspeeds. The result was that the particle size distribution of the test aerosol that entered the working section was significantly altered from what had originally been dispersed. This was not considered acceptable. So the upstream honeycomb structure was replaced by a pair of perforated aluminum plates installed in series, with circular openings 4 mm in diameter on 60° centers, resulting in 63% open area. The dimensions were chosen to minimize the downstream propagation of freestream turbulence, while largely eliminating elutriation particle losses without introducing significant losses by impaction. This modification proved successful and the new set-up then enabled experiments to be performed under all conditions of interest. Although some initial experiments had been carried out using the original set-up, the vast majority of the data described in this Report were obtained using the modified system. A quantitative comparison of inhalability results showed that there was no significant difference in the results for the original and modified system respectively.

Windspeed uniformity:

Windspeed measurement by anemometry at the extremely low air velocities pertaining to this work is known to be very difficult. Most conventional instruments, including hot-wire or pitot-static tubes, are not usable under such conditions. With this in mind, a simple 'time-of-flight' method was developed using visible smoke tracer. In this approach, streams of smoke, generated from incense sticks located in an external smoke chamber (see below in Section 3), were aspirated into the wind tunnel by the negative pressure generated by the air movement inside the tunnel. Smoke first entered into the wind tunnel via the upstream mixing chamber and traveled through the original honeycomb structure before entering the working section. A 'blip' was introduced into the smoke lines by he operator tapping on the tube through which the smoke entered the tunnel. At the low windspeeds of interest the blips remained coherent and were easy to track using the naked eye as they traveled downstream. By way of illustration, Figure 2.3 shows two time-lapse photographs of this technique. It shows two strings set 0.3 m apart, attached vertically to the back wall of the working section and extended across the wind tunnel working section from the top of the wind tunnel's back wall to the bottom of the proximate wall. This set-up was used to reduce the problem of parallax[2] by ensuring that the distance through which the smoke blips were timed was always 0.3 m regardless of the distance between the observer and the stream of smoke. This issue of parallax arose because the smoke was observed from outside the wind tunnel, at a distance up to approximately 1 m. In this system, a smoke blip was timed manually with a stopwatch as it passed between the strings, allowing a simple – and, as it turned out, quite accurate and reproducible – calculation of the windspeed.

To assess the distribution of air velocity over the working section (i.e., the uniformity along vertical and horizontal axes of the wind tunnel), the cross-section of the wind tunnel was divided into 16 equal areas, each approximately 0.9 m^2. The velocity was measured at the centerline of each section for 3 different frequency settings as displayed on the inverter control box of the fan power supply: 25, 40 and 60 Hz. These were the indices of windspeed

[2] Parallax is defined as the apparent displacement, or difference in apparent direction, of an object as seen from two different points not on a straight line with the object.

that were used for day-to-day application. By changing these settings, it was thus shown that a uniform, stable velocity could be continuously varied between 0.05 and 0.5 m/s. At windspeeds less than 0.25 m/s, the variability, as described by the coefficient of variation (CV, calculated as the standard deviation divided by the mean) was less than about 6% across the entire wind tunnel and less than about 3% in the center sections of interest. At the highest windspeed tested, approximately 0.42 m/s, the CV was somewhat higher, in the range of 12-14%. This discrepancy was likely due to measurement inaccuracy, in that the higher windspeeds were harder to time using a stopwatch due to the quick reaction time required in following the smoke. The windspeed measurements are summarized in Table 2.1 and show that the velocity distribution over the cross-section was consistent to within approximately ±12%. This was considered to be acceptable for practical purposes.

Frequency (Hz)	Pressure Drop ("H_2O)	Overall Velocity (m/s)	SD	CV (%)	Center Velocity (m/s)	SD	CV (%)
25	0.10	0.118	0.006	5.6	0.115	0.003	2.9
40	0.25	0.240	0.015	6.3	0.238	0.007	2.9
60	0.45	0.422	0.057	13.4	0.420	0.052	12.4

Table 2.1: Mean velocity measurements as a function of different frequency settings for the inverter/controller for the wind tunnel fans. Values are shown (a) averaged across both the entire wind tunnel, and (b) for just the center portion that represents the mannequin head location. Also shown are standard deviations (SD) and coefficients of variation (CV) for the air velocity measurements, along with the pressure drop across the upstream filters.

At the end of the calibration of the wind tunnel, it was found that the upper end of the useful range of windspeed that could be generated was 0.42 m/s. This will be reflected in all the experiments described in this Report.

Test aerosols and delivery system

We now move on to describe how test aerosols of well-defined characteristics were delivered to the working section of the new ultra-low windspeed facility, including the basic method by which the aerosols were dispersed from dry, narrowly-graded powders, and then how we overcame the difficult challenge of achieving aerosols that were uniformly distributed throughout the working section in terms of both aerosol concentration and particle size distribution. We also describe how aerosol particle size distributions were characterized for the full range of experimental conditions to be studied.

Method:

The test aerosols used throughout this research were generated from narrowly-graded powders of fused alumina (Duralum®, Washington Mills, Niagara, NY, U.S.A.). These were similar to those used previously in our laboratory and in many other related studies reported by other laboratories. A range of powder grades was chosen in order to generate aerosol covering the

wide range of particle sizes of interest, including F1200, F800, F500, F400, F280 and F240. These were known from long experience in wind tunnel experiments for windspeeds above 0.5 m/s to consistently provide aerosols with nominal particle aerodynamic diameters of about 6, 13, 26, 34, 74, and 90 μm, respectively, and with low geometric standard deviations (generally less than 1.30). The initial characterization of such aerosols was performed by Mark *et al.* as long ago as 1985, and yet the numerical values for the particle size parameters indicated have been found to hold very consistently over the years for aerosol generated from the same powder grades. Such consistency derives mainly from the fact that such powders, referred to as 'optical grade' and marketed primarily for industrial purposes such as grinding and polishing of lenses, are manufactured according to strict standards (as promulgated, for example, by the Federation of European Producers of Abrasives). Test aerosols generated from the powders described are not strictly monodisperse. However, because the variables of interest in research where they have been used (e.g., sampler aspiration efficiency) do not change sharply with particle size, it is allowable to accept a degree of polydispersity. Fuchs and Sutugin (1966) argued that it is acceptable in such research to use test aerosols with geometric standard deviation up to and even greater than 1.20.

Figure 2.4 shows one of the two identical mechanical dust generators (Topas SAG 410, Dresden, Germany) that were used to aerosolize and inject particles into either the top mixing cone or the upstream mixing chamber, or in both simultaneously, depending on the combination of particle size and windspeed utilized. In order to reduce inter-particle adhesion and thus ensure optimum dispersion, powder samples were conditioned overnight in an oven prior to use. During the experiments themselves, the powder contained in the feed hopper of each generator was exposed to direct radiant heat from an infrared lamp in order to maintain the desired low moisture content. The pressure of the air delivered to the aspirator of each generator was maintained above 2 bar, high enough to break up any agglomerates during aerosolization from the bulk powder (Paik and Vincent, 2002). Test aerosols in the experiments described here were not neutralized, in the light of knowledge that aerosol particle charge has insignificant effect on aspiration efficiency (Vincent, 2007).

Methods for achieving uniform aerosol concentration in the working section:

Starting from the configuration of the wind tunnel as it was originally conceived, built and delivered, we found that significant further development of the two aerosol delivery systems, the one upstream and the one above, was required in order to achieve the desired level of spatial uniformity of the various test aerosols throughout the working section. This was not unexpected.

For aerosol generation into the upstream mixing chamber, a special tracking system for the aerosol injection nozzle was built. The one shown in Figure 2.5 emerged after a considerable amount of experimental trial and error. Here, the injection nozzle was mounted on a reciprocating motor that allowed it to be moved vertically up and down cyclically. In this way, the test aerosol could be delivered alternately between the upper and the lower parts of the working section. That motor was in turn mounted onto an overhead tracking system that conveyed it laterally backwards and forwards across the width of the entrance to the working section just upstream of the conditioning screens. The nozzle itself was positioned so that the

aerosol was injected in the upstream direction, therefore ensuring enhanced spatial dispersion as it blew back over the injection system. The aim of this complex system of moving components was to generate a spatial distribution of the test aerosol in the working section that was uniform *when averaged over time*. The range of motion enabled by this bi-directional tracking system is indicated in the figure. The system described here is similar in principle to that described by Hinds and Kuo for their own mannequin studies (Hinds and Kuo, 1995). For aerosol generation from the mixing chamber above the working section, a similar reciprocating system was employed, again aiming at achieving uniform aerosol delivery – and again *when averaged over time* – to the top of the working section. That approach utilized a bi-directional tracking system that conveyed the injection nozzle alternately upstream and downstream, while simultaneously traversing a semi-circular pathway along the horizontal plane that covered the width of the wind tunnel. Here, the nozzle was pointed at approximately a 45° upward angle, which we found further added to the desired spatial uniformity. Both delivery systems, for the two mixing chambers, were adjusted by trial and error for each test aerosol and for each set of experimental conditions to arrive at the optimum placements for uniform spatial aerosol distribution within the working section.

Preliminary trials with this experimental system – before modifications were made – soon revealed some important features that represented departures from the simple idealizing assumptions implicit in the original rationale discussed earlier. In the first instance, it was found that aerosols generated from the coarsest powder grades (i.e., grades F400, F280 and F240) were not significantly present in the working section when only the upstream delivery system was in operation, even at the higher end of the windspeed range used. This was clearly due to the fact that most of the largest particles were collected by elutriation inside the individual tube-like elements of the honeycomb section located immediately upstream of the working section. Similarly, at the higher end of the windspeed range, aerosols generated from all powders delivered from above also failed to provide the desired uniform spatial distribution. That was primarily due to the large entry angle of the aerosols as they fell into the wind tunnel working section from above and were carried away by the moving air. From consideration of these initial observations it was concluded that, for the initial lay-out of the experimental system, only a limited subset of the overall range of desired experimental conditions could be examined: namely, finer grades delivered from upstream at all windspeeds and coarse grades delivered from above only at the lowest windspeeds. To overcome these limitations, wind tunnel modifications were made as described earlier (i.e., involving the removal of the honeycomb section and replacing it with a pair of vertical perforated plates) and the full set of experimental conditions were ultimately tested with this modified system in place. It is important to note that, despite these changes, which allowed for experiments to be performed at all windspeeds for all powders used, the nature of the air flow in the working section did not appear to be significantly altered from that of the original set-up.

Table 2.2 summarizes the optimal settings – as reflected in the dial settings (expressed as a %-age) for the belt speed in the generators which controlled the powder feed rate – for the two aerosol generators for horizontal and vertical aerosol delivery, respectively. These were established, by sequential measurement and modification, in order to achieve the most uniform aerosol concentration in the wind tunnel working section across the ranges of

conditions of interest. The procedure for the assessment of aerosol concentration is fully described in the next section, but a few words are necessary here with regard to the determination of the most appropriate aerosol generator settings. Initially, there were several default assumptions with regard to the aerosol generator belt speeds and the relative contribution of aerosols from each injection point. Specifically, at the lowest windspeed the default was to use both aerosol generators at the same belt speed, while at the higher windspeeds the default was to inject aerosol only from upstream, and not at all from overhead. By contrast, for the largest particle sizes at the lowest windspeed, it was assumed that injection solely from overhead would be sufficient. Starting with these assumptions, if any condition (i.e., any combination of windspeed and particle size) provided results that were not satisfactorily uniform to within the range of approximately ±10%, the settings were adjusted appropriately and the air concentration distribution was measured again. This process was repeated until acceptable spatial uniformity was achieved. As can be seen in Table 2.2, there were several sets of conditions for which these default assumptions provided adequately uniform concentrations and other conditions – not surprisingly, for the larger particles – for which multiple tests were required to optimize the results.

Powder Grade	**Windspeed (m/s)**					
	0.10		**0.24**		**0.42**	
	Upstream	**Overhead**	**Upstream**	**Overhead**	**Upstream**	**Overhead**
F1200	25%	25%	25%	0%	25%	0%
F800	25%	25%	25%	0%	25%	0%
F500	25%	5%	25%	0%	25%	0%
F400	25%	5%	25%	0%	25%	0%
F280	0%	10%	50%	5%	25%	5%
F240	0%	10%	50%	5%	40%	5%

Table 2.2: Aerosol generator settings for all combinations of windspeed and powder grade, as indicated by the percentage of the belt speed used during operation, for the contribution of aerosols from both upstream and overhead.

Aerosol concentration distribution:

From the outset, it was expected that a major challenge for this novel experimental system would be the achievement of acceptably uniform aerosol concentrations in the wind tunnel working section over the range of very low windspeeds of interest. As Table 2.2 shows, both windspeed and powder grade were variables that significantly influenced the ability to generate an appropriately uniform exposure atmosphere in the working section of the wind tunnel. Therefore, a complete assessment of concentration – as well as particle size distribution, as described in the next section – required measurements to be taken for each combination of windspeed and powder grade. The ultimate goal was to achieve an optimally uniform distribution of aerosols for each test condition by assessing the spatial uniformity, firstly within two different cross-sectional sampling planes separately and secondly between the two planes.

The initial step in the calibration process was to identify two planes in the working section at which the measurements would be made. The first one represented the location of the mannequin (which we refer to as the *'mannequin plane'*) in the center of the working section, and the second one represented the ultimate location of the reference sampler (the *'reference plane'*). The latter was located 0.75 meters upstream of the mannequin plane and 0.75 meters downstream of the entrance from the forward mixing chamber. To assess uniformity within each sampling plane separately, the distribution of aerosol concentration – covering several points on each plane – was examined for all 18 different experimental conditions. To assess longitudinal variability through the wind tunnel working section, the average aerosol concentration at the reference plane was compared to that at the mannequin plane.

Local measurements of aerosol concentration at both the reference and mannequin planes were taken using IOM personal inhalable samplers (SKC Inc, Eighty-Four, PA, U.S.A.) used facing directly upwards *as static samplers*. The selection of this particular sampler for static aerosol concentration measurements was arbitrary, as was its mode of use. The choice was based on practical considerations, including employment of the stainless steel cassette, which enabled easy gravimetric analysis with minimal sample losses and moisture uptake. Since the primary objective of this particular set of experiments was to determine the spatial uniformity of the concentration throughout the wind tunnel, the choice of this sampler and its mode of use were considered satisfactory.

For the experiments described here, the mannequin was removed from the wind tunnel and three to five IOM samplers were located at points covering the top, center and bottom of each plane. The majority of experiments were performed with the samplers located at the corners and center of a structure similar to the one shown later in Figure 2.6 (although different samplers are shown there, for reasons that will be revealed in due course). In that set-up, the four outer samplers occupied positions representing the centroids of the four quadrants of the working section cross-section, with the fifth sampler at a location representative of the position of the mannequin (when in place). For experiments utilizing three sampling points – all of which were performed *after* wind tunnel modification – the samplers were situated at the top, center and bottom positions along the central vertical axis of the wind tunnel.

Preliminary experiments performed prior to wind tunnel modification were carried out for three different powder grades (F1200, F800 and F500) and three different windspeeds (0.10 m/s, 0.24 m/s and 0.42 m/s), covering a total of 9 conditions of interest. As discussed previously, attempts to perform experiments for all other conditions proved difficult and so the full experimental regime was not tested until after the honeycomb modification was complete. An additional difference between the pre- and post-modification experiments was that aerosols were *not* injected from overhead for the initial experiments, even at the lowest windspeed.

Powder grade	Windspeed (m/s)	Reference plane					Mannequin plane				
		Top left	*Top right*	*Lower left*	*Lower right*	**Overall average (SE)**	*Top left*	*Top right*	*Lower left*	*Lower right*	**Overall average (SE)**
F1200	0.10	0.76	0.66	1.26	1.23	0.98 (0.16	0.62	0.68	0.99	1.09	0.85 (0.12)
	0.24	0.68	0.91	0.79	0.89	0.82 (0.05)	0.51	0.92	0.87	0.94	0.81 (0.01)
	0.42	0.56	0.75	0.67	0.91	0.72 (0.07)	0.62	0.83	0.74	0.99	0.80 (0.08)
F800	0.10	0.82	0.63	1.42	1.56	1.11 (0.23)	0.73	0.51	1.14	1.29	0.92 (0.18)
	0.24	0.86	0.99	1.03	0.97	0.96 (0.04)	0.69	1.08	0.91	1.01	0.92 (0.08)
	0.42	0.69	0.57	0.87	1.17	0.83 (0.13)	0.87	0.97	0.98	0.93	0.94 (0.02)
F500	0.10	0.89	1.06	1.48	1.41	1.21 (0.14)	0.87	0.93	1.46	1.52	1.20 (0.17)
	0.24	0.85	1.09	0.91	1.06	0.98 (0.06)	0.85	1.34	0.87	0.85	0.98 (0.12)
	0.42	0.36	0.65	0.48	0.82	0.58 (0.10)	0.59	0.66	0.74	0.85	0.71 (0.06)

Table 2.3: Results from preliminary experiments for the ratio of the average aerosol concentration (from 2 to 4 separate runs) at the specified sampling plane relative to the value for the center sampling point for that plane, also showing the standard error (SE) for each overall average. All results shown are for the wind tunnel prior to the modifications to the working section inlet.

Table 2.3 describes the uniformity of the measured aerosol concentration from preliminary experiments with the original, pre-modification set-up. Values are shown for each of the quadrants indicated for the wind tunnel cross-section and are expressed as the ratio of the concentration at the indicated sampling point to that at the center sampling point, shown separately for the reference and mannequin planes. These results show that the greatest *under*-sampling – relative to the center – occurred at the top of the wind tunnel, and was more pronounced at the highest windspeed. The greatest *over*-sampling occurred at the bottom of the wind tunnel at the lowest windspeed. This makes sense considering the increased influence that gravitational settling would have on aerosol behavior at these low windspeeds, particularly for the larger particles. At low windspeeds, some fraction of coarse aerosols would have a slightly downward trajectory if the particle settling velocity were not entirely outweighed by the horizontal motion associated with the freestream. This in itself would lead to a somewhat higher concentration towards the bottom of the wind tunnel. A corresponding decrease in the concentration of aerosols at the top of the wind tunnel would therefore be expected, keeping in mind that no aerosols were injected overhead in these preliminary experiments. The overall uniformity of the outer sampling points to the center point was also calculated and included in Table 2.3, with standard error estimates. On average, we concluded that the degree of uniformity within each plane before wind tunnel modification decreased with increasing windspeed and with decreasing particle size.

Powder Grade	Windspeed (m/s)					
	0.10		0.24		0.42	
	Ratio	*SE*	*Ratio*	*SE*	*Ratio*	*SE*
F1200	1.00	0.04	1.01	0.06	0.97	0.01
F800	0.99	0.03	1.01	0.04	0.97	0.04
F500	1.04	0.04	0.99	0.02	0.91	0.08

Table 2.4: Ratio of the average aerosol concentrations between the reference and mannequin planes, again pre-modification of the wind tunnel. Each value shown is based on from 2 to 4 experimental runs, and includes the standard error (SE)

Powder Grade	Windspeed (m/s)					
	0.10		0.24		0.42	
	Ratio	*SE*	*Ratio*	*SE*	*Ratio*	*SE*
F1200	0.91	0.05	1.01	0.05	1.00	0.03
F800	0.91	0.03	0.96	0.06	1.10	0.04
F500	0.98	0.01	1.06	0.07	1.11	0.02
F240	1.48	0.33	*	--	*	--

Table 2.5: Correction factors (with standard error, SE) to be applied to the reference concentration in order to establish the air concentration that would be present in the mannequin plane in the absence of the mannequin, to be used in calculating inhalability. These data were used for the pre-modification experiments only.

The ratio of the average aerosol concentration *between* the reference and mannequin plane for each experimental condition, again prior to wind tunnel modification, is shown in Table 2.4. Here it appears that, longitudinally throughout the wind tunnel, the aerosol concentration was relatively uniform, to within ± 10% for each experimental condition. While these data were obtained prior to the modification of the inlet to the working section, they provide evidence that, after aerosols enter the working section, the aerosol concentration did not change significantly as aerosols traveled through the wind tunnel, notwithstanding the within-plane differences. An additional set of concentration measurements, shown in Table 2.5, was taken along just the centerline of the wind tunnel working section, with one sampler placed at the location corresponding to the mannequin mouth in subsequent experiments and a second sampler at the location of the reference sampler. The purpose was to determine a correction factor to be applied in the later aerosol inhalability experiments with the mannequin.

Powder grade	Windspeed (m/s)	Top		Bottom	
		Ratio	*SE*	*Ratio*	*SE*
F1200	0.10	1.08	0.08	0.71[a]	0.01
	0.24	1.28	0.32	0.78	0.23
	0.42	0.65[a]	0.04	0.59[a]	0.03
F800	0.10	0.96	0.05	0.81[a]	0.05
	0.24	1.03	0.04	0.72	0.08
	0.42	0.68[a]	0.02	0.61[a]	0.03
F500	0.10	0.78	0.01	0.68	0.35
	0.24	0.99	0.06	0.82	0.01

	0.42	0.83	0.06	0.80	0.03
F400	0.10	0.87	0.27	1.00	0.10
	0.24	0.72[a]	0.09	0.72[a]	0.05
	0.42	1.47	0.55	1.48	0.49
F280	0.10	1.08	0.68	0.91	0.46
	0.24	0.98	0.01	1.03	0.27
	0.42	0.94	0.48	1.04	0.18
F240	0.10	1.01	0.34	1.16	0.14
	0.24	1.04	0.40	1.31	0.07
	0.42	0.67	0.03	1.13	0.45

[a]Difference from center is statistically different at $\alpha = 0.05$

Table 2.6: Uniformity of aerosol concentration along the vertical axis of the wind tunnel, modified by the replacement of screens at the entrance to the working section. The results are shown as the average ratio for each sampling location as referred to the center point (standard error, SE).

Only after the wind tunnel was modified (by changing the screens at the inlet to the working section, as already mentioned) was it possible to assess the uniformity of aerosol concentration for all six powder grades of interest at all three windspeeds, representing 18 experimental conditions. It was eventually noted that the variability within each of the top and bottom sections of the wind tunnel was adequately uniform such that a portion of experiments could be performed with the 3-sampler configuration described previously. Due to the change in the experimental set-up, the results for assessing spatial aerosol uniformity, as summarized in Table 2.6, are described somewhat differently than before. Now, for the subset of post-modification experiments performed with 5 samplers, the two top sampler concentrations were averaged into a single 'Top' value; and similarly for the two bottom samplers. In this way, results from the different experimental methods used in the post-modification calibration could be examined in the same way. That is, differences along the vertical axes of the wind tunnel working section were evaluated based on 3 measurements (i.e., top, center and bottom). The vertical variability of the aerosol spatial distribution, as reflected in Table 2.6, is thus expressed as the relative concentration of the top and bottom portions of the wind tunnel working section with respect to the center location. It should also be noted that the ratios calculated for the mannequin and reference planes individually were combined to enable a collective overall assessment. These results indicate that aerosol concentration was quite uniform for most conditions, but that there were several situations in which the concentration measured for the top and bottom sampling points showed significant differences relative to the center concentration. Typically, the largest differences were seen at the highest windspeeds and for the smallest particles. For the top section of the wind tunnel, there was significant under-sampling with respect to the center using the smallest particles at the higher windspeed. For the bottom section of the wind tunnel, there was also significant under-sampling with respect to the center for the smaller particles, but at both the highest and lowest windspeed. As expected, over-sampling was typically seen for the largest particle sizes, but those differences were not statistically significant (at a significance level of $\alpha = 0.05$).

Powder grade	Windspeed (m/s)					
	0.10		0.24		0.42	
	Ratio	*SE*	*Ratio*	*SE*	*Ratio*	*SE*
F1200	1.03	0.05	0.95	0.16	0.96	0.04
F800	1.02	0.04	1.06	0.10	0.97	0.05
F500	0.89	0.26	0.93	0.04	0.87	0.04
F400	0.89	0.20	1.08	0.09	0.71[a]	0.11
F280	2.50	1.66	0.67[a]	0.13	0.87	0.30
F240	6.95[a]	2.33	1.22	0.34	1.00	0.33

[a]Difference from center is statistically different at $\alpha = 0.05$

Table 2.7: Uniformity between the reference and mannequin planes for the modified wind tunnel, represented by the average concentration ratio for each sampling point, based on 3 measurements for each plane, for all powder grades and windspeeds.

The ratios of the aerosol concentrations between the reference and mannequin planes for the modified wind tunnel are shown in Table 2.7, corresponding to the results for the pre-modified tunnel shown in Table 2.4. Differences here were typically less than about 10%, and were only statistically significant for powder grade F400 at 0.42 m/s, grade F280 at 0.24 m/s, and grade F240 at 0.10 m/s.

Powder grade	Windspeed (m/s)					
	0.10		0.24		0.42	
	Ratio	*SE*	*Ratio*	*SE*	*Ratio*	*SE*
F1200	1.04	0.06	1.07	0.02	0.98	0.08
F800	1.03	0.11	1.06	0.02	1.06	0.02
F500	1.26	0.02	1.00	0.01	1.15	0.04
F400	1.19	0.04	0.80	0.03	0.98	0.17
F280	0.94	0.07	0.71	0.05	1.22	0.08
F240	2.90	0.73	0.65	0.06	0.78	0.01

Table 2.8: Correction factors (with standard error, SE) to be applied to the reference concentration in order to establish the air concentration that would be present in the mannequin plane in the absence of the mannequin, to be used in calculating inhalability. These data were used for the experiments using the modified version of the wind tunnel.

Finally, Table 2.8 shows the ratios of the aerosol concentration between the reference and mannequin planes for the modified wind tunnel (and hence corresponding to the results shown in Table 2.5 for the pre-modified version of the tunnel). As before, these would be used as correction factors to be applied to the reference sampler concentration measurements in order to provide accurate estimates of the actual aerosol concentration to which the mannequin and samplers were exposed. Although these values essentially describe the same relationship as that shown in Table 2.7, there were important experimental differences that enabled the use of these numbers as correction factors. Firstly, these results were obtained from measurements taken only at the locations where the reference sampler and mannequin mouth would ultimately sit, nominally along the center-line of the win d tunnel working section. Secondly, and importantly – and distinctly different from the results shown in Table 2.5 – the aerosol concentration values on which these latest results were based were obtained using the thin-walled cylindrical sampling probes that served as the actual reference samplers for the subsequent inhalability experiments (details of which are given later in this Report).

Aerosol particle size distribution:

Based on considerations along the lines already described, it was reasonable to expect that, in the ultra-low windspeed environment of the new facility, particle size distributions would be significantly modified during dispersal into the tunnel and conveyance into the working section, more so than in wind tunnels featuring higher windspeeds (as is typical of nearly all previous research in this area). We therefore set out to examine the extent to which the mass median aerodynamic diameter (*MMAD*) and Y6(wheredoesitallgo?)LBJaerosols generated from each powder grade differed from the nominal values reported previously (Mark *et al.*, 1985 and others) for aerosols dispersed into those other wind tunnels.

The particle size distribution in the working section of the wind tunnel was measured for each of the experimental conditions already identified, with the exception of the aerosols generated from the upper mixing chamber for the coarsest-grade particles (F280 and F240) at the lowest windspeed (0.10 m/s). For the latter, it was reasonably assumed that there were no significant losses during entry downwards into the test section, and so the original, nominal particle size distributions were considered appropriate. For the rest, measurements were taken using versions of the Marple personal cascade impactor (Model 290, from SKC Inc., Eighty Four, PA, U.S.A.) that had been modified with an additional, porous plastic foam top stage to extend the upper end of the sampler's useful particle size range (see Figure 2.7, full details are described by Wu and Vincent, 2007). The *MMAD* and σ_g were subsequently obtained by inputting the mass collected on each impactor stage into a simple inversion algorithm (Wu, 2005). This algorithm was originally developed for aerosol sampler studies in calm air, in which case the aspiration efficiency parameters were based on the assumption of calm air. In the present work, the model for aspiration efficiency needed to be adapted to account for the low-windspeed conditions of interest. This in turn produced an interesting circular dilemma since the matter of aspiration efficiency, for both inhalability and personal sampler performance, was itself the primary subject of investigation. To approach this problem, we sought appropriate estimations. In these, approximations for aspiration efficiency at ultra-low windspeeds were obtained by linear interpolation between what is already known from published models for moving and calm air respectively. Since the version of the modified-Marple sampler that was used in the present work did not feature the cap that was present in the modified device described by Wu and Vincent, it was considered to be roughly equivalent to an upwards-facing cylindrical tube. Models are available for such tubes. For the moving air extreme, we used the model suggested by Vincent *et al.* (1986), described by

$$A = \frac{1}{1 + 4GStR^{1/2}} \qquad (2.1)$$

where *St* is the Stokes number referred to the windspeed and tube diameter and *R* is the ratio of the windspeed to the inlet velocity, and the coefficient $G = 2.1$. For the calm air extreme we used the model described by Su and Vincent (2004), given by

$$A_{tube-up} = 1 - 0.8(4St_C R_C^{3/2}) + 0.08(4St_C R_C^{3/2})^2 - 0.12R_C^{-0.4}(e^{-p} - e^{-q}) \qquad (2.2)$$

where St_C is the Stokes number in calm air (referred now to the inlet velocity and tube diameter) and R_C is the ratio of the particle settling velocity to the inlet velocity, and where the coefficients p and q are given by

$$p = 2.2R_C^{1.3}St_C \tag{2.3}$$

$$q = 75R_C^{1.7}St_C \tag{2.4}$$

Using the model embodied in these equations, interpolated estimates for the aspiration efficiency at ultra-low windspeeds (A_U), to be used in the inversion algorithm for estimates of particle size distribution, were obtained using

$$A_U = A_{0.05} - \left[(A_{0.05} - A_{0.5}) \times \left(\frac{U}{0.5} \right) \right] \tag{2.5}$$

where U is the windspeed, $A_{0.5}$ is the estimated aspiration efficiency in moving air (with U = 0.5 m/s), and $A_{0.05}$ is the estimated aspiration efficiency in calm air (for U = 0.05 m/s). Assuming a linear relationship between the models for moving and calm air, the preceding equations were combined and folded into the inversion algorithm to provide the best available estimate of *MMAD* and σ_g for the range of ultra-low windspeeds studied.

The results are shown in Table 2.9 (for the pre-modification wind tunnel) and Table 2.10 (for the modified wind tunnel). At this point, a few words of clarification are needed. It is noted that the estimates for *MMAD* and σ_g for each individual sample taken were the result of inputting into the algorithm the data from 11 different impactor stages for each sample – the foam insert, 9 impaction plates, and the back-up filter, respectively. For each combination of windspeed and powder grade, one option for obtaining an overall estimate of *MMAD* based on multiple samplers would be simple arithmetic averaging. But the same cannot be done in order to estimate the σ_g. With this in mind, therefore, for each individual impactor stage the mass ratio (i.e., the proportion of the overall sample that was collected on that stage) was averaged across all experimental repeats and it was those new 11 *averaged* values that were entered into the algorithm to generate the best estimates for the average *MMAD* and the corresponding σ_g-values. In other words, each impactor stage was treated as a specific measurement point for which an average was obtained across all samples for each set of experimental conditions.

Prior to the wind tunnel modification, only a subset of experimental conditions was used for determination of the particle size distributions. Five modified-Marple cascade impactors were placed in the four quadrants and center point of the wind tunnel working section, respectively, over the mannequin plane. Samples were taken of 20-minute duration, with 2 repeats for each experimental condition. In Table 2.9 for the pre-modification set-upmeasurements, each value shown represents the average of 10 samples obtained for a specific set of conditions. The results show a surprising pattern in the relationship between windspeed and *MMAD* in that, for a given powder grade, the largest *MMAD* was observed for the *middle* windspeed (0.24 m/s). This trend was noted for all three powders. Nonetheless, for each windspeed, the *MMAD* increased as the powder grade became coarser, as would be expected. Additionally,

the σ_g-values were significantly greater than the corresponding nominal ones (for faster moving air), indicating that the test aerosols in our new experimental system were less narrowly dispersed than for aerosols generated using the same powder in faster moving air.

Powder Grade	Windspeed (m/s)						Nominal Value	
	0.10		0.24		0.42			
	MMAD (μm)	σ_g	*MMAD* (μm)	σ_g	*MMAD* (μm)	σ_g	*MMAD* (μm)	σ_g
F1200	6.83	1.81	9.57	1.88	7.75	1.53	6	1.36
F800	9.84	1.57	18.16	1.95	12.73	1.47	13	1.38
F500	13.89	2.15	27.93	1.77	18.58	1.35	26	1.30

Table 2.9: Particle size distributions measured using modified Marple-type cascade impactors prior to wind tunnel modification, represented by the mass median aerodynamic diameter (MMAD) and geometric standard deviation (σ_g).

Powder Grade	Windspeed (m/s)						Nominal Value	
	0.10		0.24		0.42			
	MMAD (μm)	σ_g	*MMAD* (μm)	σ_g	*MMAD* (μm)	σ_g	*MMAD* (μm)	σ_g
F1200	9.6	1.28	9.5	1.32	9.3	1.34	6.0	1.36
F800	13.9	1.49	12.8	1.47	12.4	1.56	13.0	1.38
F500	28.8	1.62	32.7	1.71	28.7	1.93	26.0	1.30
F400	37.7	1.62	44.3	1.59	40.0	1.74	34.0	1.20
F280	74.0[a]	1.19[a]	62.4	1.42	66.9	1.45	74.0	1.19
F240	89.5[a]	1.29[a]	60.1	1.45	63.0	1.49	89.5	1.29

[a] Nominal value used for this condition

Table 2.10: Particle size distributions, measured by modified Marple-type cascade impactors, for all powder grades and windspeeds of interest in the fully modified wind tunnel, represented by the mass median aerodynamic diameter (MMAD) and geometric standard deviation (σ_g).

After the wind tunnel modification, samples with the modified Marple sampler were taken just at the center of the reference and mannequin planes, again over a 20-minute period with two repeats for each set of conditions. In Table 2.10 the results show that, for the various powder grades (with the exception of grade F800), the particle size distributions were indeed significantly different (at $\alpha = 0.05$) from the nominal values. For these results, however, the pattern seen for the preliminary measurements of *MMAD* – in which the largest value was observed in the middle windspeed of 0.24 m/s – had disappeared. And although the estimated σ_g-values were still typically higher than the nominal ones, they were generally smaller than the pre-modification estimates shown in Table 2.9. This difference is likely to be associated with the fact that the wind tunnel modification enabled increased penetration of aerosols into the working section.

Heated, breathing mannequin

We now describe the realization of a heated breathing mannequin system that would be sufficiently representative of an actual human subject that might be exposed by inhalation to aerosols. Once again, as for the wind tunnel, there was no off-the-shelf equipment that would meet what was required. So development from scratch was once more required. The basic principles underlying the design are described, leading up to the actual design and construction of the facility itself, featuring in particular the ability to accurately and consistently recover the particulate matter that had been inhaled and collected inside the head of the mannequin, along with its integration into the working section of the ultra-lowspeed wind tunnel.

Principles:

As previously stated, the current research is concerned with measuring the *inhalable fraction* of aerosols at ultra-low windspeeds. It is important to note that the only human physiological structures that might significantly impact aerosol inhalability, and so must be taken into account in the mannequin design, were the external body surfaces, orifice openings, and breathing patterns. That is, it was necessary only to accurately reproduce the external anatomical structure of a typical human (i.e., the nose and mouth openings). Since there was no interest in finer aerosol fractions, it was not necessary to incorporate features relating to any internal respiratory system configuration beyond the provision of the capability to provide representative ranges of values for relevant breathing parameters (e.g., tidal volume, breathing cycles per minute, etc.).

An important consideration when discussing inhalability is that the air jet produced during expiration will disturb the air flow approaching the mannequin and in turn have the potential to impact the inhalation of aerosols in the next part of the breathing cycle. This has rarely been studied during previous research, a notable exception being the work reported by Wood and Birkett (1979). It was considered to be particularly important in the context of the ultra-low windspeeds featured in the current work, where it would be reasonable to expect a more marked effect than at higher windspeeds. So the capability to examine this needed to be built into the mannequin. In addition, it was important to avoid the possibility of re-entrainment of aerosols already collected onto the filter or deposited onto surfaces along the inhalation pathway – which may have occurred in some reported studies. Therefore, an additional requirement of the new mannequin system was to allow entirely different pathways for inspiration and expiration. To achieve this, the mannequin was designed such that oral inspiration took place through one mouth and expiration through an identical one located immediately below the first. Further details on these design features are discussed below.

Another important consideration for the design of the mannequin system was the possibility of effects associated with body heat. Several workers have previously speculated about the possibility of air movement that might derive from buoyancy effects associated with warmer air close to the body. Again, any such effects, if they exist at all, are likely to be more pronounced at the ultra-low windspeeds of the present work than at the higher windspeeds of

earlier studies. With this in mind, therefore, the mannequin was designed to incorporate the ability to simulate body heat to typical surface temperatures.

Finally, it is well known that inhalability is strongly dependent on orientation of the mannequin with respect to the wind. Yet it was always recognized that, in striving to achieve a particle size-selective standard for inhalability, the only practical option was to assume that there was no preferred orientation with respect to the wind. In the earliest experimental studies of inhalability (e.g., Ogden and Birkett, 1978; and others), although the individual experiments were carried out for a single orientation, the results were averaged uniformly over all the orientations from 0 to 360°. Later studies, however, built the desired feature directly into the experiments by providing for the mannequin to be rotated slowly about a vertical axis. This was done in the present research. With this in mind, the mannequin was therefore designed to fit onto a rotating mechanism integrated into the wind tunnel structure, allowing for slow rotation in a continuous, albeit reciprocal manner – that is, one full rotation in one direction, and the next in the other, and so on, as will be described later.

Mannequin construction and integration into wind tunnel:

Mannequin design and construction were completed in cooperation with Measurement Technology Northwest, Seattle, WA, U.S.A., who had previously built heated, breathing mannequins for other applications elsewhere. The goal for this apparatus was to: (a) realize a life-sized mannequin with accurately modeled external human features; (b) simulate continuously-variable, representative breathing parameters (e.g., tidal volume, breathing frequency, etc); (c) allow for inspiration and expiration through either the nose or mouth, in any combination; (d) enable collection – or recovery – of all inhaled particles; (e) be heated to a representative range of body temperatures; and (f) be integrated into the new wind tunnel (described above) with the ability to rotate slowly (at a rate between 1 and 3 rpm) and continuously through 0 to 360° about a vertical axis.

The resultant system is shown in the photographs in Figure 2.8. The mannequin is shown in Figure 2.8a fully assembled and located in the working section of the wind tunnel. Figure 2.8b shows a detailed view of the mannequin with the face-piece dropped down to reveal the 47-mm filter holder, along with the various connections that could be manually adjusted to achieve any desired combination of nose and mouth breathing. What cannot be shown in this representation are the heating coils located just under the surface of the mannequin – at the front and back torso, in each arm and on the head – to simulate the desired body temperature. Figure 2.8c shows the mannequin with the associated breathing machine (in the suitcase) and the laptop computer that was programmed to operate and control all heating and breathing functions, including maintaining the desired body temperature, breathing minute volume, and breathing cycles per minute. Figure 2.9 shows the open breathing machine suitcase revealing the two pneumatic cylinders – each of volume 1.4 L, for a total of 2.8 L – that could be cycled in and out by a servo-linear actuator, resulting in a sinusoidal breathing pattern. The control system allowed for tidal breathing volumes from 0.1 to 2.5 L (as governed by the distance the pistons traveled), and breathing frequency from 5 to 30 cycles per minute (as governed by the speed of travel). Airflow rates were monitored by means of integrated spirometers. Body

temperatures were monitored and controlled by means of thermocouples located at strategic locations just beneath the mannequin surface.

During the aerosol inhalability experiments that will described later in this Report, it was an essential feature that the inspired air passed through a filter, which allowed for collection of the inhaled aerosol, and also that particles collected on the inner walls of the nose and/or mouth before reaching the filter during inspiration were recoverable. It was considered especially important that air flowing through the system during the expiration cycle should *not* follow the same route as during inspiration. There was serious concern that, were the two pathways were to be the same, particles having been collected on the filter or deposited on the internal walls during inspiration might be re-entrained during the expiration part of the cycle, and so exit the mannequin in the exhaled air. With these concerns in mind, the mannequin was designed so that inspired and expired air followed different pathways. This required a complex system of pathways and connectors inside the head, as shown in Figure 2.10. Here, the breathing manifold has been removed from the mannequin, revealing the nose and mouth inlets, the internal tubing connections, and the filter holder.

For nose breathing, separation of the airflows was achieved by allowing air to be inspired through one nostril and out through the other, each measuring 12 mm in diameter such that it would be roughly equivalent in area to a pair of actual human nostrils, thus ensuring approximately the same air velocity during entry and exit. For mouth breathing, the same objective was achieved by providing the mannequin with two mouths, each with dimensions equivalent to a typical human mouth, measuring 40 mm long and 3 mm wide, and located vertically adjacent to one another. Due to constraints of the tubing connections inside the mannequin head, oral inhalation was always through the upper mouth and oral exhalation was always through the lower mouth. For consistency, nasal breathing was established to always be in through the left nostril and out through the right nostril.

For the collection of inhaled particles, the 47-mm filter holder shown in Figure 2.10 was situated in mannequin's inspiration pathway. The aluminum holder consisted of a conical-inlet filter holder fitted with a thick silicone O-ring that secured the filter in place onto a metal backing that sat in the outlet portion, all of which was secured together by a threaded metal ring that allowed the two sections to be firmly screwed together. On the inside of the mannequin head, the breathing manifold that included the pathways from each nose and mouth opening contained a quick-release device from which the filter holder inlet could be easily snapped in and out. The outlet of the filter holder was attached to flexible tubing that ran through the mannequin body and ultimately passed through the floor of the wind tunnel to connect to the breathing machine.

The fully-installed mannequin system also contained a mechanism that allowed for 360° slow rotation about a vertical axis. This was achieved by means of a shaft and motor system mounted in the center of the floor of the working section of the tunnel. The shaft was installed in the middle of a hollow tube on which the mannequin sat, and through which the wires connecting the breathing and heating functions were fed. Continuous rotation of the mannequin in the same direction, while desirable, was impractical due to the need for these tubing and wire connections without tangling. So the rotating mechanism was connected to a

relay system that was triggered after one full rotation, at which point the rotation of the mannequin would be reversed and thus follow the same path back through another 360°. This reciprocating motion – at the equivalent of about 3 revolutions per minute – was continued for as many cycles as required (i.e., to enable the desired sampling duration). By this arrangement, we were able to ensure that, averaged over time, there was no preferred orientation with respect to the wind.

Overview

In the preceding sections we have outlined the new facilities that were developed and built for the study of aerosol transport at ultra-low windspeeds. These included a novel hybrid wind tunnel into which well-characterized aerosols –generated from narrowly-graded powders of fused alumina – may be introduced, as well as a life-sized mannequin capable of breathing and heating to body temperature. It was expected from the beginning that realizing such a system would present many practical difficulties. But through modifications made during the commissioning and calibration of the experimental system, a reliable working system was achieved meeting our experimental design requirements to the desired level of satisfaction. The work in achieving all this was an essential part of the project and required a commensurate amount of time and effort, accounting for more than half of the overall time and effort in the overall project. Ultimately, however, this important task was accomplished successfully, laying the foundation for the experimental program to investigate human inhalability and personal sampler performance at ultra-low windspeeds.

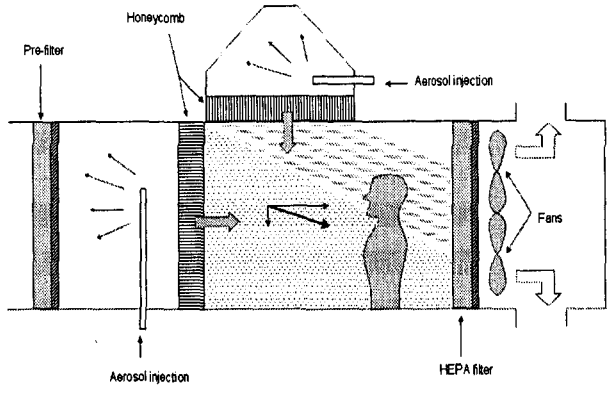

Figure 2.1: Conceptual sketch of the new ultra-lowspeed wind tunnel, showing aerosol injection from both overhead and upstream and the resultant expected particle trajectories.

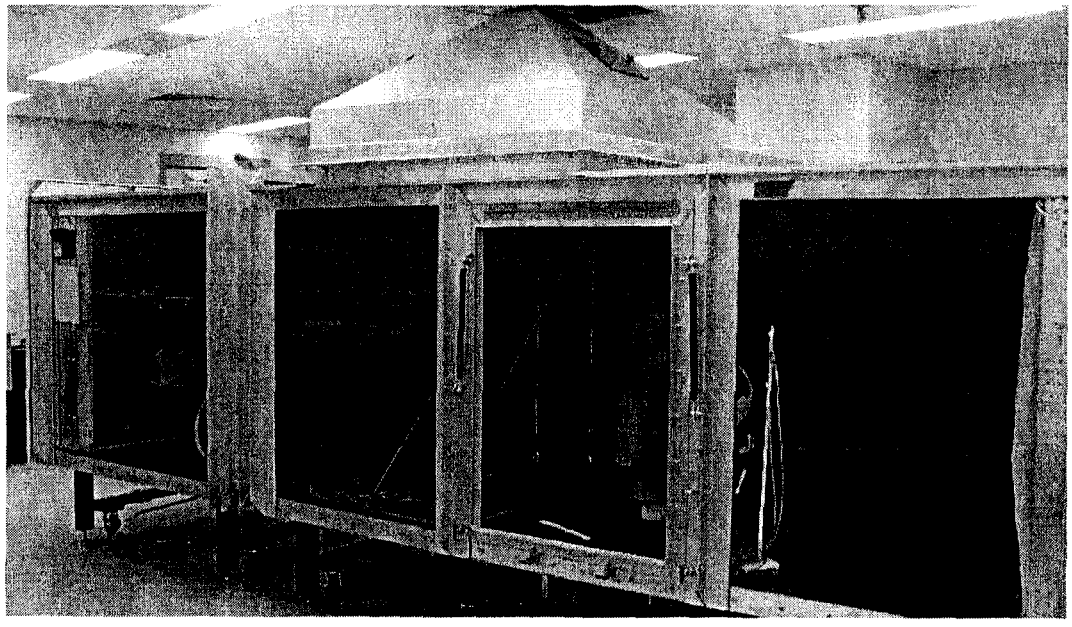

Figure 2.2: The new ultra-lowspeed wind tunnel facility, showing the heated, breathing mannequin installed in the working section.

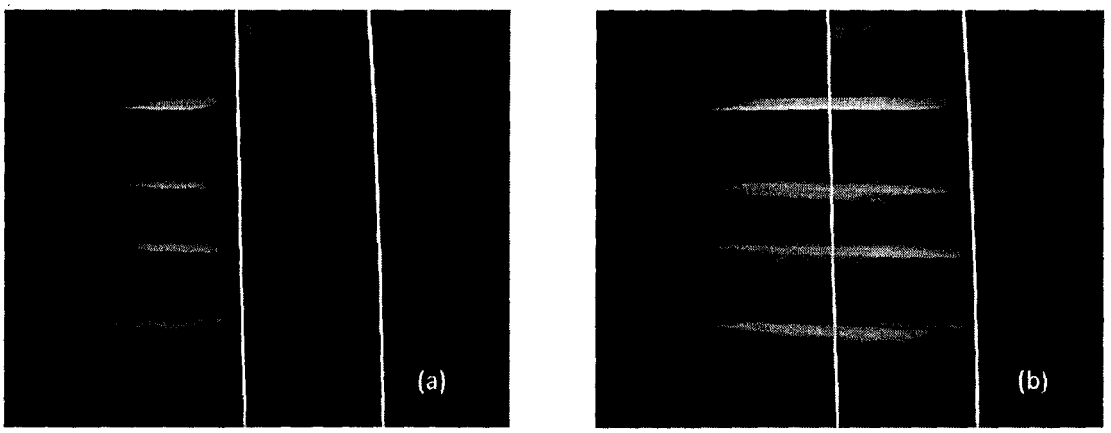

Figure 2.3 Time-lapse photographs to illustrate the technique that was developed for measuring windspeed; it shows several smoke 'blips' as they travel across the section in which they were timed. Also shown are the strings that demarcated the timing section and assisted in dealing with the problem of parallax for the viewer.

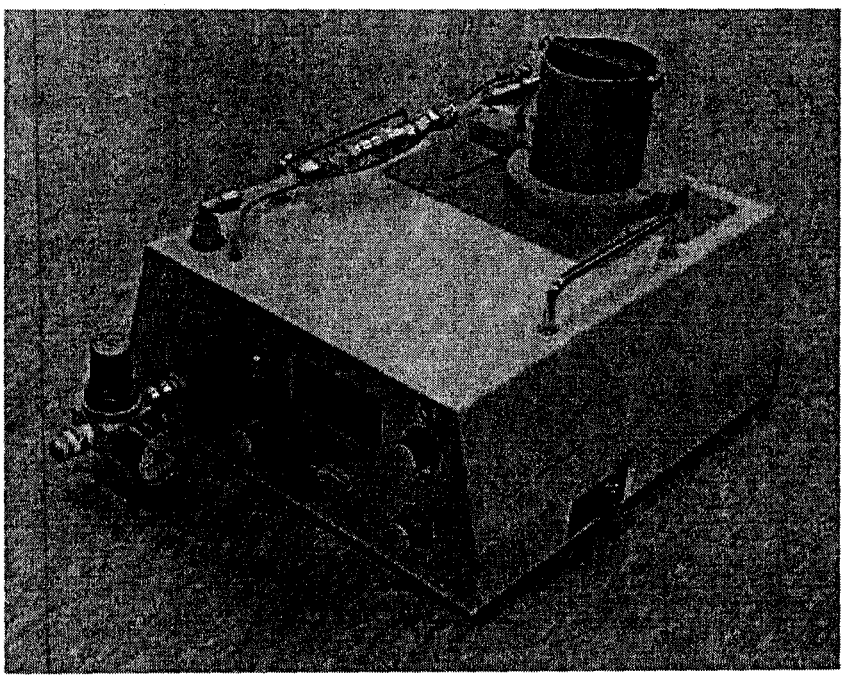

Figure 2.4: One of the Topas dust generators used to aerosolize and inject narrowly graded powders of fused alumina into the wind tunnel.

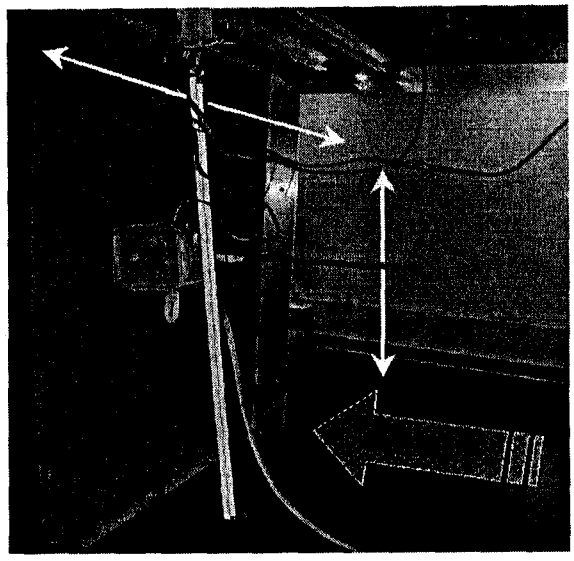

Figure 2.5: Bi-directional tracking system used to fully disperse aerosols injected into the upstream mixing chamber, with the white arrows indicating the range of motion of the injection nozzle provided by the tracking system and the gray arrow indicating the direction of airflow.

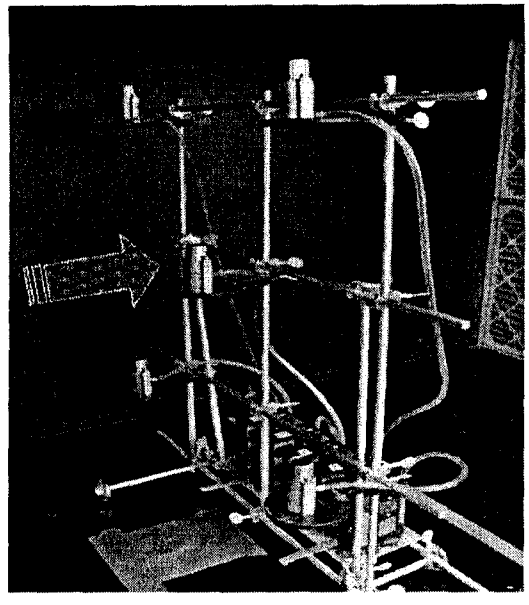

Figure 2.6: Structure used for wind tunnel calibration measurements, in this case shown with the Marple cascade impactors used to measure particle size distribution, but also used to measure aerosol concentration distribution with IOM samplers facing upwards as static samplers. The gray arrow indicates the direction of airflow.

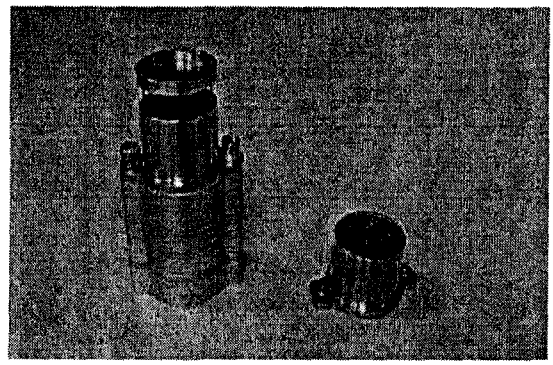

Figure 2.7: Modified Marple-type cascade impactor used to measure particle size distributions, shown assembled with the cap (not used here). Also shown is one of the disassembled top foam stages.

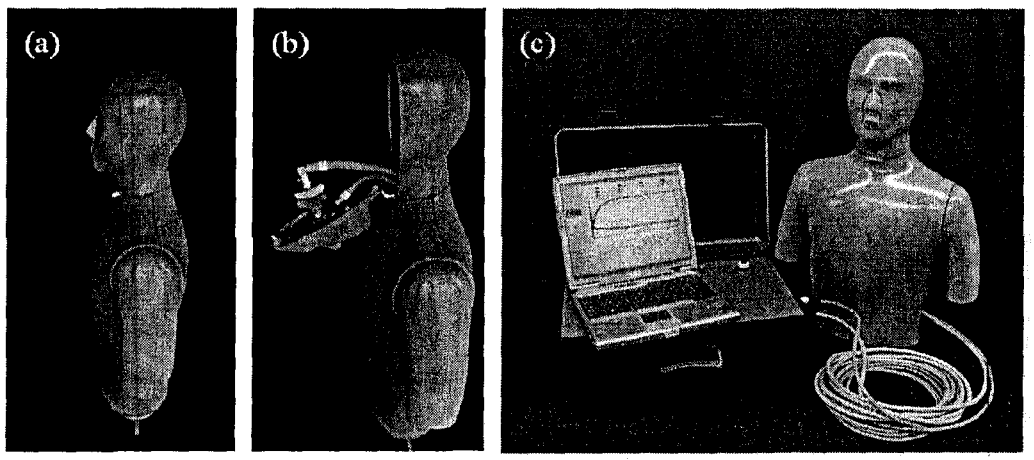

Figure 2.8: New mannequin system shown (a) fully assembled inside the wind tunnel, (b) with the face piece opened to reveal the internal filter holder, and (c) with all peripheral components.

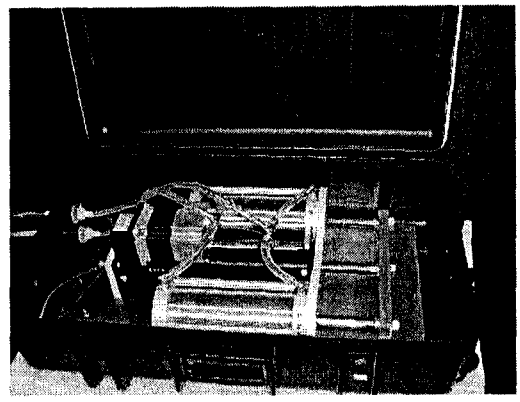

Figure 2.9: Mannequin breathing machine, consisting of two pneumatic cylinders and a servo-linear actuator that cycles in and out to produce a representative range of human breathing flowrates.

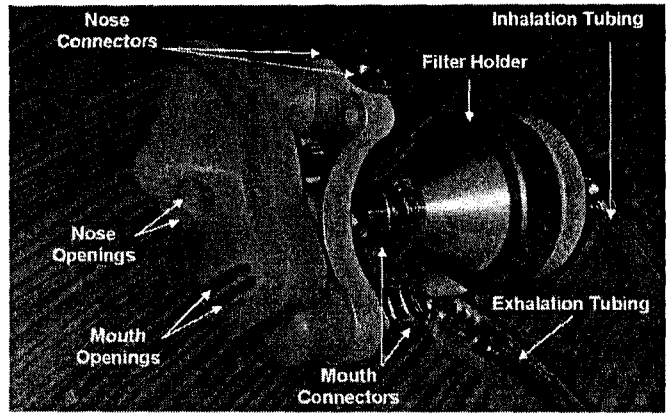

Figure 2.10: Mannequin breathing manifold with attached filter holder, indicating the various nose and mouth orifices as well as the separate internal tubing connections.

3. Visualization of the air flow around the heated breathing mannequin

In the same way that most of the research on human inhalability has not included the ultra-low windspeeds of interest, experimental characterization of air movements around the human body at low windspeeds has also never been studied to any significant extent. Some relevant studies have been reported for higher windspeeds, greater than 0.5 m/s. For example, Wood and Birkett (1979) performed some rudimentary flow visualizations and showed qualitative evidence of air disturbances resulting from the breathing action of a mannequin. However no attempts were made to link these findings in any way with inhalability. There has also been some rudimentary mathematical modeling to understand the physical processes that influence human aspiration (Erdal and Esmen, 1995; Dunnett and Ingham, 1986; and others). Most recently, numerical modeling of human aspiration included computer simulations of airflow patterns around the human body under calm air and ultra-low windspeed conditions close to those of interest here (Gilmutdinov and Zivilskii, 2008). However, laboratory experiments to examine airflow patterns around a simulated human – both breathing and heated – have not been attempted in the more relevant ultra-low range of windspeeds pertaining to this Report.

Flow visualization experiments are described here that were intended to provide qualitative insights of the nature of the airflow near the mannequin under the conditions of interest, and how this might have some influence on inhalability, depending not only on the windspeed itself but also various breathing parameters (e.g., minute volume, breathing mode, etc.) relating to the mannequin. The results of such an investigation were intended to complement – and provide additional insight into – the results of our human inhalability studies that will be described later.

Flow visualization methods

A visible tracer method was sought that would accurately reflect the motion of the air, in effect graphically identifying the streamlines that describe the airflow pattern in the wind tunnel and around the mannequin. The free stream turbulence in the new wind tunnel – in its original unmodified version – was low enough that such flow visualization was possible, aided in part by the upstream honeycomb that served to straighten the airflow as it entered the working section.

For purposes of the present work, several methods of flow visualization were considered or attempted. Initially, the helium bubble technique was thought to be potentially useful, having been widely used for such purposes by aerodynamicists for many years (e.g., Kerho and Bragg, 1994; Mueller, 1996). A commercially available helium bubble generator (Sai™, Sage Action, Inc., Freeville, NY, U.S.A.) was acquired for this purpose and set-up outside the wind tunnel, with a stainless steel connecting tube for the introduction of neutrally-buoyant bubbles directly into the working section. However it was soon found that the bubbles could not be introduced without significantly disturbing the freestream. So this approach was eventually abandoned. We then considered the alternative hot-wire smoke generator, which has been widely used in other wind tunnel studies for smoke generation purposes (e.g., Sreenath *et al.*, 1997). But this would require the installation of an overly complex apparatus directly within the working section of the wind tunnel, and so this too was abandoned. Ultimately, the technique that proved most promising was the simplest. It involved the use of smoke generated from incense sticks inside an external chamber and drawn into the tunnel by virtue of the negative pressure there (relative to

outside). Figure 3.1 depicts the system that was eventually realized. Figure 3.1a shows the external smoke chamber, which was constructed of particle board on 5 sides with a plexiglas top and steel brackets holding all sides together. In each experiment, eight incense sticks (Florasense Incense, Blyth HomeScents International, Des Plaines, IL, U.S.A) were lit and placed inside the chamber, and allowed to burn for at least five minutes before turning on the wind tunnel, allowing a sufficient concentration to build up inside the chamber. A flexible tube leading from the chamber was connected inside the tunnel to a long rigid plastic tube of diameter about 5 cm that extended from the top to the bottom of the upstream mixing chamber (see Figure 3.1b). Twelve small, equally-spaced holes were drilled into the rigid tube. When the tube filled up with the smoke from the smoke generation chamber, the negative pressure inside the wind tunnel was sufficient to draw in the smoke which then appeared as a set of 12 thin parallel, horizontal and highly-visible strands, entering into the wind tunnel working section through the honeycomb at its entrance. Experience showed that very striking flow visualizations could be obtained by this method, as will be shown below in the photographs that are presented.

A sketch of the wind tunnel configuration ultimately used for the flow visualizations is given in Figure 3.2. An important feature of this set-up, as seen in the figure, was the lighting system that was developed in order to enable adequate illumination of the smoke traces as they moved through the wind tunnel working section. This was achieved by placing a set of five 250-watt floodlight bulbs inside the upper mixing chamber, sitting directly atop the honeycomb structure that separated that chamber from the main exposure section. The honeycomb provided collimation of the light and excellent illumination of the smoke lines and mannequin. Since it was important to limit sources of heat inside the wind tunnel, the lighting system remained off and was turned on only for the brief duration of each experiment.

As described earlier, the mannequin was attached to a rotational mechanism to obtain orientation-averaged sampling results for the subsequent inhalability and personal sampler studies. For the flow visualization studies described here, however, the mannequin was placed only at fixed orientations, mostly (unless stated otherwise) facing into the freestream. Most of the experiments were performed with an unclothed mannequin. But a small number of experiments were also conducted to examine the effects of added garments.

Of course, the usefulness of this flow visualization study would be heavily dependent on the ability to obtain high quality images of the flow patterns around the mannequin. With this in mind, appropriate photographic equipment was purchased, in the form of a digital camera (Panasonic, DMC-FZ50 Lumix) that was capable of producing not only high-resolution photographs, but also high-quality video clips, from which high-quality individual 'still' frames could also be extracted. During each experiment, the camera was placed on a fixed tripod outside the wind tunnel. In order to optimize contrast, black matte paper was installed on the far wall of the tunnel. In addition, thick black cloths were draped over the wind tunnel viewing windows to significantly reduce the ingress of stray ambient light. Each of the final videos obtained using this system lasted for approximately 40 seconds and incorporated from 5 to 10 full breathing cycles.

Experimental conditions

The parameters that were modified for the flow visualization experiments are listed below in Table 3.1.

Windspeed (m/s)	Mode of breathing	Breathing flowrate (L/min)	Body temperature (°C)	Orientation (° From wind direction)	Clothing
Combinations of the following parameters					
0.10	Nose in/Nose out	6	Heated (33°C)	0	Lab coat
0.24	Mouth in/Mouth out	20	Unheated	90	Hard hat
0.42	Nose in/Mouth out			180	Safety glasses

Table 3.1: Summary of ranges of conditions for the flow visualization experiments.

These were chosen to complement those conditions for which the inhalability and personal sampler performance measurements, the primary object of the research, would to be carried out (as described later in this Report), including

- Windspeed (m/s)
- Breathing flowrate (minute volume, L/min)
- Mode of breathing (i.e., nose or mouth breathing)
- Body temperature (°C)
- Orientation
- Clothing

Three different windspeeds (0.10 m/s, 0.24 m/s and 0.42 m/s) were chosen to examine the range of environments that are considered 'ultra-low.' Two different breathing flowrates, expressed in terms of minute volume, were chosen to simulate '*at rest*' breathing and a '*moderate work*' (6 L/min and 20 L/min, respectively). Those values were based on either 12 or 20 breaths per minute with either 0.5 L or 1.0 L tidal volume, respectively. The modes of breathing that were used included mouth-only breathing (in and out through the mouth), nose-only breathing (in and out through the nose), and in through the nose and out through the mouth (nose-mouth breathing). The additional possibility of breathing in through the mouth and out through the nose was not included because this was not considered to be a mode of breathing normally to be found among workers in real situations. At the higher breathing flowrate (20 L/min), nose-only breathing was not examined because this too was not considered a common breathing pattern[3] (Saibene *et al.*, 1978). Combining the parameters of breathing flowrate and mode of breathing

[3] The term 'breathing pattern' as used here refers to the various combinations of flowrate and breathing mode, so that ultimately 5 different breathing patterns were examined: mouth-only at 6 L/min, mouth-only at 20 L/min, nose-only at 6 L/min, nose-mouth at 6 L/min and nose-mouth at 20 L/min.

provided 5 different breathing 'patterns: 6 L/min mouth, 20 L/min mouth, 6 L/min nose, 6 L/min nose-mouth, and 20 L/min nose-mouth. Mannequin body temperature was either unchanged (i.e., room temperature) or heated to typical human skin temperature (33 °C).

Analysis of orientation effects was completed under a more limited set of conditions, with the mannequin operated – unheated – with either nose-only or mouth-only breathing and for each of the three windspeeds and two flowrates indicated. The orientations that were studied included facing into the wind (0°), at a right angle to the wind direction (90°), and facing downstream from the wind direction (180°). The effects of clothing – lab coat, safety glasses and hard hat – were tested to a limited extent for the mannequin both heated and unheated, but not breathing.

For mouth-only breathing, inspiration took place through one mouth orifice and expiration through the other. Due to the size of the filter holder located along the inhalation pathway – for use during later studies where inhaled aerosols are collected – the inhalation tubing was always attached to the upper mouth, with expiration through the lower mouth. Although the present study of air patterns around the breathing mannequin did not require the use of any filters, the same configuration was used here for consistency.

Similarly, for nose-only breathing, inspiration was through one nostril and expiration was through the other nostril. In this case, each orifice was available for either inspiration or expiration. But again for consistency, inspiration was established always to be through the left nostril with expiration through the right nostril. It is important to acknowledge that in these simulations, the jet produced by breathing through only one nostril, as opposed to normal human breathing through both nostrils at once, was not entirely representative picture of real human nasal breathing. However, the size of each nostril was designed such that the air velocity in the expired air jet was the same as would have been achieved for the two nostrils at actual size. Preliminary observations confirmed that no difference in air disturbance was visible based on which nostril was chosen for expiration.

Basis for qualitative analysis

A few words are needed to explain the basis on which the results of the flow visualizations were used to make useful conclusions. For each condition of interest, the primary question was: Is the airflow approaching the mannequin significantly modified by the breathing action of the mannequin? If so, it was asked: Does the modification persist long enough to disturb the airflow through the subsequent inspiration phase? If the answer was affirmative in both cases, it could reasonably be concluded that the perturbation introduced into the freestream might be sufficient to significantly influence aerosol transport in the approaching air during the whole breathing cycle, and hence – by extension – affect aspiration efficiency.

An additional research question of interest was: Is the body temperature of the mannequin sufficient to cause any air movements around the mannequin derived from the effect of buoyancy in the warmer air near the body?

Results and discussion

The ultimate product of the flow visualization experiments was a library of movie videos – 30 in total – depicting the breathing mannequin under the various sets of conditions specified above. The movie records cannot be presented here, but are available from the PI on request. From those records, still photographs at various points in the mannequin breathing cycle were extracted and compiled into the figures shown here. In each case, the pictures represent what was observed at the peak of the inspiration and expiration phases, respectively. Those points were determined both by visually identifying the moment at which the smoke disturbance was closest to and farthest from the breathing orifice in question and by noting the audible sounds emanating from the pump system – also captured in the recordings – that accompanied inspiration and expiration.

Effect of windspeed:

Figure 3.3 shows typical results for the effect of windspeed on air movements around the breathing mannequin when unheated and breathing through the mouth at 6 L/min. It is clearly evident that there was a clear difference in airflow disturbances around the mannequin, to an extent strongly dependent on the windspeed. It is noted that the smoke tracers for the higher windspeeds were somewhat less smooth, containing small eddies that tended to increase the width of the smoke lines. Most of this, we believe, was associated with the slightly higher level of freestream turbulence at the higher windspeeds.

The results show that, during expiration for the lowest air velocity (0.10 m/s), there was a region of disturbed air directly in front of the mannequin face that was larger than for the higher air velocities. For this windspeed, the disturbance due to the air jet during exhalation persisted even into the inspiration part of the breathing cycle. That is, the airflow pattern did not fully recover. In contrast, at the higher windspeeds of 0.24 m/s and 0.42 m/s the smooth smoke pattern *did* fully recover by the time of arrival of the subsequent inspiration phase. As expected, for a given windspeed, the actual degree of disturbance – in terms of how far the plume of expired air extended out in front of the mannequin – was also dependent on both the mode of breathing and the breathing flowrate. Looking at the collection of videos for each breathing pattern, similar results with regard to the effect of windspeed (i.e., more disturbed flow in the lowest windspeed) were seen for all but one combination of breathing mode and breathing flowrate. That exception was for nose-only breathing at the low flowrate (6 L/min), where the air disturbances were minimal and not persistent for all windspeeds.

Effect of breathing flowrate:

Figure 3.4 shows typical results for the effect of breathing flowrate, illustrated for the case of the unheated, mouth-only breathing mannequin at a windspeed of 0.24 m/s. It is seen, for every combination of windspeed and mode of breathing, that the lower flowrate produced a plume of expired air that did not extend upstream as far as that from the higher flowrate. Not surprisingly, there was also an inverse relationship between the flowrate and the windspeed, such that the least amount of disturbance was observed when the mannequin was breathing 'at rest' in the higher windspeeds. Conversely, the most disturbed air was seen when the mannequin was breathing at the higher flowrate ('moderate work') at the lowest windspeed.

Effect of breathing mode:

Figure 3.5 shows typical results for the effect of the mode of breathing. On the one hand, it is seen that expiration through the mouth created a jet that was projected upstream directly into the region immediately in front of the mannequin head. On the other hand, for expiration through the nose the jet was instead directed at a downward angle close to the body, disturbing the air in front of the mannequin torso. For the condition of inspiration through the nose with expiration through the mouth, the results looked similar to those for mouth-only breathing, with disturbances seen immediately upstream of the head. However, for mouth-only breathing the disturbance appeared always to be greater than for nose-only breathing. Overall, the results show that, for the same breathing flowrate, the air was more highly disturbed when mannequin expiration took place through the mouth.

An important consideration with respect to nose versus mouth breathing relates to the possible effect on the performances of personal samplers mounted onto the body. It is a reasonable assumption that the observed differences – in the direction of the expired air jet for nose and mouth breathing, respectively – could potentially produce corresponding differences in sampler performance.

Effect of body temperature:

Figure 3.6 shows typical results for the effect of body temperature, obtained for the non-breathing mannequin for the same range of windspeeds already indicated. For the two higher windspeeds (0.24 and 0.42 m/s), there appears to be no noticeable influence of body heat on the air flow pattern. At the lowest windspeed (0.10 m/s), however, a comparison of the smoke patterns around the heated and unheated mannequin reveals an interesting phenomenon which needs discussion. We see here that the smoke patterns appear to be 'flattened' downwards (when compared to all the corresponding cases where the body was unheated). It is believed that what is seen here is associated with the plume of heated (and hence buoyant) air rising from the body and moving towards the top of the wind tunnel, where a slowly-recirculating eddy is formed above the mannequin. In other words, the appearance of the smoke pattern for this particular set of conditions is an experimental artifact arising from the relatively confined space occupied by the mannequin in the wind tunnel, and hence should not be interpreted as having any potential impact on the questions posed in this part of the research.

Effect of body orientation:

As mentioned previously, an ideal, complete assessment of the flow around the heated, breathing mannequin would require experiments at orientations other than forwards-facing. However, due to the complex flow around the mannequin body, including associated flow separation and turbulence, it was not possible to obtain video recordings of sufficient quality to be very useful. Therefore, the results described here are based on written observations based on visual observations made at the time of the experiments, and are tentative.

When the mannequin was placed at 90° angle to the freestream, it was noted that there was very little affect of breathing on the smoke patterns around the mannequin. Eddies were observed on the downstream side of the head as a result of separation of the air flowing over the mannequin and re-circulating in the near wake of the body. But these secondary air movements were those typical of a bluff body flow without aspiration, of the type widely studied and understood by aerodynamicists, and were clearly not the result of the breathing action of the mannequin. When the mannequin was placed at 180°, facing downstream, the smoke pattern in the breathing zone of the mannequin – which was now in the near wake of the bluff mannequin body – was seen to be highly disturbed due to the same eddy formation just described. But again, affects of breathing on the overall nature of the flow appeared to be small.

Effect of clothing and personal protective equipment:

From the flow visualizations that were carried out, it was generally the case that the presence of garments – including lab coat, safety glasses, hard hat – did not significantly impact the movement of smoke around the unheated mannequin. However, it is worth noting that, when the mannequin was heated, the presence of the lab coat and hard hat had a slight cooling effect such that the surface of the garments displayed a lower temperature than for the 'nude' mannequin body, as measured by a remote infrared thermometer. This suggests that, any effects of body heat would be even further reduced for a clothed human subject.

Conclusions

Breathing Parameter	Windspeed (m/s)		
	0.10	0.24	0.42
Mouth			
6 L/min	YES	NO	NO
20 L/min	YES	YES	NO
Nose			
6 L/min	NO	NO	NO
Nose-Mouth			
6 L/min	YES	NO	NO
20 L/min	YES	YES	NO

Table 3.2: Summary of results from all flow visualizations, indicating those conditions for which significant, persistent disturbances were noted (shaded area, 'YES') and where no such effects were observed ('NO').

Table 3.2 shows an integrated summary of the findings we have described, indicating the conditions for which the impact of expired air was substantial enough to noticeably and continuously destabilize the air upstream of the mannequin. For some sets of conditions, there was little or no affect of expiration during the subsequent inspiration part of the breathing cycle. But for other conditions, most notably for the highest breathing flowrate at the lowest windspeed, the influence of the expired air was clearly seen to persist into the subsequent inspiration phase. There was a strong dependence on whether expiration took place through the nose or mouth, with mouth breathing providing the greatest influence. The table, which was based on careful inspection of all the video recordings, summarizes the ranges of conditions pertaining to each of these two outcomes. Although not shown in the table, it is reiterated that dependencies on body temperature, orientation and clothing were weak.

Although this study was focused on the impact that *expiration* had on the *air* motion in the vicinity of the breathing mannequin in the wind tunnel, these results provide an interesting insight about the possible impact that the route of *inspiration* (i.e., nose versus mouth) might have on *aerosol* transport in the vicinity of the breathing orifice. For the conditions where significant affects were observed on the flow pattern persisting into the inspiration phase, it is reasonable to expect there to be significant influences on aerosol transport, and in turn on the aspiration efficiency of the human head and of personal samplers worn on the body in the breathing zone. Further discussion of such possibilities will be presented later in this Report.

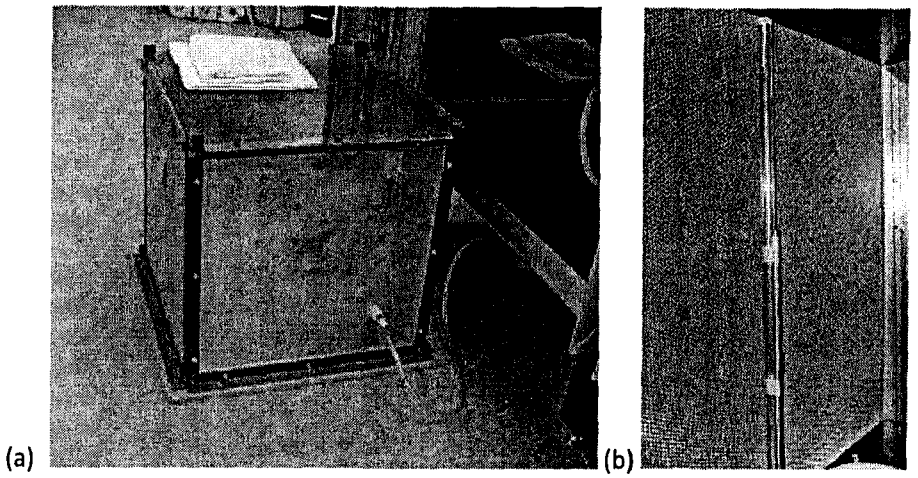

Figure 3.1: Smoke generating equipment for flow visualization studies, including (a) remote smoke chamber with flexible tubing connection and (b) rigid plastic tube for ultimate dispersal into wind tunnel working section.

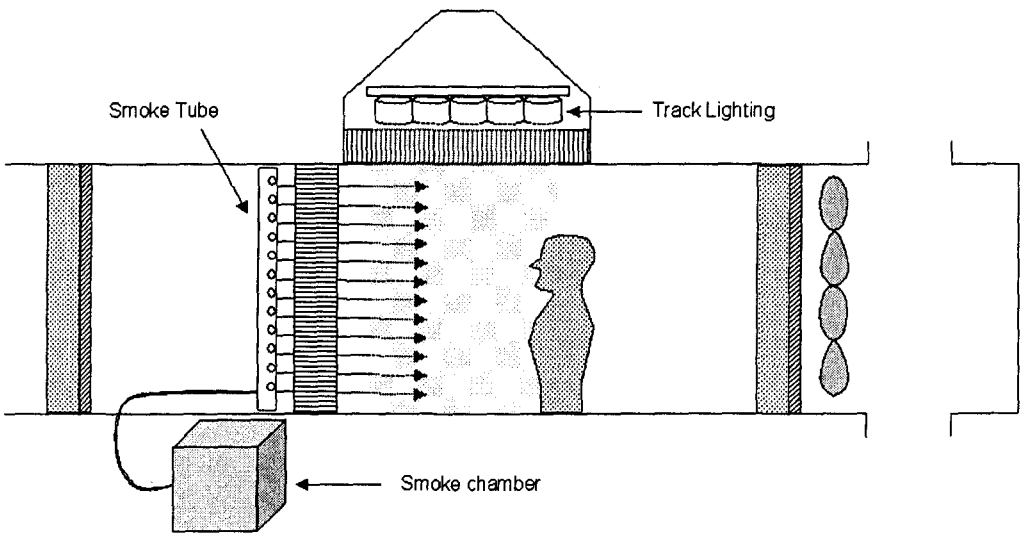

Figure 3.2: Wind tunnel set-up for smoke generation and flow visualization.

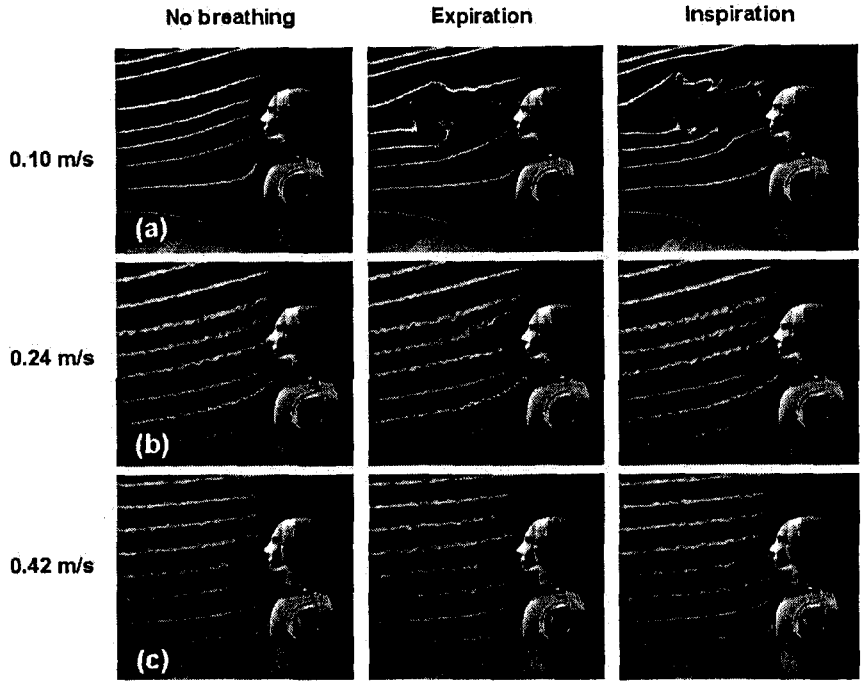

Figure 3.3: Still photographs extracted from flow visualization videos depicting the air disturbances in front of an unheated mannequin, breathing through the mouth only at 6 L/min, in windspeeds of (a) 0.10 m/s, (b) 0.24 m/s and (c) 0.42 m/s.

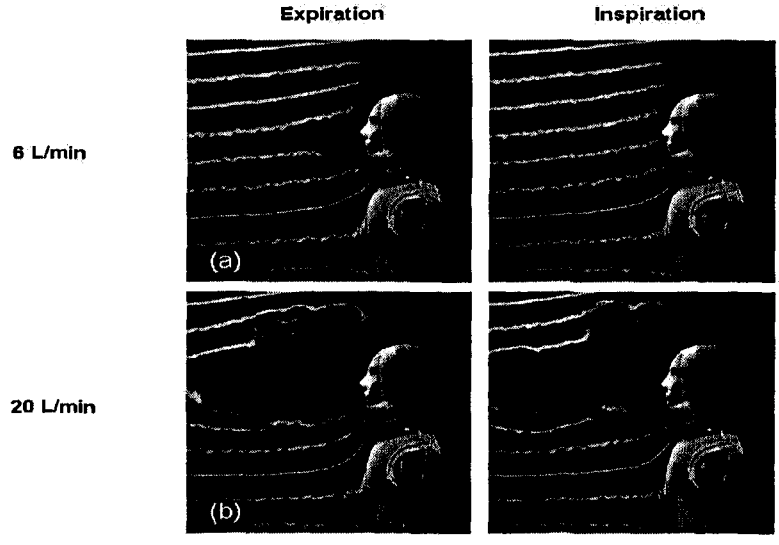

Figure 3.4: Still photographs extracted from flow visualization videos depicting the air disturbances in front of an unheated mannequin, breathing through the mouth only, at 0.24 m/s, for breathing flowrates of (a) 6 L/min and (b) 20 L/min.

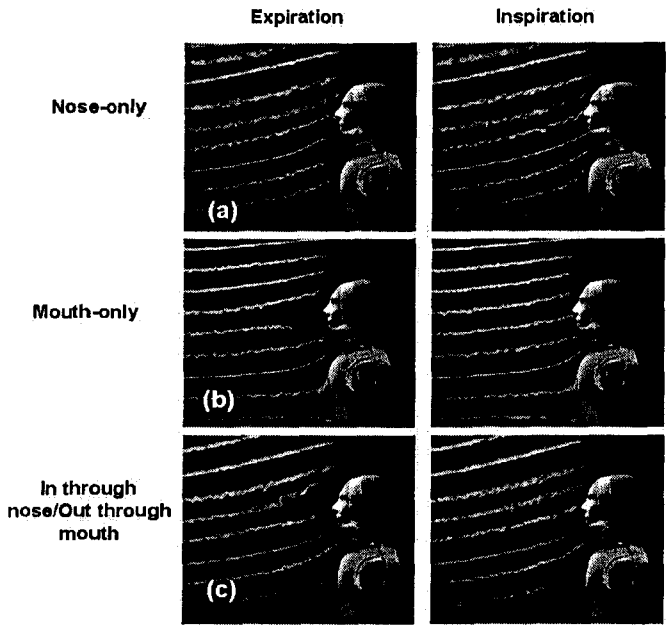

Figure 3.5: Still photographs extracted from flow visualization videos depicting the air disturbances in front of an unheated mannequin at 0.24 m/s windspeed, breathing at a flowrate of 6 L/min using (a) nose-only, (b) mouth-only and (c) nose-mouth breathing.

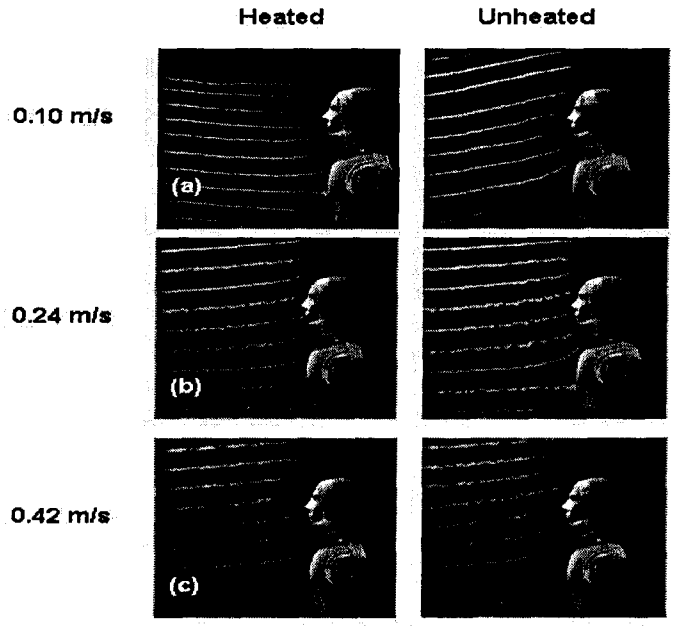

Figure 3.6: Still photographs extracted from flow visualization videos depicting the non-breathing mannequin, both heated and unheated, at external windspeeds of (a) 0.10 m/s, (b) 0.24 m/s and (c) 0.42 m/s.

4. Aspiration efficiency of the breathing mannequin

We now move on to describe the experiments that were carried out to assess inhalability at ultra-low windspeeds, using the inert mannequin to simulate an actual human subject. A new, large set of experimental data was obtained and examined with respect to the factors potentially influencing aspiration efficiency, including particle aerodynamic diameter, windspeed and the various mannequin breathing parameters. Discussion will include reference to the flow visualizations from the preceding section, and how that largely-qualitative work may provide additional insight into these quantitative measurements. Ultimately, this part of the research was aimed at providing a more complete understanding of human aspiration efficiency at the ultra-low windspeeds of interest in most occupational settings.

Experimental methods

The experimental methods for this part of the research involved measuring the aerosol concentration inhaled by a breathing mannequin and relating it to the aerosol concentration as measured by a reference sampler. The mannequin was located in the center of the wind tunnel working section, approximately 1.5 meters downstream of the forward mixing section. For all the experiments that are described, the mannequin was rotated slowly in order to simulate *no-preferred-orientation.*

The mannequin sample:

For each experiment, the 47-mm glass fiber filter that was to be placed inside the head of the mannequin was conditioned overnight in a desiccator to stabilize the mass – by reducing the moisture content – then weighed and inserted into the filter holder. The entire device was then snapped into place along the inhalation pathway inside the mannequin head. Tweezers were used to transfer the filters into and out of the holder and powder-free latex gloves were also worn to reduce contamination. The filters were analyzed gravimetrically using an electronic analytical balance (Model MC210S, Sartorius, Elk Grove, IL, U.S.A.) located in a room adjacent to where the wind tunnel was operating. After sampling, the entire filter holder was removed from inside the mannequin head for transport to the balance room, care during handling being taken to avoid any possible loss of sample from the filter. The conical cover piece of the filter holder was set aside for wipe sampling and the filter was removed and placed in a covered glass dish inside the desiccator, to be conditioned again and re-weighed the next day. Any particulate material that was deposited inside the conical piece – including on the O-ring – was collected using small cotton balls impregnated with isopropyl alcohol. These were similarly conditioned and weighed – when thoroughly dry – prior to and after sampling. The mass stability of the cotton balls was shown to be comparable to that for the glass fiber filters when similarly allowed to stabilize in a desiccator for at least 24 hours. Finally, particulate matter deposited inside the mannequin head, along the inhalation pathway between the entry (i.e., the nose or mouth opening) and the filter, was similarly recovered and weighed. Filter and cotton blanks were prepared each day, typically during the first experiment of that day. Since the filter holder inside the mannequin was the only one of its type, during the experiments the filter blank was put into a covered glass dish similar to that in which the loaded filters were placed in after sampling. The cotton blanks were also placed

into glass dishes after being dipped into the isopropyl alcohol in a similar manner as the cotton balls used for sampling. If any of the blanks were found to be questionable or unusable, another group was set-up for a later experiment. Ultimately, all reported values were blank-corrected; that is, the differences in the weight of the filter blank or cotton blank were subtracted from the corresponding loaded substrates.

The mass of particulate matter collected (i.e., inhaled) during sampling – including the portion recovered by the cotton balls afterwards – was obtained by taking the difference in the mass of the filter before and after sampling, and similarly for the cotton balls. The resultant filter (m_F) and wall (m_w) particulate masses were combined – minus the resultant masses on the filter blank (b_F) and cotton blank (b_c) – to provide the total inhaled aerosol mass. From the breathing flowrate (Q, the minute volume, expressed in [L/min]), and the sampling time (t), the corresponding total volume of inhaled air (V) was calculated from

$$V = Q \cdot t \tag{4.1}$$

The inhaled aerosol mass concentration (C_M) was then obtained directly using

$$C_M = \frac{(m_F - b_F) + (m_W - b_C)}{V} \tag{4.2}$$

The reference sample:

An additional important experimental consideration was to obtain an accurate measurement of the 'true' aerosol concentration in the wind tunnel, which would be used as a reference concentration for calculating inhalability. The best method for this was a cylindrical isokinetic sampler – defined earlier – for which the flowrate was chosen to provide an inlet air velocity that exactly matched the freestream air velocity. For relatively fast- moving air (i.e., $U > 0.5$ m/s), the isokinetic sampling concept is straightforward because convective inertial forces alone largely govern particle motion. That is, there is no deflection in particle trajectory associated with gravitational settling. However, for situations where the freestream air velocity is close to zero (i.e., $U < 0.05$ m/s), isokinetic sampling is inappropriate because particle motion is dominated by gravitational settling. Here, we need to consider how isokinetic sampling might apply to the intermediate (i.e., ultra-low) of interest in this work. Ultimately, it was reasoned that, despite the additional affect of gravity at low windspeeds to the extent that particles follow trajectories that are significantly influenced by gravitational settling, the concept of isokinetic sampling *could* still be applied. It was argued that the volume of air aspirated by the isokinetic sampler would experience some downwards loss of particles due to gravitational settling, but that loss would be simultaneously – and equally compensated for – by particles falling into the aspirated air from above. One anticipated result of this would be enhanced deposition of particles onto the inside walls of the reference sampler. So it was determined that, in practice, such wall losses should be subsequently analyzed along with the filter.

As required for isokinetic sampling, the device used here, shown in Figure 4.1, was a thin-walled cylindrical tube, with a plastic conical piece fit over the probe to minimize the effect of

the bluntness imposed by the filter holder. For the current situation, where the desired inlet velocity (U_S) would be equal to the windspeed (U), the appropriate flowrate (Q) for each individual windspeed scenario was calculated from

$$Q = \frac{\pi \delta^2 U_S}{4} \tag{4.3}$$

where the tube diameter δ = 0.01 m for the reference sampler that was used. Although a full assessment of the windspeed inside the wind tunnel had initially been performed for calibration purposes (as described earlier), windspeeds were measured again for these experiments to ensure an accurate calculation of the required flowrates. It was then determined that pump flowrates of 0.51, 1.03 and 1.65 L/min were required for the reference sampler at the corresponding nominal windspeeds of 0.10, 0.24 and 0.42 m/s, respectively.

For these relatively low required flowrates it was possible to use a personal sampling pump (Model XR5000, SKC Inc, Eighty Four, PA, U.S.A.) to create the desired inlet velocity for the isokinetic samplers. The reference sampler pump was calibrated using a primary flow meter (DryCal DC-Lite, Model 20k rev 1.06, BIOS International), both before each test and then again after sampling was completed. The average of these two values was used to determine the total volume of air sampled. If the change in flowrate throughout an experiment was greater than 5% – as per the manufacturer recommendations – then the sample was deemed unusable and the experiment was repeated. In addition, the pump was programmed with a delay so that before sampling began there was ample time to turn on the wind tunnel, the mannequin breathing machine and the aerosol generating systems. For the latter, approximately one minute was allowed for the aerosols to properly mix and disperse into the working section. By following the procedure described, it was ensured that the reference sampler was operating during exactly the same time period as the mannequin itself.

The reference sampler was placed in the reference plane approximately 0.75 meters upstream of the mannequin, a distance close enough to ensure similar aerosol exposure and yet far enough so that any mannequin breathing disturbances would not impact airflow at the reference sampler. Due to do the length of the probe and the expectation of internal wall deposits, alcohol-soaked cotton was used to recover any particles that deposited before reaching the filter. The cotton was handled in the same manner as that for the deposits in the mannequin head. That is, it was allowed to sit in the desiccator overnight before weighing, both prior to and after sampling. In order to get the most accurate estimate of the wind tunnel aerosol concentration at the mannequin itself, a correction factor (a) was applied to the concentration collected at the reference sampler based on the determination of the concentration ratio between the two planes, as discussed previously. The true reference sampler concentration (C_R) was calculated from

$$C_R = a \cdot \frac{(m_F - b_F) + (m_W - b_C)}{V} \tag{4.4}$$

where m_F refers to the mass collected on the reference sampler filter, b_F refers to the blank filter weight, m_w refers to the mass recovered from inside the reference sampler walls, b_c refers to the blank cotton weight and V is the volume of air sampled, calculated as before.

Mannequin aspiration efficiency:

From Equations (4.2) and (4.4), it was a simple matter to calculate the mannequin aspiration efficiency (A) from the ratio of the mannequin concentration (C_M) to the reference concentration (C_R), thus

$$A = \frac{C_M}{C_R} \tag{4.5}$$

The nature of the sampling environment and the range of aerosol particle sizes of interest required that slightly different experimental set-ups needed to be used for each combination of windspeed and powder grade. As discussed earlier, the relationship between the external windspeed and the particle settling velocity necessitated a different proportion of aerosols be injected in each mixing chamber to optimize the spatial uniformity of aerosol concentration and particle size distribution. Aerosols were thus introduced into the test section of the wind tunnel at a range of injection mass flowrates from both upstream and above (as described earlier in this Report).

Each sampling run lasted for 20 minutes and included the breathing mannequin, heated up to body temperature (33 °C) and dressed in a laboratory coat, and the reference sampler located 0.75 meters upstream of the mannequin. Each experiment included a combination of three different parameters: windspeed (0.10, 0.24 or 0.42 m/s), particle size (as given by the calculated MMAD for powder grade F1200, F800, F500, F400, F280 or F240, representing a particle size range from 9.3 μm up to 89.5 μm), and breathing pattern (6 L/min mouth, 20 L/min mouth, 6 L/min nose, 6 L/min nose-mouth or 20 L/min nose-mouth). Two or three tests were performed for each combination of conditions for a total of 183 experiments.

As mentioned earlier, a limited set of preliminary experiments was carried out prior to modification of the wind tunnel. The ranges of conditions at which those were performed included combinations of the three finest powder grades (F1200, F800 and F500) at the same three windspeeds (0.10, 0.24 and 0.42 m/s), essentially representing 9 particle sizes from about 7 μm up to about 28 μm. For these tests, the mannequin was always breathing through the mouth at 20 L/min. Additional tests were performed for powder grade F500 (representing *MMAD* of 13.9, 18.6 and 27.9, depending on the windspeed) with the mannequin breathing through the mouth at 6 L/min at all three windspeeds, and also for powder grade F240 (*MMAD* = 89.5 μm) with breathing through the mouth at 20 L/min at 0.10 m/s windspeed only. In those early tests, all test aerosols were injected upstream for the three smaller aerosol particle sizes and were injected only from above for the largest aerosol particle sizes. Otherwise, the procedure was the same as for the later full set of experiments. These preliminary tests represented 26 experiments and are included here for completeness. So a total of 209 experiments were performed.

The statistical analyses that are described below were performed using SAS 9.1 (SAS Institute, Cary, NC, U.S.A.) and Sigma Plot 2000 (SPSS, Inc., Chicago, IL, U.S.A.).

Pre-modification versus post-modification experiments

Before a full analysis of the full body of data could be undertaken, it was essential to compare the results obtained before and after the wind tunnel was modified. To reiterate, the discovery of losses of particles by elutriation of larger particles in the honeycomb at the entrance to the working section of the wind tunnel required a modification in order to enable testing over the full set of conditions of interest, specifically by replacing the honeycomb with a pair of perforate-plate screens. Prior to the modification, preliminary experiments had been carried out to determine the aspiration efficiency of the mannequin for a subset of the desired conditions listed above. It was important to know how inhalability measurements taken before and after modification compared, hopefully to confirm the validity of proceeding with the modified system. It is noted that the flow visualizations discussed in the previous section of this Report were performed prior to modification and so any utilization of those results as they relate to inhalability required that the main features of the airflow not be substantially different after modification. Comparison of the pre- and post-modification results would therefore provide an important bridge between earlier studies and the main body of aerosol studies that followed.

Table 4.1 shows the mean aspiration efficiency results from both before and after the wind tunnel modification, indicating the similar experimental conditions used.

Powder Grade	Breathing Pattern	Windspeed (m/s)	A_{pre}	A_{post}
F1200	20 L/min Mouth	0.10	0.71	1.03
		0.24	0.84	0.85
		0.42	0.66	0.57
F800	20 L/min Mouth	0.10	0.82	0.77
		0.24	0.72	0.58
		0.42	0.72	0.57
F500	6 L/min Mouth	0.10	1.21	0.85
		0.24	0.98	0.73
		0.42	0.87	0.71
F500	20 L/min Mouth	0.10	0.92	0.79
		0.24	0.87	0.76
		0.42	0.58	0.62
F240	20 L/min Mouth	0.10	0.58	0.76

Table 4.1: Mean aspiration efficiency measurements obtained before (A_{pre}) and after (A_{post}) wind tunnel modification at the same experimental conditions.

Figure 4.2 shows graphically the comparison between the pre-modification results with the post-modification results, containing experimentally-obtained values for aspiration efficiency for conditions where there are data from experiments with both experimental configurations. The

solid line represents an idealized relationship with perfect agreement (slope = 1) and the dashed line represents the actual relationship (slope = 0.88). In general, it is seen that the pre-modification aspiration efficiency values tend to be somewhat larger than the post-modification ones. One explanation is that the elutriation of larger particles into the honeycomb structure shifted the particle size distribution in the working section towards smaller MMAD-values, leading to somewhat higher values for aspiration efficiency. However, the paired t-test that was carried out to assess the magnitude of this observed difference revealed no statistically-significant difference between the two sets of data (*p-value* = 0.214). Thus support was provided for the inclusion of the pre-modification data in the overall analyses.

Results

The research that is now described represents an important set of experiments that, we believe, will bridge the gap between the previous aspiration efficiency studies conducted at high windspeeds in traditional wind tunnels and those performed at essentially zero windspeed in calm air aerosol chambers. The data are displayed graphically in Figure 4.3, where aspiration efficiency (A) is plotted as a function of particle aerodynamic diameter (d_{ae}). The entire set of raw data is shown, including experimental results obtained before the wind tunnel was modified. This figure provides a picture of the overall spread of the data, but – obviously -- cannot reveal differences associated with the individual variables for the various sets of experimental conditions. Figures 4.4 through 4.8 present graphical depictions of the same data. Each point on the graphs represents the average of all repeat experiments performed under the same conditions, with error bars in the vertical axis showing one standard deviation (*SD*). For each set of unique experimental conditions, straight lines were drawn between adjacent points to better delineate between the data points for each windspeed.

A 3-way analysis of variance (ANOVA) was carried out that examined the mannequin's aspiration efficiency as a function of particle size, windspeed and breathing pattern. The overall interaction model was highly significant (*p-value* < 0.0001), indicating that those three factors explaining 58% of the variability. Each individual variable was also found to be significant (*p-value* <0.0001, 0.0037, and 0.0178, respectively). We now provide an examination of each of these parameters as directly tested in these experiments. The subsequent discussion sets about to understand how the same parameters, when combined into relevant dimensionless groups, reflect the roles of the physical processes relevant to human inhalability at ultra-low windspeeds, leading in turn to a new semi-empirical model.

Particle aerodynamic diameter:

As mentioned earlier in this Report (see Tables 2.9 and 2.10), the particle size distribution for the test aerosols is represented by the mass medium particle aerodynamic diameter (*MMAD*) and the geometric standard deviation (σ_g). Including the pre-modification data, the size range of the particles tested in these experiments ranged from 6.8 to 89.5 μm, covering a significant portion of the inhalable aerosol size fraction. For each set of 'parent' test powder and conditions, the values indicated were measured directly. Most indicated a slight shift upward from the nominal values as determined by Mark *et al.* (1985). The fact that each combination

of powder grade and windspeed constituted a different *MMAD* and σ_g meant that effectively, 9 different particle sizes were tested before modification and 18 after modification.

Figure 4.9 shows the mean aspiration efficiency as a function of particle aerodynamic diameter, averaged across all tests performed at each particle size. Here the horizontal error bars represent the 16th (d_{16}) and 84th (d_{84}) percentiles given by

$$d_{16} = \frac{d_{50}}{\sigma_g} \tag{4.6}$$

$$d_{84} = d_{50} \cdot \sigma_g \tag{4.7}$$

where d_{50} represents the mass median aerodynamic diameter (*MMAD*) and σ_g represents the geometric standard deviation. It is noted that there will be additional systematic trends or biases within these data, relating to changes in other experimental conditions, such as windspeed or breathing pattern. Therefore, statistical error estimates for the mean aspiration efficiency on the vertical axis are not strictly appropriate. The effect of these other variables will be discussed in further detail below.

For the entire set of data presented here, ANOVA showed that particle size was highly significant (*p-value* < 0.0001), with the values for aspiration efficiency generally decreasing with increasing particle size. It is interesting to observe that the general broad trend for aspiration efficiency as a function of particle size also appeared to agree with the currently-accepted inhalability criterion, as can be observed in Figure 4.9, approaching unity for the smallest particles and decreasing with increasing particle size, leveling off at about $A = 0.50$ for the largest particle sizes.

Windspeed:

Attention is now turned to the effect of windspeed on mannequin aspiration efficiency. Figure 4.10 shows the complete set of data, again represented by the mean aspiration efficiency (A) at each particle aerodynamic diameter (d_{ae}), but now separated out by windspeed. All breathing flowrates and modes of breathing are embodied within these means. For an indication of the variability, Figure 4.11 shows the results for A as a function of d_{ae} at 0.10, 0.24 and 0.42 m/s, respectively, with data separated into the five sets of mannequin breathing conditions (e.g., 6 L/min for mouth breathing, etc) and error bars in the vertical axis reflecting one standard deviation.

The results show that inhalability at lower windspeeds, irrespective of the mannequin's breathing pattern, was consistently greater than at higher windspeeds. The ANOVA results for windspeed confirm that aspiration efficiency was significantly greater at 0.10 m/s than for 0.24 m/s and 0.42 m/s, and was also significantly greater at 0.24 m/s than at 0.42 m/s (all *p-values* < 0.0001). On first inspection of Figure 4.11, it also appears that the mean aspiration efficiency values for 0.10 m/s lie somewhat above the curve for the current convention. For 0.24 m/s the results lie close to the curve, and for 0.42 m/s the results tend to lie below it.

Referring back to Figures 4.3 to 4.7, it is also useful to look more closely at the effect of windspeed within each breathing pattern separately, especially since – as reflected in the equations presented earlier for aspiration efficiency – the relationship between windspeed and mean inlet velocity is expected to be influential. Here it was found that the only condition for which windspeed was *not* a significant factor was for 6 L/min nose-mouth breathing (*p-value* = 0.1280). For all other breathing conditions, aspiration efficiency was significantly different based on windspeed (for a significance level of $\alpha = 0.05$), with the lowest windspeed always associated with the highest inhalability.

Breathing parameters:

Breathing parameters are reflected in both the breathing flowrate *and* mode of breathing. First, however, we examine the combinations of these, including mouth breathing at 6 L/min and 20 L/min, nose breathing at 6 L/min and nose-mouth breathing at 6 L/min and 20 L/min. The ANOVA showed that aspiration efficiency was significantly different based on the breathing pattern of the mannequin across all windspeeds (*p-value* = 0.0034). However, looking at each windspeed separately (see Figure 4.11), there were no significant differences for aspiration efficiency based on the mannequin breathing pattern at windspeeds 0.10 m/s and 0.24 m/s (*p-values* = 0.0866 and 0.6786, respectively). However, differences *were* significant for 0.42 m/s (*p-value* = 0.0217).

Next, the individual impacts of breathing flowrate and mode of breathing were analyzed separately. A 2-way ANOVA was performed to look at these effects, as well as their interaction, which showed that while flowrate was not significant (*p-value* = 0.1214), mode of breathing (*p-value* = 0.0320) and the interaction between the two parameters (*p-value* = 0.0263) *were* significant factors for determining aspiration efficiency.

	Mouth - 20	Nose - 6	Nose/Mouth - 6	Nose/Mouth - 20
Mouth - 6	0.0767	0.1703	0.0154[a]	0.0105[a]
Mouth - 20		0.5271	0.8897	0.1038
Nose - 6			0.5022	0.0369[a]
Nose/Mouth - 6				0.1727

[a] Statistically significant difference at $\alpha = 0.05$

Table 4.2: Results from t-tests comparing all breathing patterns to one another, as expressed by the p-value.

In order to more fully understand the effect of each breathing parameter individually (i.e., breathing flowrate, inlet orifice and outlet orifice), t-test comparisons between each breathing pattern were carried out, the results of which are shown in Table 4.2. It was shown that the results for mouth breathing at 6 L/min was not significantly different from those for mouth breathing at 20 L/min; also that the results for nose-mouth breathing at 6 L/min were not significantly different from those for nose-mouth breathing at 20 L/min. This finding supports the view that breathing flowrate by itself was not an important factor for determining inhalability.

Looking next at the breathing mode, a direct comparison of mouth-only to nose-only breathing suggested that, for the same breathing flowrate, in this case, 6 L/min – breathing mode was not an important factor for determining inhalability (*p-value* = 0.1703). This contrasts with the ANOVA results discussed previously, which had indicated that mode of breathing was significant across all experiments. In order to understand this further, it is therefore instructive to examine the relative importance of the separate inhalation and exhalation orifices as they relate to inhalability. This is possible here because different orifices for inhalation and exhalation were used for some tests. With this in mind, it is interesting to note that the results for mouth breathing at 6 L/min were significantly different from those for nose-mouth breathing at 6 L/min. However, the same was not true for 20 L/min mouth breathing, where the results were not significantly different from those for nose-mouth breathing at the same flowrate. On the one hand, that leaves it ambiguous as to the influence of the orifice of inhalation (i.e., inhaling through the mouth versus inhaling through the nose) on inhalability. On the other hand, it was shown previously that the interaction of flowrate and mode of breathing was significant. Therefore, it is not surprising that different flowrates might show different levels of importance for the orifice of inhalation as it relates to aspiration efficiency. In contrast, with respect to the orifice of exhalation, for the same breathing flowrate of 6 L/min, the results for nose breathing were found not to be significantly different from those for nose-mouth breathing. That suggests that the orifice of exhalation was not an important factor for determining inhalability. In fact, across all experiments, the inlet orifice was shown to be statistically significant (*p-value* = 0.0191), with mouth breathing consistently being associated with higher inhalability. At the same time, the orifice of exhalation was not significant (*p-value* = 0.9857). Finally, it is also interesting to note that the most significant difference was between the results for mouth breathing at 6 L/min and those for nose-mouth breathing at 20 L/min, again suggesting that the combination of differences in breathing flowrate and inhalation orifice was the most important factor determining inhalability.

Discussion

We now move on to a discussion of human aspiration efficiency at ultra-low windspeeds in the light of what is known about the physical principles that govern the sampling – including human aspiration – of aerosols. The mechanics of aerosol sampling, and in turn the aspiration efficiency of a blunt sampler (of which the human head is one example), are governed by a number of different variables, including: sampler size (width of sampler body), *D; s*hape of sampler, *B; o*rifice dimension (diameter of sampling orifice), δ; *w*indspeed, *U*; inlet velocity, U_S; *o*rientation, Θ; and *p*article size (aerodynamic diameter), d_{ae}. From the principles of aerosol mechanics, we may deduce that the aspiration efficiency of aerosols for single-orifice sampling systems in moving air may be expressed in the general functional form (Vincent, 2007)

$$A = f\{St, R, r, B, \Theta\} \tag{4.8}$$

where inertial forces are represented by the Stokes number (*St*), defined as

$$St = \frac{(d_{ae}{}^2)\gamma U}{18\eta\delta} \tag{4.9}$$

where γ is the density of water (1000 kg/m^3) and η is the viscosity or air (1.78 x 10^{-5} kg/m·s). In addition, R is the ratio of the windspeed (U) to the inlet velocity (U_S)

$$R = \frac{U}{U_S} \tag{4.10}$$

and r is the ratio of the sampler orifice diameter (δ) to the sampler width (D) given by

$$r = \frac{\delta}{D} \tag{4.11}$$

while B is quantity that represents the aerodynamic bluntness of the sampler and Θ is the orientation of the sampler with respect to the wind.

A similar expression exists for calm air, thus

$$A = f(St_c, R_c, r, \theta, B) \tag{4.12}$$

which is analogous to the expression given earlier for moving air. Here, however, we have the modified Stokes' number (St_c) and velocity ratio (R_c), along with the dimension ratio (r), along with orientation (θ, this time with respect to the upwards vertical) and sampler body shape (as represented by bluntness, B). The two new terms, St_c and R_c, are given by

$$St_c = \frac{d_{ae}\gamma^* v_s}{18\eta\delta} \tag{4.13}$$

$$R_c = \frac{v_s}{U_s} \tag{4.14}$$

while the other terms are the same as before for the moving air case. Equation (4.12) embodies the fact that, for calm air sampling, it is the action of gravity, expressed in terms of the particle settling velocity, v_s, that brings the particles into the vicinity of the sampler inlet, in contrast to the moving air case (where this was achieved by virtue of convection), and hence is dependent on U.

For the intermediate case where the windspeed is not zero but is low enough that the trajectories of particles are significantly influenced by gravitational settling, a further modified expression is appropriate, thus

$$A = f\{St, R, r, B, \Theta, Fr\} \tag{4.15}$$

where we have introduced a new parameter, the Froude number (Fr) given by

$$Fr = \frac{U^2}{gD} \tag{4.16}$$

This reflects the ratio between the inertial and gravitational forces. Written in this way, instead of the more cumbersome one that simply merges Equations (4.8) and 4.12), we avoid unnecessary redundancy. Equation (4.16) provides a useful working relationship that may be used in the development of a semi-empirical model.

Stokes number at ultra-low windspeeds:

We first examine the aspiration efficiency (A) of the human head with respect to Stokes number (St), one of the predominant governing parameters, for each set of experimental conditions. Table 4.3 lists the relevant Stokes numbers, based on windspeed, particle size, and sampler orifice diameter as defined in Chapter 5, with the mouth and nose having different sampler dimensions of 0.003 meters and 0.012 meters, respectively. Figure 4.12 then displays the entire set of raw data for aspiration efficiency (A) as a function of Stokes number (St). What quickly emerges is the impact that the different pathways of inhalation (i.e., nose versus mouth) have on the value of Stokes number. In the facility used for this research, the mannequin nose measured 4 times as wide as the mouth, resulting in lower Stokes numbers for nose breathing.

	Windspeed (m/s)								
Powder Grade	**0.10**			**0.24**			**0.42**		
	d_{ae}	*St*		d_{ae}	*St*		d_{ae}	*St*	
		Mouth	*Nose*		*Mouth*	*Nose*		*Mouth*	*Nose*
F1200	9.6	0.010	0.002	9.5	0.023	0.006	9.3	0.038	0.009
F800	13.9	0.020	0.005	12.8	0.041	0.010	12.4	0.067	0.017
F500	28.8	0.086	0.022	32.7	0.267	0.067	28.7	0.360	0.090
F400	37.7	0.148	0.037	44.3	0.490	0.123	40.0	0.699	0.175
F280	74.0	0.570	0.142	62.4	0.972	0.243	66.9	1.956	0.489
F240	89.5	0.833	0.208	60.1	0.902	0.225	63.0	1.734	0.434

Table 4.3: Stokes numbers (St) calculated for each set of experimental conditions tested.

As defined, Stokes number increases with increasing windspeed (U), increasing particle size (d_{ae}), and decreasing orifice diameter (δ). For most practical sampling scenarios, it has been observed that A decreases with St. Based on these tendencies, it is therefore expected that A should decrease with an increase in windspeed, increase in particle size, and decrease in the orifice diameter. More specifically, A decreased as U increased within the ultra-low speed range, A decreased as d_{ae} increased from about 7 up to about 90 μm, and A was generally greater for inspiration through the larger-dimension mouth than for the smaller-dimension nose. Therefore it is not surprising that, as is clearly evident in Figure 4.12, the same

relationship between aspiration efficiency and Stokes number was also observed in the present study at ultra-low windspeeds, with a downward trend in A as St increased. This was also confirmed by ANOVA, which found a significant difference in mannequin aspiration efficiency based on Stokes number ($p\text{-}value < 0.0001$).

Inlet velocity and its relation to windspeed:

The second parameter of interest, R, represents the ratio of the windspeed (U) to the mean inlet velocity (U_S). The different breathing flowrates used in these experiments were obtained by changing both the tidal volume and the breathing frequency, but the actual inlet velocity was also different depending on the dimension (width) of the sampling orifice (δ). The inlet velocities for each breathing condition, the ones shown in Table 4.4, were calculated from

$$U_S = \frac{4Q}{\pi\delta^2} \tag{4.17}$$

where $\delta = 0.003$ m for oral inhalation and $\delta = 0.012$ m for nasal inhalation.

ANOVA showed that there was a significant dependence of A on R ($p\text{-}value < 0.0001$). In particular, increases in A were associated with decreases in R. So again, as for St, the relationship with R, and hence with the ratio between breathing parameters and external windspeed, was clearly a significant factor in determining inhalability.

Breathing orifice	***Q (L/min)***	***U_S* (m/s)**	***R***		
			0.10 m/s	*0.24 m/s*	*0.42 m/s*
Nose	6	0.88	0.114	0.273	0.477
	20	2.95	0.034	0.814	0.142
Mouth	6	14.15	0.007	0.017	0.030
	20	47.16	0.002	0.005	0.009

Table 4.4: Mannequin inlet velocity (U_S) and R-values for each experimental condition tested.

Inspection of the data as they are displayed in the graphs, it is notable that aspiration efficiency exceeded unity for several conditions. However, this discussion of the importance of the velocity ratio, R, may help explain that result. First, all of the results where $A > 1$ were obtained at the lowest windspeed and the lower breathing rate – one for particle size 28.8 μm during 6 L/min mouth breathing and the other three for particle size 9.6 μm at 6 L/min mouth breathing, 6 L/min nose breathing and 6 L/min nose-mouth breathing. In an ideal situation, assuming no external air effects (i.e., no net loss or gain of particles from the air stream that enters the breathing orifice), the aerosol concentration inhaled by the human head would not be expected to be higher than the ambient air concentration. In reality however, the inlet velocity of the human nose and/or mouth will typically be much greater than the external windspeed (see Table 4.4). That creates the potential for over-sampling with respect to the

measured ambient air concentration. In addition, as previously discussed, when the windspeed decreased relative to a constant mean inlet velocity, aspiration efficiency increased. Therefore it is not at all surprising that all of the instances where aspiration efficiency was greater than unity were at the lowest windspeed.

Mannequin dimensions and orientation:

Other parameters in Equation (4.15) relate to the size and shape of the mannequin in its capacity as a sampler, specifically its dimensions and orientation. The first of these, r, was the ratio of the sampler orifice diameter (δ) to the sampler width (D). For these purposes, the sampler width was given by the size of the mannequin head, with $D = 0.2$ m, making it essentially a constant for all experiments. In that way, analysis of the role of the r-parameter was simply an assessment of the impact of the orifice diameter. As previously discussed, the orifice diameter was already determined to be a significant factor for determining aspiration efficiency – in this case, for the inspiration orifice but not the expiration orifice – and with mouth breathing having a greater impact relative to nose breathing. In addition, it will be remembered that the Stokes number accounted for the influence of orifice dimension on aspiration efficiency in its calculation. Therefore, the r-parameter may be disregarded for these purposes. The next parameter that could influence measurements of aspiration efficiency was sampler shape (B). But since the effective sampler shape was the same for all experiments performed here, this parameter too may be ignored in the present discussion. Finally, the orientation parameter (Θ), representing the mannequin orientation with respect to the wind, was also eliminated from our discussion by the fact that the mannequin was continuously rotated so that there was no preferred orientation of sampling with respect to the wind.

Froude number at ultra-low windspeeds:

The final parameter that will be discussed is the Froude number (Fr). As noted previously, the sampler width was essentially constant, and so for the three windspeeds used here (0.10, 0.24 and 0.42 m/s) the Froude number was calculated to be 0.005, 0.029 and 0.090, respectively. This implies that increasing the windspeed from 0.10 m/s to 0.42 m/s would increase the influence of gravity on aspiration efficiency by a factor of about 18. The true usefulness of the Froude number lies in its relationship to Stokes number. Where Fr is smaller than St, the influence of gravity should not be ignored. Looking at the St-values in Table 4.3, it can be seen that the Fr-values cited above were close to or smaller than St for most of the conditions studied. As expected, therefore, ANOVA results indicated that Fr was associated with significant differences in mannequin aspiration efficiency, with greater aspiration efficiency being associated with lower Fr-values. In general, it is clear that, as expected, gravity was highly influential in aerosol transport at the ultra-low windspeeds pertaining to our experiments.

Empirical model for aspiration efficiency at ultra-low windspeeds:

We now proceed towards bringing together the results from this part of the research to provide a cohesive picture of human aspiration efficiency at ultra-low windspeeds. This

involves incorporating the data that have been obtained with the functional framework that has been proposed in the form of Equation (4.15). In the first instance, this expression may be simplified by reference to the fact that – as already discussed above – the parameters namely r, B, and, Θ are inconsequential as far as our experiments are concerned and so may be ignored. In this way, we are left with

$$A = f\{St, R, Fr\} \tag{4.18}$$

It is now a question of what actual mathematical combination of the parameters identified in this expression is appropriate. Discussion begins from the position that there is *no* known physical model that may be derived from first principles to describe the aspiration process for the system of interest. So we must seek a relationship that is empirical, albeit – through Equation (4.18) – rooted in physical ideas. There are many options, but it was decided to opt for the arbitrary simple combination

$$A = a(St^b \cdot R^c \cdot Fr^d) \tag{4.19}$$

where the coefficients a, b, c and d would be sought by non-linear regression. By this approach a good fit with the experimental data was achieved using

$$A = 0.362(St \cdot R \cdot Fr)^{-0.062} \tag{4.20}$$

Here, $r^2_{adj} = 0.30$ and the model, including each individual coefficient, was significant (all *p-values* < 0.0001).

Figure 4.13 shows the relationship between this newly-developed model and the experimental data. It is seen that agreement between the model and the actual experimental data is quite good. It should be noted, however, that the usefulness of such a model is limited and should not be generalized beyond the present context.

Relation of flow visualization results to inhalability measurements:

In the previous section of this Report, flow visualization studies were described for the heated, breathing mannequin at ultra-low windspeeds. It was determined that the very lowest windspeeds, coupled with high breathing flowrates and expiration through the mouth, were associated with significant and persistent flow disturbances in the freestream approaching the mannequin. In the context of the experiments described here, it is to be expected that such disturbances might have a significant effect on the transport of aerosols during inhalation.

There does indeed appear to be a correlation between the conditions for such flow disturbances and an apparent systematic shift in aspiration efficiency of the human head. Notably, although the new results for the highest windspeeds and lowest breathing flowrates were broadly consistent with what has already been reported many times in previous research with mannequins in moving air (and which underpin the current inhalability convention), we now see a distinct shift towards higher aspiration efficiency at the lowest windspeeds. However, the effect of breathing flowrate – where, on the basis of the flow visualizations, we

might have expected to see a similar shift in aspiration efficiency for mouth breathing at the highest breathing flowrates – was less clear.

Conclusions

From an examination of the complete set of mannequin aspiration efficiency data obtained in these experiments, the most important conclusion that can be drawn is that inhalability is influenced by windspeed. Specifically, the lowest-windspeed environments were found to be clearly associated with a shift towards higher values for inhalability. These observations were confirmed in the statistical analyses and were supported – at least in part – by our interpretation of the flow visualization studies described earlier. As expected, based on the many previous studies, dependence on particle aerodynamic diameter was also found to be highly significant, with aspiration efficiency decreasing for increases in aerosol particle size. So too were the effects of the combination of breathing flowrate and orifice of inspiration.

The combination of the influential variables into dimensionless groups and the development of an empirical relationship between these and aspiration efficiency were instructive, especially in the way in which the role of gravitational settling could be incorporated into explaining the results.

Taken as a whole, the results of these new experiments provide an important contribution to the understanding of aerosol inhalability for relevant workplace environments – that is, at the ultra-low windspeeds which we now know pertain to most workplaces. In turn they will provide a new basis for thinking about the inhalability convention which is applied in aerosol exposure standards.

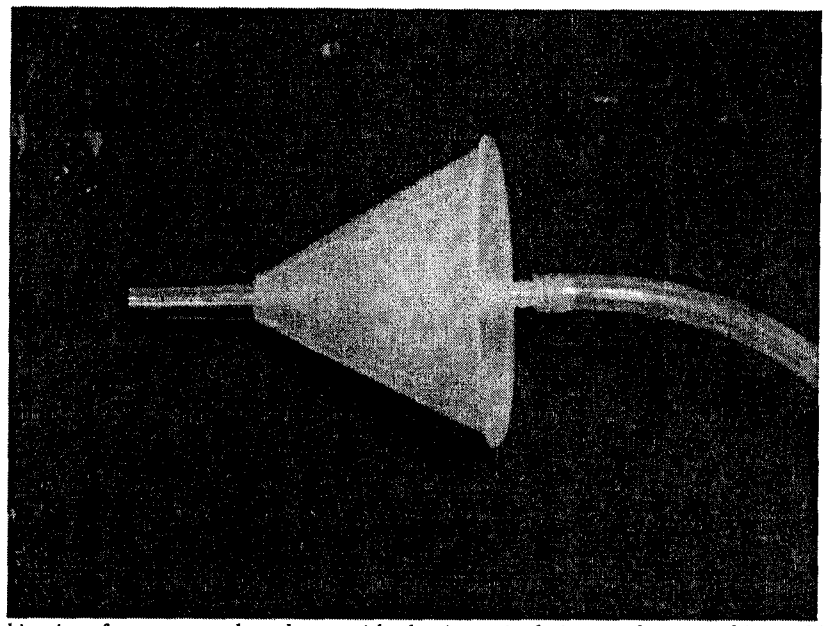

Figure 4.1: Isokinetic reference sampler, shown with plastic conical piece and pump tubing, which was used to measure the actual aerosol concentration inside the wind tunnel.

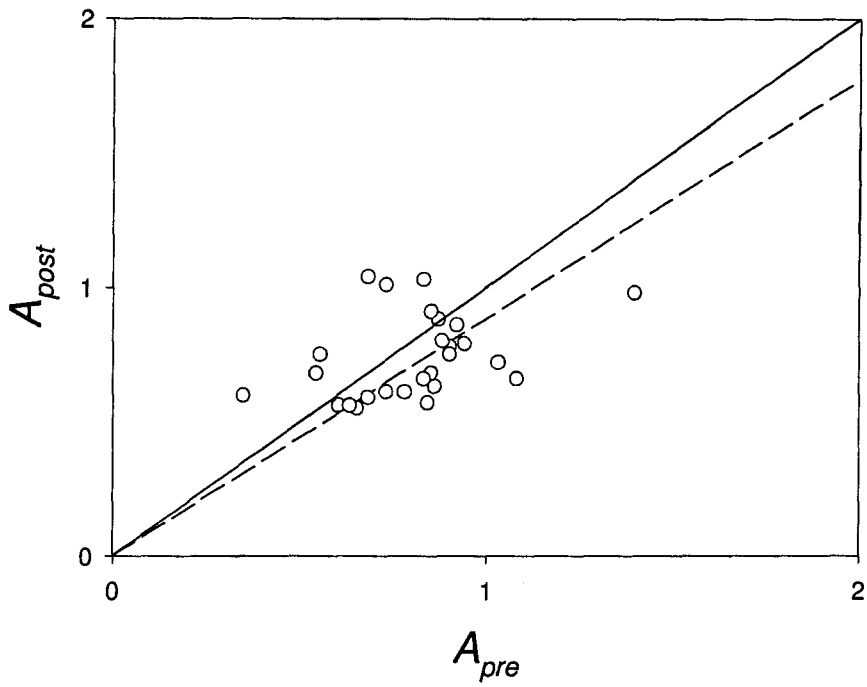

Figure 4.2: Comparison of aspiration efficiency measurements before (A_{pre}) and after (A_{post}) wind tunnel modification. The solid line represents an ideal relationship and the dashed line represents the actual relationship (slope = 0.88).

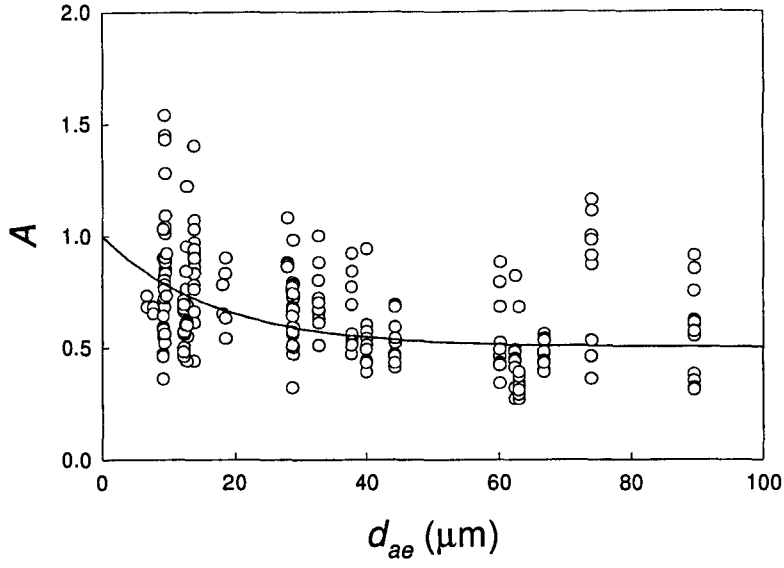

Figure 4.3: All data for mannequin aspiration efficiency (A) as a function of particle aerodynamic diameter (d_{ae}). The current inhalability convention (solid line) is shown for comparison.

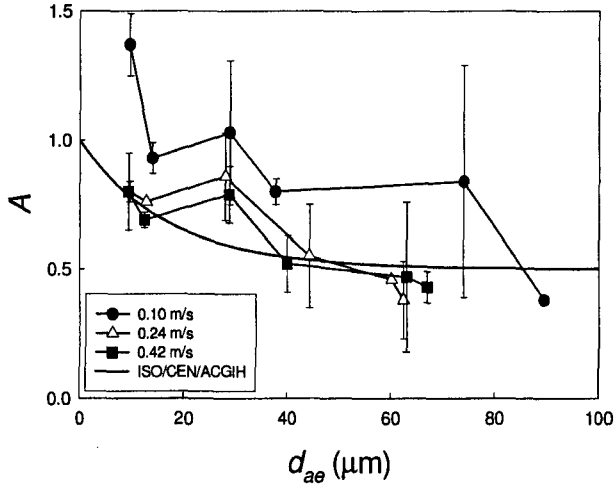

Figure 4.4: Mannequin aspiration efficiency (A) as a function of particle aerodynamic diameter (d_{ae}) for 6 L/min mouth breathing, at each windspeed separately, shown with the current inhalability convention. Error bars represent one standard deviation.

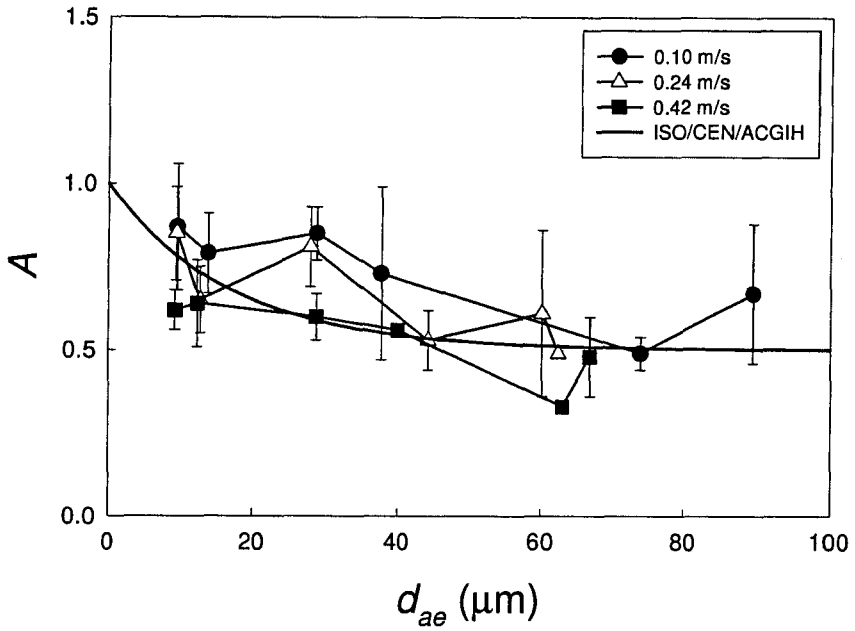

Figure 4.5: Mannequin aspiration efficiency (A) as a function of particle aerodynamic diameter (d_{ae}) for 20 L/min mouth breathing, at each windspeed separately, shown with the current inhalability convention. Error bars represent one standard deviation.

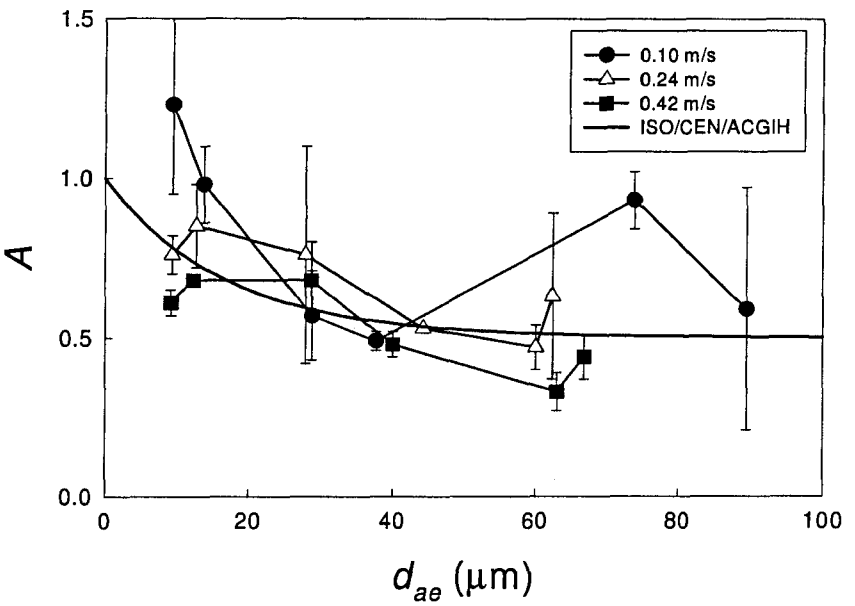

Figure 4.6: Mannequin aspiration efficiency (A) as a function of particle aerodynamic diameter (d_{ae}) for 6 L/min nose breathing, at each windspeed separately, shown with the current inhalability convention. Error bars represent one standard deviation.

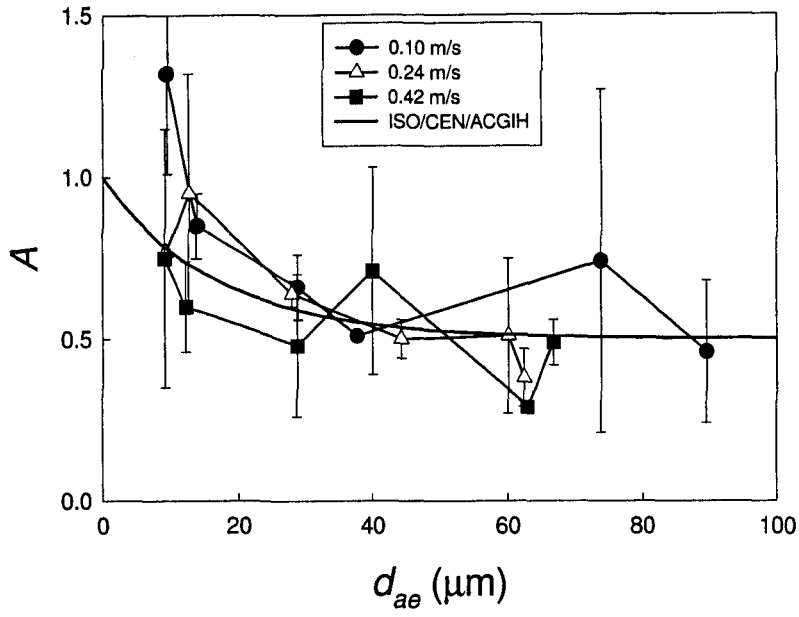

Figure 4.7: Mannequin aspiration efficiency (A) as a function of particle aerodynamic diameter (d_{ae}) for 6 L/min nose-mouth breathing, at each windspeed separately, shown with the current inhalability convention. Error bars represent one standard deviation.

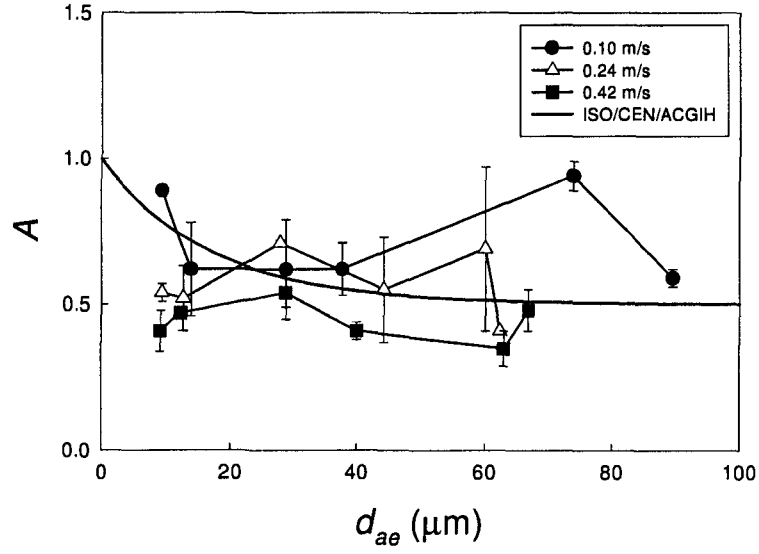

Figure 4.8: Mannequin aspiration efficiency (A) as a function of particle aerodynamic diameter (d_{ae}) for 20 L/min nose-mouth breathing, at each windspeed separately, shown with the current inhalability convention. Error bars represent one standard deviation.

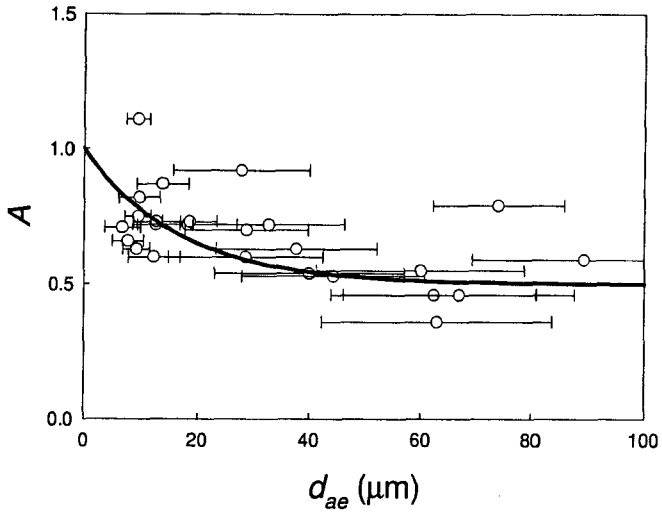

Figure 4.9: Aspiration efficiency (A) as a function of particle aerodynamic diameter (d_{ae}) for each particle size tested. Horizontal error bars represent the 16th and 84th percentiles calculated from the geometric standard deviation. The current inhalability convention is shown for comparison.

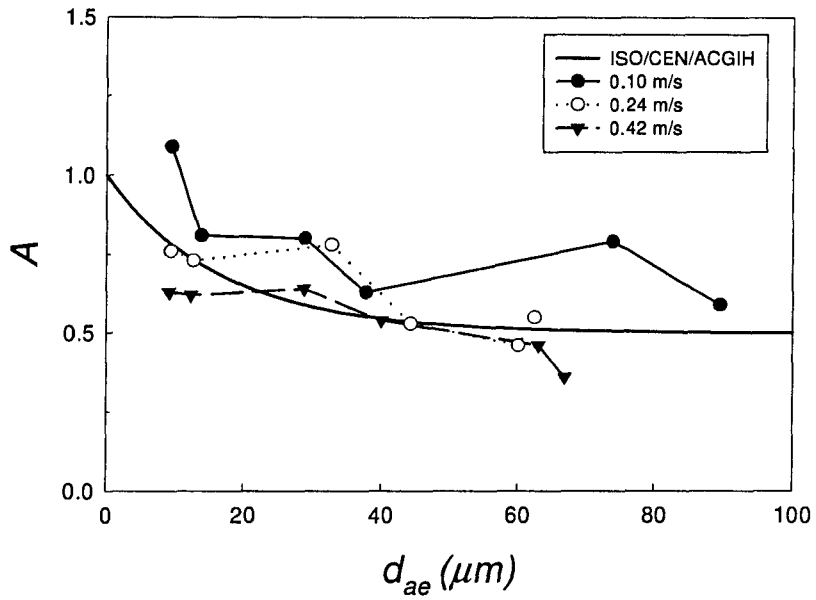

Figure 4.10: Aspiration efficiency (A) as a function of particle aerodynamic diameter (d_{ae}) at each windspeed, across all experiments. The current inhalability convention is also shown for comparison.

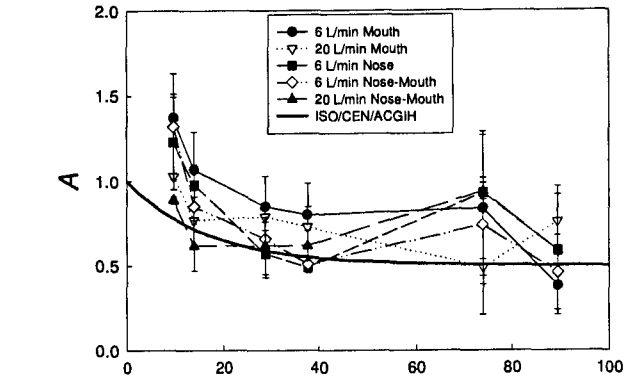

(a)

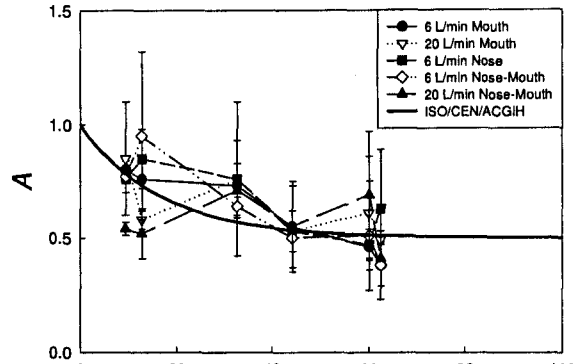

(b)

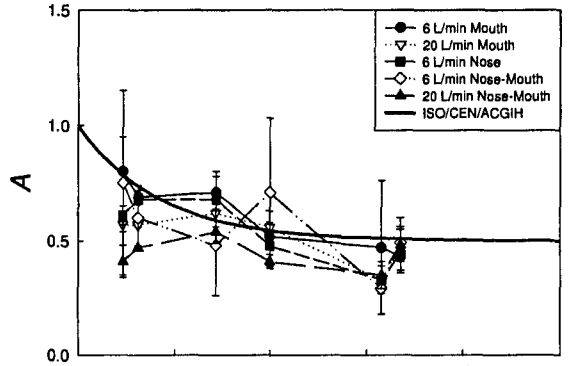

(c)

Figure 4.11: Mean aspiration efficiency (A) as a function of particle aerodynamic diameter (d_{ae}) for different mannequin breathing conditions at windspeeds of (a) 0.10 m/s, (b) 0.24 m/s and (c) 0.42 m/s. Error bars represent one standard deviation. The current inhalability convention is also shown for comparison.

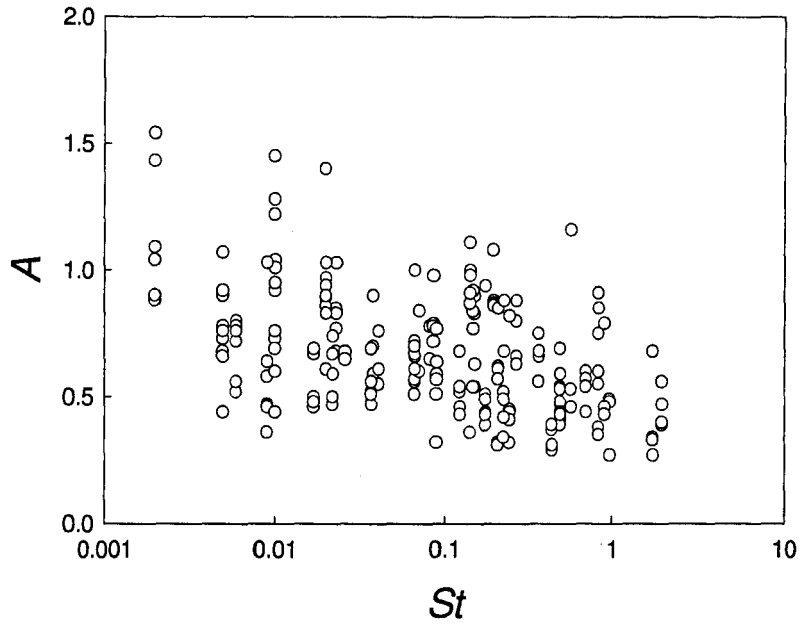

Figure 4.12: Mannequin aspiration efficiency (A) as a function of Stokes Number (St), across all experiments.

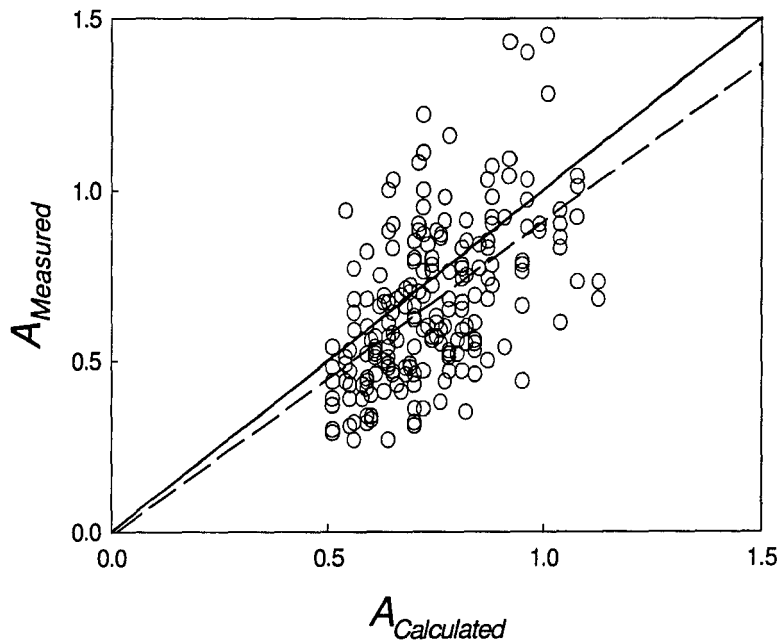

Figure 4.13: Comparison of the aspiratreportion efficiency calculated the newly developed model ($A_{Calculated}$) to that measured by the mannequin ($A_{Measured}$). The solid line represents perfect agreement and the dashed line shows the actual relationship (r^2_{adj} = 0.30).

5. Personal sampler performance

Understanding the performance characteristics of sampling devices is essential in order to effectively choose the best method for estimating personal exposures to workplace aerosols. There are a large number of factors that will determine which sampler is appropriate for a given situation (e.g., sensitivity, interferences, portability, etc.). However, most of these are beyond the scope of this work. Here, the focus of the sampler performance study discussed in this chapter is on the effectiveness of various aerosol samplers for collecting the inhalable aerosol fraction at ultra-low windspeeds. More specifically, how well does a given sampler reflect what is actually inhaled at such low windspeeds, taking into account the significant shifts in inhalability that were noted in the previous section of this Report? This part of the research therefore set out to assess the applicability of a number of personal sampling devices currently suggested for collecting the inhalable fraction to ultra-low windspeed environments.

Experimental methods

Four different personal sampling devices were tested in this study: the 2 L/min IOM inhalable aerosol sampler, the 4 L/min Button inhalable aerosol sampler, the 3.5 L/min GSP conical inlet sampler and the 2 L/min CFC sampler.[4] The first three samplers were chosen because they are widely used around the world to measure personal exposures to the inhalable aerosol fraction and are commercially available to industrial hygienists. The fourth sampler, the CFC, is not specifically an inhalable aerosol sampler, but it is the sampler still the most commonly used by industrial hygienists in the United States for collecting what is referred to as 'total aerosol'. Further details of these will be given later.

During each experiment, the samplers were all operated concurrently with the heated, breathing, rotating mannequin and the isokinetic reference sampler. We have previously described in detail the experimental methods for the mannequin and reference sampler operation and so only relevant details will be repeated here. It should also be noted that all personal sampler data were obtained after the wind tunnel was modified. The variables that were studied included: particle size (fused alumina powder grades F1200, F800, F500, F400, F280 and F240, a range of particle sizes from 9.3 μm up to 89.5 μm), windspeed (0.10, 0.24 and 0.42 m/s), and mannequin breathing pattern (6 L/min mouth-only, 20 L/min mouth-only, 6 L/min nose-only, 6 L/min nose-mouth and 20 L/min nose-mouth). The mannequin to which the samplers were attached was always heated to skin temperature (33 °C) and continuously rotated in order to achieve orientation-averaged sampling. For each of the experimental conditions tested, 2 repeats were performed with 20 minutes per sampling period. As shown in Figure 5.1, the personal samplers were attached to a lab coat worn by the mannequin. To eliminate any biases associated with sampler position – and with specific regard to the fact that the mannequin was always exhaling through the left nostril, as discussed earlier – each sampler was moved to the opposite coat lapel

[4] IOM refers to the Institute of Occupational Medicine (Edinburgh, Scotland, UK) where the sampler was developed, the Button sampler was named by researchers at the University of Cincinnati where it was developed, GSP is the name given by its German manufacturer to a sampler that elsewhere is known as the 'conical inlet sampler' (or CIS), and CFC refers to the closed-face plastic cassette sampler that is widely used by industrial hygienists in the United States and elsewhere. The flowrates indicated are those recommended by the manufacturers to achieve the desired performance.

for the second test. Otherwise, placement of the samplers was arbitrary. In this way, it was reasonable to assume that any effect associated with reversing the direction of mannequin rotation after every complete turn would be negligible.

Each sampler was operated with its own individual personal sampling pump, similar to what was used for the reference sampler described earlier (Model XR5000, SKC Inc, Eighty Four, PA, U.S.A.). Initially, there was a significant issue with respect to attaching the sampling pumps to the mannequin, due to the shape of the mannequin body and the need for continuous rotation. So the pumps were all placed in a small backpack situated at the back of the mannequin torso. The pack was secured by a single strap that sat across the mannequin chest. As shown in Figure 5.1, each sampler was connected to its respective pump with flexible tubing long enough to reach around the body, allowing easy rotation of the mannequin with all equipment in place.

During sampling, we deployed either 25-mm (IOM, Button) or 37-mm (GSP, CFC) glass fiber filters. Each filter was conditioned overnight in a desiccator to remove moisture, both before and after sampling. With the exception of the disposable CFC samplers, the IOM, Button and GSP samplers were all washed with soap and water and re-used for subsequent experiments. Blanks were obtained for each sampler type once per day, prepared during the first experiment of that day, alongside the filter and cotton blanks prepared for the mannequin and reference sampler, as in the protocol described in the previous section of this Report. Again, it was expected that issues associated with moisture build-up on the filters should not arise. Nonetheless, all reported results were blank-corrected.

The pump flowrate required for each personal samplers (i.e., between 2 and 4 L/min) was calibrated using a primary flow meter both before each test and then again after sampling was completed. Again, samples were rejected if changes in flowrate exceeded 5%. Otherwise, the average of the two flowrates was used to determine the total volume of air sampled. The concentration of sampled material (C_S) was determined using

$$C_S = \frac{[(m_2 - m_1) - (b_2 - b_1)]}{Q} \tag{5.1}$$

where Q is the sampling flowrate. This value was then compared to the reference sampler concentration (C_R), as defined in the previous section, to obtain the sampling efficiency (A_S), thus

$$A_S = \frac{C_S}{C_R} \tag{5.2}$$

The sampler filter mass concentration was compared to the inhaled concentration as collected by the mannequin (C_M) using

$$A_I = \frac{C_S}{C_M} \tag{5.3}$$

All the statistical analyses of the results that are described below were performed using SAS 9.1 (SAS Institute, Cary, NC, U.S.A.) and Sigma Plot 2000 (SPSS, Inc., Chicago, IL, U.S.A.).

Sampling and analysis of individual sampler types

The IOM inhalable aerosol sampler (SKC, Inc., Eighty Four, PA) is shown on the mannequin in Figure 5.1 on the far right side of the photograph. The version used in all the work described here included a stainless steel cassette insert that held a 25-mm glass fiber filter, all of which was weighed together. In use, the entire cassette was placed in the desiccator overnight prior to weighing, which included both before the experiment was carried out and after the sample was obtained. A fitted cap was placed over the cassette inlet while the samples were located inside the desiccator in order to prevent dust from settling onto the loaded filters, and care was taken to wipe off the outside of the cassette with a dry cloth prior to weighing. This sampler required sampling at 2 L/min, and the fully-assembled sampler was clipped to the lab coat of the mannequin so that its inlet pointed directly outwards from the body. From inter-sampler comparisons based on extensive earlier work at the higher windspeeds, this sampler has been identified as the best reference sampler for the current inhability convention (Bartley, 1998).

The Button sampler (SKC, Inc., Eighty Four, PA) is shown on the center-right side of the mannequin pictured in Figure 5.1. For this sampler, a 25-mm glass fiber filter that had been desiccated overnight was weighed – on its own – before and after sampling. The O-ring that held the filter in place tended to be quite snug against the filter, and so extra care was taken when removing it from atop the filter in order to prevent sample loss. As required for this sampler, the flowrate was set at 4 L/min, and the sampler itself was attached to the lab coat again with the inlet again pointing out from the body.

The GSP conical inlet sampler (BGI, Inc., Waltham, MA, U.S.A.) is shown attached to the mannequin lab coat in the center-left portion of the photograph in Figure 5.1. It included a removable plastic cassette that held a 37-mm glass fiber filter. For these experiments, the filter – again, desiccated overnight – was removed from the cassette and weighed separately before and after sampling. The plastic cassette was not included, as is customary in the use of this sampler. The sampling flowrate was set at 3.5 L/min, and the sampler was clipped to the lab coat with the inlet pointing directly away from the body.

Lastly, the 37-mm closed-face cassette (CFC) (SKC, Inc., Eighty Four, PA) is shown in the far left of Figure 5.1, draped over the mannequin shoulder. The version of the CFC used for these experiments consisted of 3 polypropylene stages that fitted snugly together and was certified 'Leak-Free' by the manufacturer. In each experiment, a 37-mm glass fiber filter was weighed individually and placed on top of a supportive pad inside the cassette. All pieces of the sampler were kept in the desiccator overnight with the filter before and after sampling to control moisture uptake. One concern with the CFC sampler, as noted previously, was that it had been consistently shown to suffer from high levels of internal wall deposits, which are not analyzed when only the filter is weighed. Although it is possible to collect these deposits, such as wipes or specially-designed inserts, it was decided for this research that analysis of the CFC sampler would be carried out in the manner traditionally used by practicing industrial hygienists – that is, by analyzing *only* the filter. Again, care was taken when removing the filter from the sampler to

avoid potential sample loss due to mishandling. In contrast to the other samplers described, this sampler was not clipped to the mannequin's lab coat, but was instead draped over one shoulder so that the inlet was pointed downward at an angle of approximately 45°. The sampling flowrate was set at 2 L/min.

Individual sampler results and discussion

We will now present the results for each personal sampler individually, both in terms of its overall sampling efficiency and its direct relationship to the aspiration efficiency of the breathing mannequin.

IOM inhalable aerosol sampler:

Figure 5.2 shows all the experimental data for the aspiration efficiency of the IOM sampler. They are separated out into each of the mannequin breathing conditions (i.e., 6 L/min mouth-only, 20 L/min mouth-only, 6 L/min nose-only, 6 L/min nose-mouth and 20 L/min nose-mouth, respectively), with further separation in each graph based on the three different windspeeds tested. Each data point represents the mean of all the experimental runs for the conditions indicated, with error bars reflecting one standard deviation. The curve for the current inhalability convention is also included in the figure for the purpose of comparison.

ANOVA results indicated that the IOM sampling efficiency was significantly different based on the windspeed (*p-value* < 0.0001), with sampling efficiency decreasing as windspeed increased. There were no statistically-significant differences based on the breathing pattern of the mannequin (*p-value* = 0.1900) or for the mode of breathing (*p-value* = 0.2712). However, sampling efficiency was significantly dependent on mannequin breathing flowrate (*p-value* = 0.0180) where greater IOM sampling efficiency was associated with higher breathing rate. This suggests a possible influence of the disturbance to the incoming freestream during expiration under such conditions.

Figure 5.2 also shows that, at the lowest windspeed (0.10 m/s), IOM sampling efficiencies lay consistently above the inhalability curve. Furthermore, the sampling efficiency at the lowest windspeed is considerably greater than unity for many conditions. At the two higher windspeeds (0.24 and 0.42 m/s), the IOM sampler follows the criterion somewhat better, but even there the bulk of the data appear to lie above the inhalability curve.

Another detail to note in those figures is the magnitude of the calculated standard deviations, which appear to especially large for the largest particle sizes and at the lowest windspeed. This may be associated with the fact that the uniformity of air velocity and aerosol concentration was less good under these conditions.

Figure 5.3 shows the direct comparison between IOM sampling efficiency and the mannequin aspiration efficiency, plotting the results obtained across all ranges of conditions. The solid line represents perfect agreement ($A_{Mannequin} = A_{IOM}$) and the dashed line represents a simple linear regression of the data ($r^2_{adj} = 0.35$) given by

$$A_{IOM} = 0.27 + 1.00 A_{Mannequin} \quad (5.4)$$

It is interesting to note here that the slope of the estimated relationship is 1:1, as desired in an ideal inhalable aerosol sampler, yet there is a small but significant offset. Overall, it is shown that the IOM sampler consistently exhibited higher sampling efficiency relative to the mannequin for each given set of conditions. Indeed, a t-test comparison of those data indicated that the difference was statistically significant (*p-value* < 0.0001). Furthermore, looking at each windspeed separately, the same trend was apparent (all *p-values* < 0.0001).

Button inhalable aerosol sampler:

Figure 5.4 shows the results for the mean sampling efficiency of the Button sampler as a function of particle aerodynamic diameter. The data are again organized into the five previously described breathing pattern combinations (i.e., 6 L/min mouth-only, 20 L/min mouth-only, 6 L/min nose-only, 6 L/min nose-mouth and 20 L/min nose-mouth, respectively), and the same three windspeeds. Again, the error bars represent one standard deviation, and the current inhalability curve is shown.

ANOVA results showed that the Button sampling efficiency was significantly dependent on the windspeed (*p-value* < 0.0001), with sampling efficiency increasing with decreasing windspeed. This is clearly apparent in Figure 5.4, which shows that the Button sampler exhibited higher sampling efficiencies at 0.10 m/s compared to those for 0.24 m/s and 0.42 m/s. In addition, it can also be seen that the lowest windspeed was consistently associated with sampling efficiencies greater than the current inhalability convention. For the two higher windspeeds however, there was better agreement with the convention. With respect to the mannequin breathing parameters – breathing pattern, flowrate and mode of breathing – no significant differences (at a significance level of $\alpha = 0.05$) were observed.

Figure 5.5 shows the direct relationship between the Button sampling efficiency and the mannequin aspiration efficiency. A paired t-test showed that the differences between the two data sets were statistically significant (*p-value* < 0.0001). However, when separated out by windspeed, the results for the highest windspeed (0.42 m/s) were not significantly different (*p-value* = 0.2317). On the other hand, at the two lower windspeeds (0.10 m/s and 0.24 m/s), the differences remained statistically different (*p-values* <0.0001 and 0.0076, respectively). This indicates that, only at the highest windspeed, the Button sampler corresponded quite well with the inhalable fraction – as measured here by the mannequin – at the highest of the windspeeds tested. Figure 5.5 also includes the result of linear regression ($r^2_{adj} = 0.36$) of all the data, shown by the dashed line and described by

$$A_{Button} = 0.02 + 1.25 A_{Mannequin} \quad (5.5)$$

It is seen that the sampling efficiency of the Button sampler was steeper relative to the aspiration efficiency of the mannequin. However, the intercept was now very close to zero, so that it can be said that the Button sampler consistently provided a sampling efficiency which was approximately 25% greater than for the mannequin.

GSP conical inlet sampler:

Figure 5.6 shows the results for the sampling efficiency of the GSP conical inlet sampler. The figure is organized in the same way as for the other samplers. The ANOVA results showed that the sampling efficiency of the GSP sampler was significantly different based on windspeed (*p-value* < 0.0001), with sampling efficiency again increasing with decreasing windspeed. There were no statistically-significant differences (at $\alpha = 0.05$) for the sampling efficiency of the GSP based on any mannequin breathing parameters tested – including pattern, flowrate or mode of breathing. Similar to what was seen for the performance of the Button sampler, the GSP sampling efficiency was typically greater than the current inhalability convention at the lowest windspeed, but was more consistent with it for both the higher windspeeds tested.

An additional consideration with respect to the GSP sampling methods is worth mentioning. As indicated previously, the plastic cassette that held the filter in place inside the sampler was not included for gravimetric analysis. However, it was visually observed that a portion of aspirated particulates was clearly deposited onto this cassette. But it was not analyzed, consistent with the customary use of this sampler. So it should be noted that inclusion of the cassette for gravimetric analyses might be expected to result in a higher sampling efficiency than has been reported here.

Figure 5.7 shows the relationship between the GSP sampling efficiency and the mannequin aspiration efficiency. Analysis of that relationship using a paired t-test showed a statistically significant difference (*p-value* < 0.0001). When separated out by windspeed, the highest windspeed (0.42 m/s) was not significantly different relative to the mannequin aspiration efficiency (*p-value* = 0.1944). However, significant differences remained for the two lower windspeeds (0.10 m/s and 0.24 m/s) (*p-values* <0.0001 and 0.0085, respectively). Linear regression ($r^2_{adj} = 0.57$) yielded

$$A_{GSP} = -0.11 + 1.36 A_{Mannequin} \tag{5.6}$$

The overall fit – as indicated by the r^2_{adj} value – of this regression for the GSP to the mannequin was better than for the other inhalable aerosol samplers. However, in contrast to the IOM and Button samplers, there is a greater bias between the GSP and the mannequin.

Closed-face cassette sampler:

Figure 5.8 shows the corresponding results for the CFC sampler. The ANOVA results showed that sampling efficiency was significantly different based on windspeed (*p-value* < 0.0001), but not significant (at $\alpha = 0.05$) based on any of the breathing parameters – pattern, flowrate or mode of breathing. It is clearly seen that, for each experimental condition, the sampling efficiency dropped off sharply quickly and approached zero for particles larger than about 20 μm. The only conditions for which the CFC provided a sampling efficiency similar to the current inhalability convention were for the smallest particles (approximately 9 μm) at the lowest windspeed (0.10 m/s). These tendencies are generally similar to what has previously been observed for the CFC at higher windspeeds.

Figure 5.9 depicts the direct relationship between the sampling efficiency for the CFC sampler and the mannequin aspiration efficiency. As expected, a t-test comparison of those data showed a statistically-significant difference (*p-values* < 0.0001). Looking at each windspeed separately also indicated significant differences between the CFC and the mannequin (all *p-values* < 0.0001). In contrast to the other samplers tested, differences associated with the CFC were in the opposite direction, indicating much lower sampling efficiency than the mannequin. Linear regression ($r^2_{adj} = 0.32$) yielded

$$A_{CFC} = -0.17 + 0.56 A_{Mannequin} \tag{5.7}$$

This indicates that the CFC consistently collected less than half of what was inhaled by the mannequin.

Inter-sampler comparisons

We now set out to directly compare the tested samplers with one another. As discussed, the IOM sampler has – until now – been considered as the best reference sampler for the inhalable fraction convention (Bartley, 1998). This is not surprising since, of all the samplers tested, this is the only instrument that had been designed with performance specifically matching the current inhalability criterion. With this in mind, it was deemed useful to compare the performances of the other samplers with that of the IOM sampler. But, noting that the CFC remains the most popular personal sampler in use today by American industrial hygienists, it will also be instructive to understand how the performance of that device compares to that of each of the other samplers.

Figure 5.10 shows the relationship between the IOM and Button samplers for all concurrent experiments ($r^2_{adj} = 0.62$). From visual inspection of the graph, it appears that the sampling efficiencies of these two samplers are in quite close agreement, with the IOM typically providing slightly greater values compared to the Button. Despite this observed similarity, however, there was a statistically-significant difference for these two samplers across all the ultra-low windspeeds tested (*p-value* < 0.0001). But it is interesting to note that, when separated out by windspeed, this difference was less significant at 0.10 m/s (*p-value* = 0.0396) than at the higher 0.42 m/s (*p-value* < 0.0001). That suggests that a decrease in windspeed may be associated with better agreement between the sampling efficiencies of the IOM and Button samplers.

Figure 5.11 shows the corresponding relationship between the IOM and GSP inhalable aerosol samplers ($r^2_{adj} = 0.53$). Here, the difference between the samplers is clearly greater than for the IOM and Button samplers. But, again, the results for the IOM sampler were higher compared to those for the GSP. A paired t-test showed a significant difference between these two samplers (*p-value* < 0.0001). That difference also remained highly significant within each individual windspeed.

Figure 5.12 shows the relationship between the IOM and the CFC samplers ($r^2_{adj} = 0.14$). Here, it is clear that the IOM consistently collected more than the CFC. Therefore, it is not surprising to find that the difference between these two samplers was highly significant across all windspeeds

(all *p-values* < 0.0001). Again, this result is broadly consistent with the body of previous work on these two samplers.

Although the IOM is the most commonly-used sampler nowadays for collecting the inhalable fraction, it is also informative to make some inter-sampler comparisons of the other instruments tested in this research. This will help form a more complete picture of the relative performances of these personal samplers. For that purpose, Figure 5.13 shows the relationship between the Button and GSP samplers for all concurrent experiments (r^2_{adj} = 0.55). A paired t-test indicated that, for all windspeeds, there was a significant difference between the Button and GSP samplers (*p-value* = 0.0208), with the Button typically indicating higher sampling efficiencies compared to the GSP. However, when separated out by windspeed, these two samplers were not significantly different at 0.10 m/s or 0.24 m/s (*p-value* = 0.3404 and 0.2142, respectively), and there was only a slightly significant difference at 0.42 m/s (*p-value* = 0.0249). The results suggest that an increase in the windspeed corresponded to an increase in the difference between the performances of these two samplers. In other words – similar to what was seen for the comparison of the IOM and Button samplers – agreement between these inhalable aerosol samplers was best at the lowest windspeed.

Figure 5.14 shows the corresponding relationship between the Button and the CFC samplers (r^2_{adj} = 0.16). Here, it is seen that the Button nearly always provided a greater sampling efficiency than the CFC. Paired t-test comparisons showed that those differences were statistically significant across all windspeeds and within each windspeed separately (all *p-values* < 0.0001). Finally, Figure 5.15 shows the relationship between the GSP and CFC samplers (r^2_{adj} = 0.53). Here, the relationship was similar to that found for the IOM and Button samplers, with the GSP almost always providing a sampling efficiency greater than the CFC. As expected, paired t-test comparisons showed that, once again, these differences were highly statistically significant across all windspeeds and within each windspeed separately (all *p-values* < 0.0001).

Possible correction factors for sampler use at ultra-low windspeeds

As the preceding discussion has shown, the three nominally inhalable aerosol samplers – in contrast to the CFC sampler – appeared to over-sample the inhalable fraction at ultra-low windspeeds. However, the consistency in those data suggests the possibility of applying correction factors to enable usage of these three samplers in practical very-low windspeed environments. To explore this, the sampling efficiency of each sampler in relation to what was inhaled by the mannequin is now examined more closely.

The experimental results for the IOM sampler show a mixed picture, as reflected in Equation (5.4) obtained from the linear regression analysis of the results. On the one hand, the slope of the relationship between A_{IOM} and $A_{Mannequin}$ is satisfyingly 1:1. However, there is a large offset of 0.27, suggesting that the plot of A_{IOM} versus $A_{Mannequin}$ does not pass through the origin. That is physically not plausible since both sampling systems should indicate zero when the actual aerosol concentration falls to zero. The appearance of the results on which Equation (5.4) was based suggests the possibility of an experimental artifact. In terms of using Equation (5.4) to obtain a correction factor, this presents a problem. However, the only option at present – albeit unsatisfactory – is to recalculate the linear regression, forcing the new expression through the

origin. That modified relationship is shown in Figure 5.16a, which suggests that concentrations obtained using the IOM sampler should be multiplied by a factor of 0.73 to better correlate them with the inhalable aerosol fraction at ultra-low windspeeds. Now, not surprisingly, the r^2_{adj} for the regression fell to 0.30 during the recalculation, compared to 0.35 for the initial regression. However the suggested correction factor may be useful for the practical use of the IOM sampler at ultra-low windspeeds.

The search for a correction factor for the other samplers is, fortunately, more straightforward because the offset between the samplers – as determined by linear regression – is small, indeed small enough to be ignored. With this in mind, the linear regressions were repeated where the relationship was forced through the origin. Figure 5.16b shows the simplified relationship between the Button sampler and the mannequin, indicating that the correction factor to be applied to the Button sampler in order to match the inhalability exhibited by the mannequin at ultra-low windspeeds of this research should be 0.78 (with the new r^2_{adj} remaining the same at 0.36). Similarly, Figure 5.16c shows the same relationship for the GSP sampler and the mannequin aspiration efficiency where the correction factor to be applied to the GSP sampler in order to match the inhalability exhibited by the mannequin at ultra-low windspeeds of this research should be 0.83 (with the new r^2_{adj} reduced only slightly from 0.57 to 0.56).

Ultimately, such correction factors are merely 'suggested' by inspection of the actual experimental data. But they are very simplistic and do not taken into account the various complicating factors that will be found in sampling in actual workplaces, including higher-vs-lower windspeeds, coarser-vs-finer aerosols, etc. So they should be used only with considerable caution.

Relation of physical principles and new empirical model

The physical principles governing aerosol sampling discussed briefly above and elaborated extensively elsewhere (e.g., Vincent, 2007) are of course applicable to discussion of the performances of the sampling devices tested here. A simple empirical model was described in the preceding section that adequately describes the data that were obtained for the aspiration efficiency of the human head under ultra-low windspeed conditions. But even that was considered not to be particularly useful beyond drawing together the data within a plausible scientific framework. The physical situation for the personal samplers discussed here is essentially the same. But the differences in geometry, orientation on the body, etc. make things still more complicated. So any attempt to model our results along the same lines will be even less helpful, and therefore no such attempt was made.

Conclusions

Studies were carried out of the performances of three personal samplers – the IOM, the Button, and the GSP samplers – that have been touted as appropriate for collecting the inhalable fraction as defined by the current convention defined by ACGIH and other standards-setting bodies. The closed-face cassette (CFC) widely used for collecting 'total aerosol' by industrial hygienists in the United States was also included in the experimental program. Previous work had suggested that sampling efficiency for samplers like those tested was not significantly dependent on

windspeed for air velocities in the range 0.5 and 1 m/s, (Aizenberg *et al.*, 2001). It was an important finding from the present work that the windspeed in the wind tunnel *was* indeed – and unambiguously – a significant factor influencing the performances of all four personal aerosol samplers tested. More specifically, the sampling efficiency increased with decreasing windspeed for each sampler type. The shift was most marked for the lowest windspeed tested (0.10 m.s), matching what was found for the aspiration efficiency of the human head. This is a very important finding.

The other potentially influential factors that were examined for each sampler related to the mannequin; namely, the breathing pattern, the mode of breathing and the breathing flowrate. Here, it was shown that the breathing pattern of the mannequin (i.e., the *combination* of breathing flowrate and mode of breathing) had no significant impact on the sampling efficiency of any personal samplers attached to the body. The breathing mode (i.e., nose, mouth or nose-mouth breathing), looked at independently, was also not a factor for determining sampling efficiency for any of the samplers. However, where the breathing flowrate was looked at as a separate factor, only the IOM sampler showed significant differences, albeit small. Overall, these results suggest that differences in human aspiration do not have any substantial effect on the performance of personal samplers attached to the body.

An important aspect of the research just described is that the performance of each sampler was assessed *directly relative* to the mannequin aspiration efficiency as determined during the same experiments. This, in truth, provides the *ideal* evaluation of sampler performance in relation to what is inhaled. Here, when experiments for all ultra-low windspeeds were taken together, all the samplers tested performed in a manner that showed significant differences from the mannequin. More specifically, the those samplers identified as suitable for collecting the inhalable fraction – the IOM, Button, and GSP samplers – indicated sampling efficiencies that exceeded that of the mannequin. But the CFC sampler consistently provided lower sampling efficiencies. However, when the data were separated out into the three different windspeeds, both the Button and GSP were statistically similar to the mannequin at the highest windspeed (0.42 m/s). On the other hand, both the IOM and CFC remained statistically different from the mannequin at each windspeed. This suggests that, at the higher end of the ultra-low windspeeds used in this work, the Button and GSP samplers may provide reasonably accurate measurements of the inhalable fraction of aerosols. In contrast, at both lower windspeeds (0.10 m/s and 0.24 m/s), none of the samplers provided accurate estimates of the inhalable aerosol fraction as reflected by direct comparison with the mannequin.

In general, the results described in this chapter suggest that, if current samplers are to be used in ultra-low windspeed environments, correction factors to better correlate those sampler measurements to the inhalable aerosol fraction may be appropriate. In addition, for the practical application of these samplers for use under the realistic workplace windspeeds we have identified, modified criteria against which to compare those measurements would also be required. That is, ACGIH and other standards setting bodies should re-visit the particle size selective criteria as they apply to inhalable aerosol.

Taken as a whole, the body of research described here represents an important addition to the knowledge and understanding of common personal samplers in use today. In general, many of

the findings are consistent with what has been learned about the relative performances of these samplers in other studies, both in laboratory and field tests. However, laboratory assessment of inhalable aerosol samplers at ultra-low windspeeds – being more representative of typical working environments – had not been performed previously.

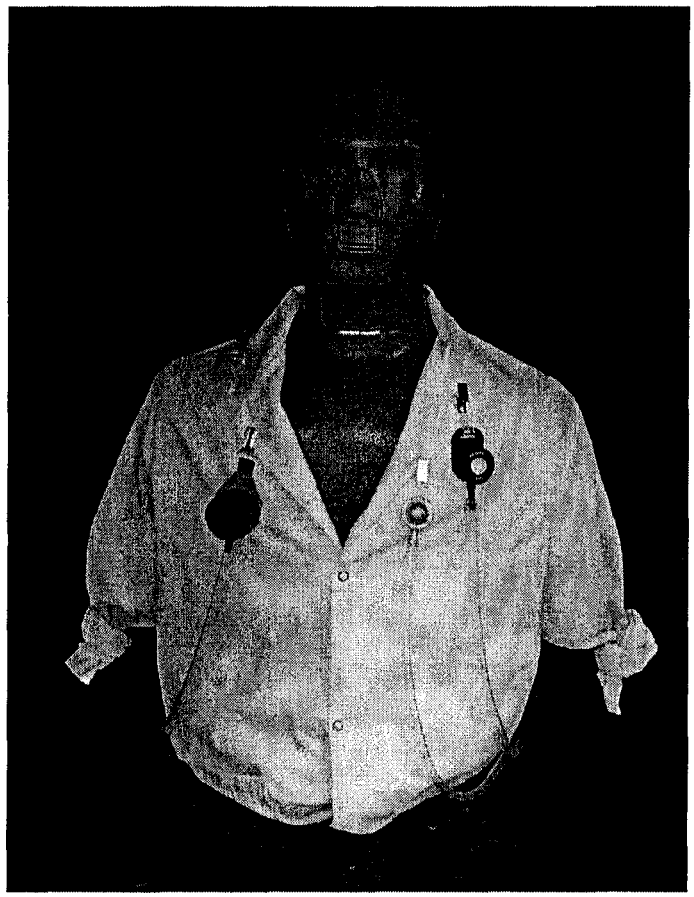

Figure 5.1: Experimental set-up for assessing personal sampler performance at ultra-low windspeeds, showing the mannequin with all four personal samplers tested. Not shown is the bag situated on the back of the mannequin torso that held the four sampling pumps.

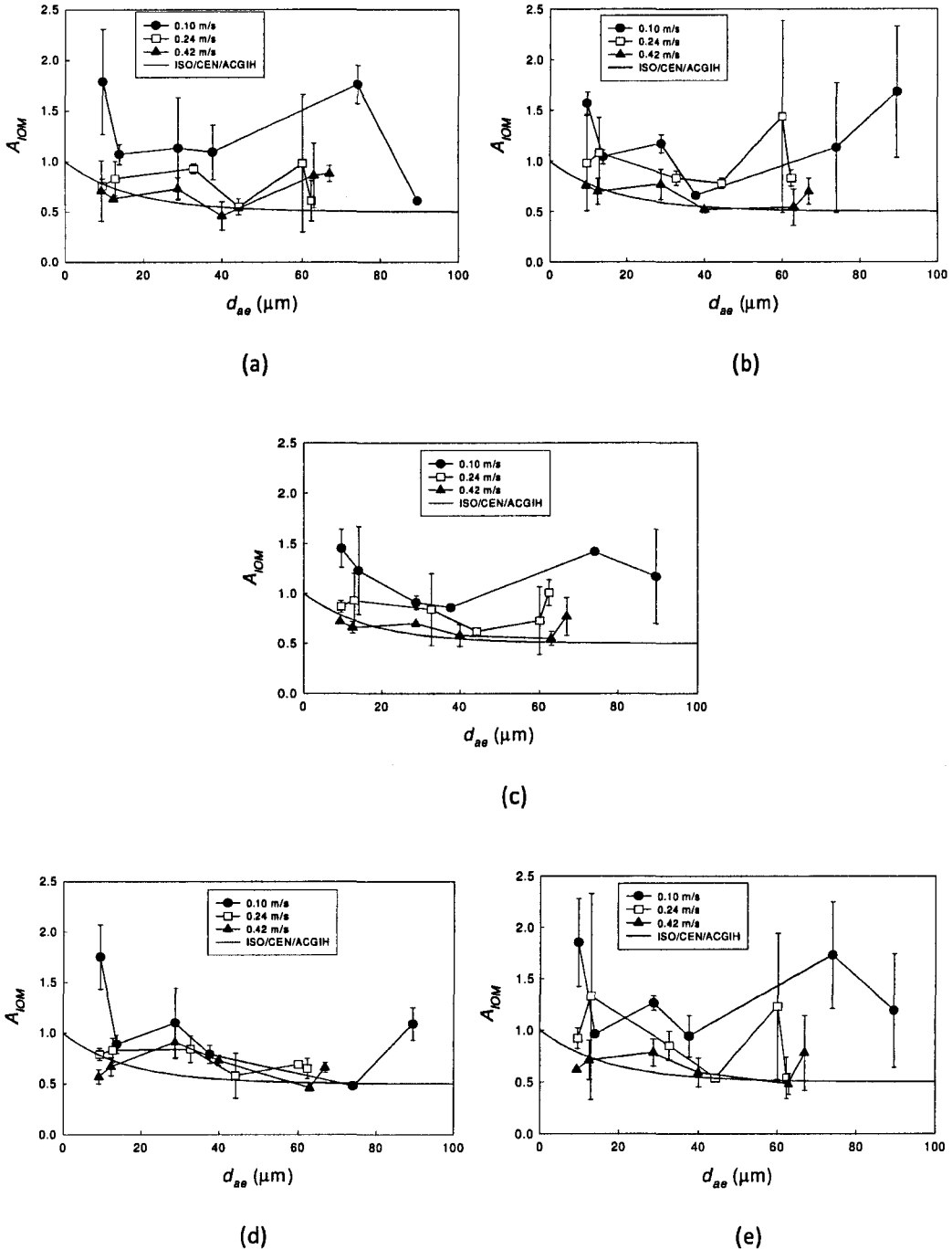

Figure 5.2: Mean sampling efficiency of the IOM sampler (A_{IOM}) as a function of particle aerodynamic diameter (d_{ae}) when attached to a heated mannequin with breathing patterns of (a) 6 L/min mouth, (b) 20 L/min mouth, (c) 6 L/min nose, (d) 6 L/min nose-mouth and (e) 20 L/min nose-mouth. The current inhalability convention is also shown.

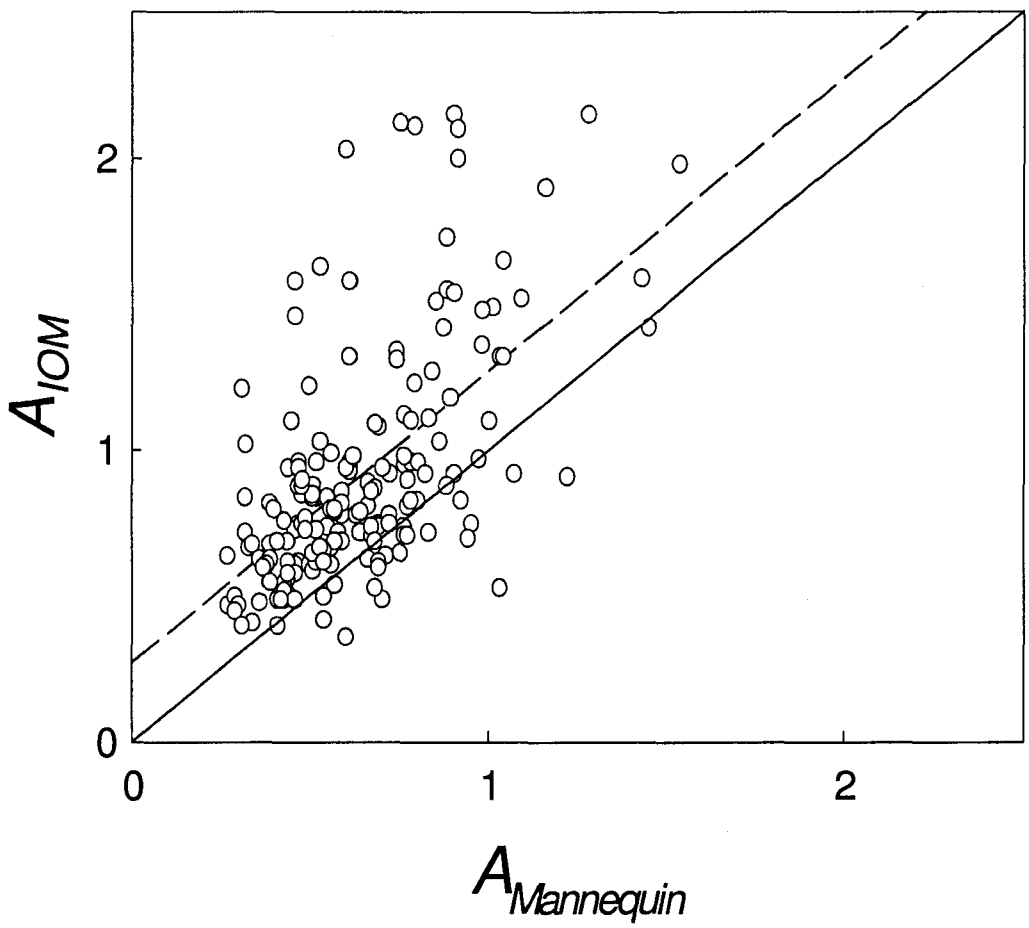

Figure 5.3: Comparison of the sampling efficiency for the IOM sampler (A_{IOM}) to the mannequin aspiration efficiency ($A_{Mannequin}$), for all concurrent experiments. The solid line shows perfect agreement and the dashed line is the actual relationship ($r^2_{adj} = 0.35$).

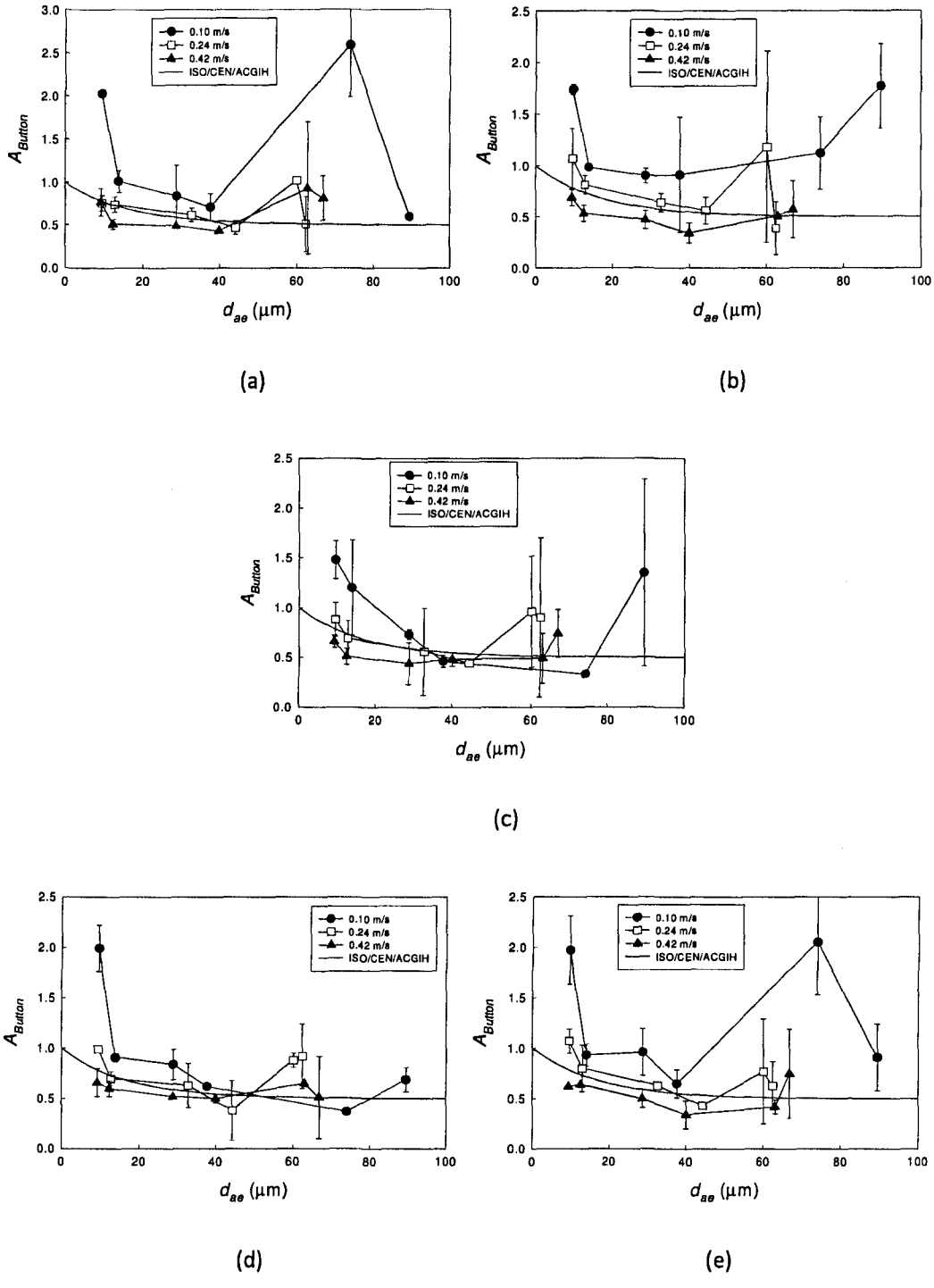

Figure 5.4: Mean sampling efficiency of the Button sampler (A_{Button}) as a function of particle aerodynamic diameter (d_{ae}) when attached to a heated mannequin with breathing patterns of (a) 6 L/min mouth, (b) 20 L/min mouth, (c) 6 L/min nose, (d) 6 L/min nose-mouth and (e) 20 L/min nose-mouth. The current inhalability convention is also shown.

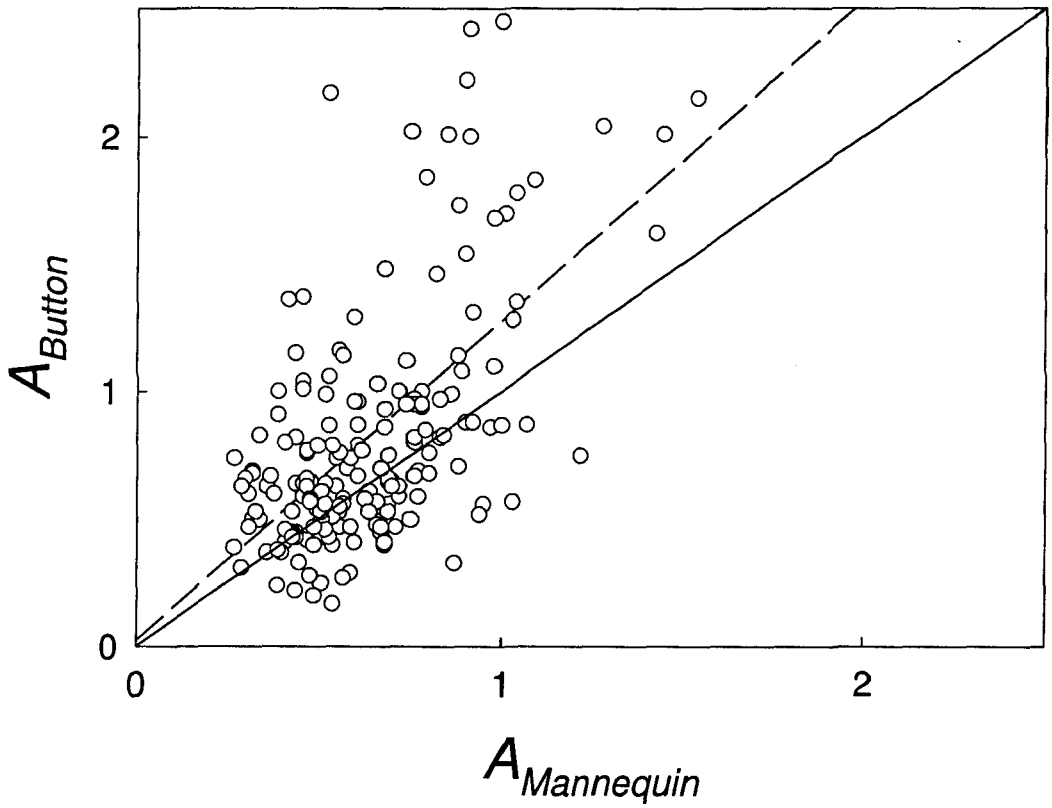

Figure 5.5: Comparison of the sampling efficiency for the Button sampler (A_{Button}) to the mannequin aspiration efficiency ($A_{Mannequin}$), for all concurrent experiments. The solid line shows perfect agreement and the dashed line is the actual relationship ($r^2_{adj} = 0.36$).

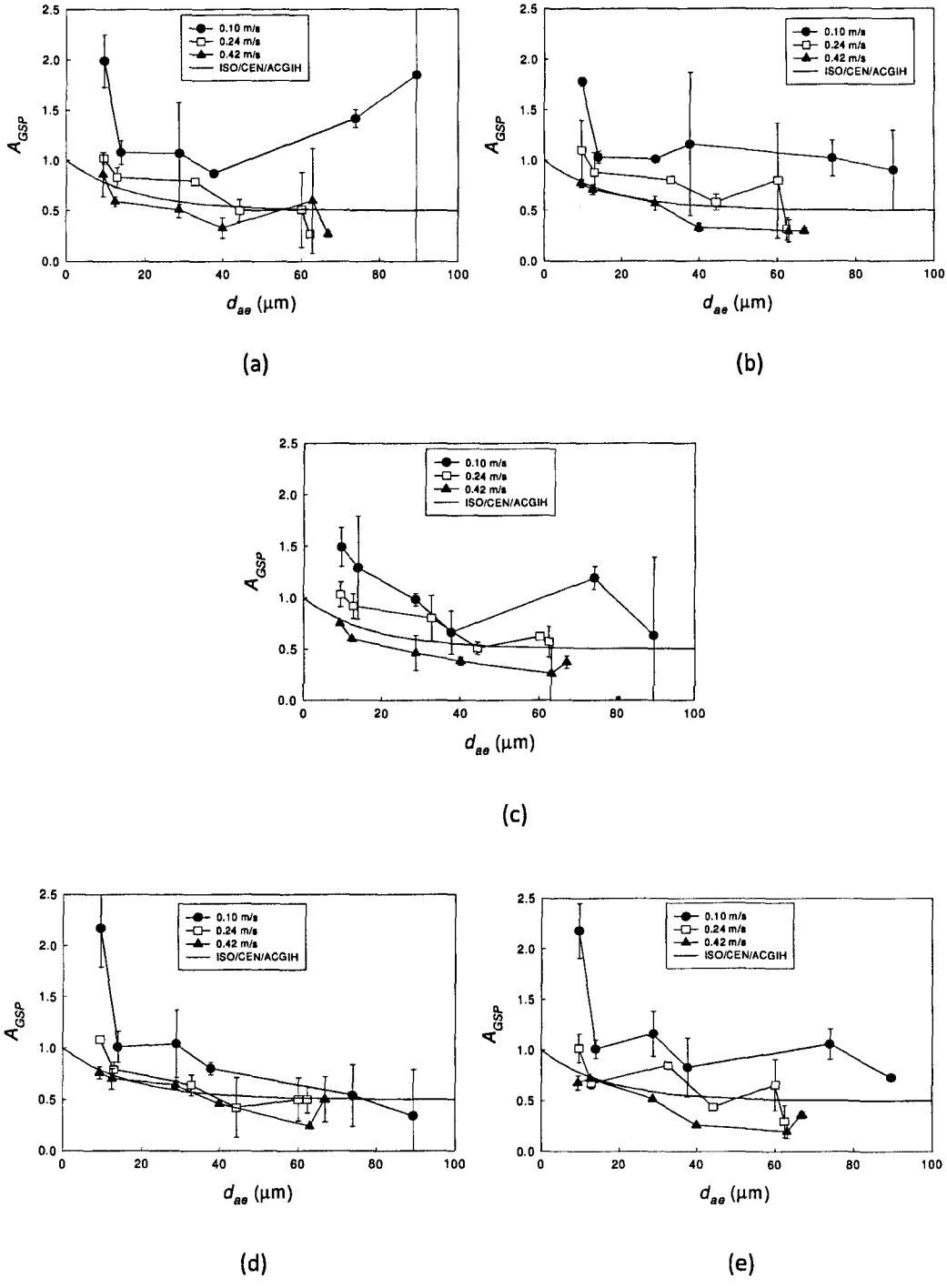

Figure 5.6: Mean sampling efficiency of the GSP sampler (A_{GSP}) as a function of particle aerodynamic diameter (d_{ae}) when attached to a heated mannequin with breathing patterns of (a) 6 L/min mouth, (b) 20 L/min mouth, (c) 6 L/min nose, (d) 6 L/min nose-mouth and (e) 20 L/min nose-mouth. The current inhalability convention is also shown.

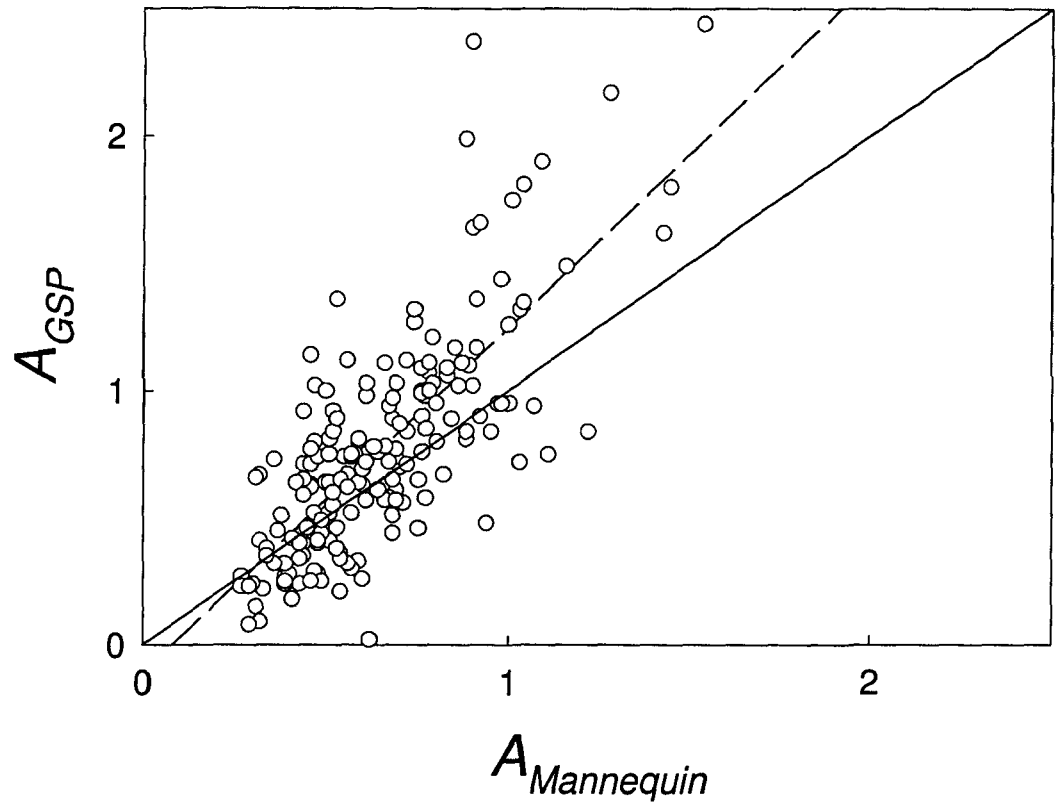

Figure 5.7: Comparison of the sampling efficiency for the GSP sampler (A_{GSP}) to the mannequin aspiration efficiency ($A_{Mannequin}$), for all concurrent experiments. The solid line shows perfect agreement and the dashed line is the actual relationship ($r^2_{adj} = 0.57$).

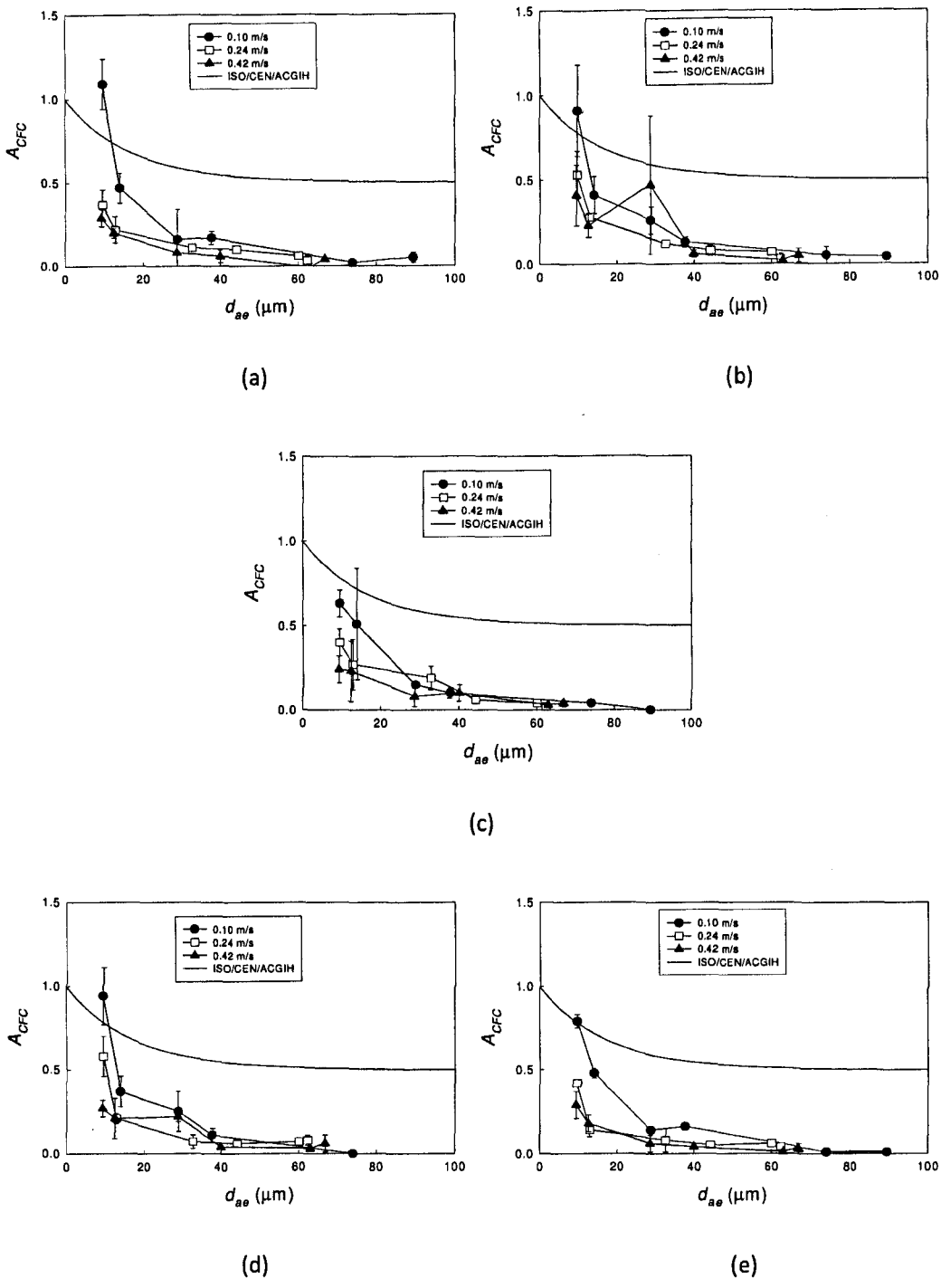

Figure 5.8: Mean sampling efficiency of the CFC sampler (A_{CFC}) as a function of particle aerodynamic diameter (d_{ae}) when attached to a heated mannequin with breathing patterns of (a) 6 L/min mouth, (b) 20 L/min mouth, (c) 6 L/min nose, (d) 6 L/min nose-mouth and (e) 20 L/min nose-mouth. The current inhalability convention is also shown.

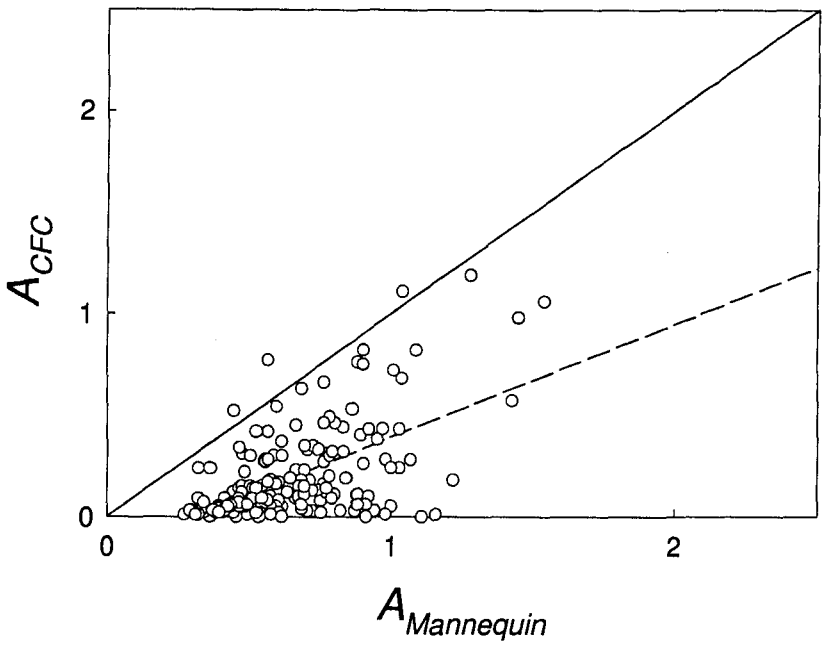

Figure 5.9: Comparison of the sampling efficiency for the CFC sampler (A_{CFC}) to the mannequin aspiration efficiency ($A_{Mannequin}$), for all concurrent experiments. The solid line shows perfect agreement and the dashed line is the actual relationship ($r^2_{adj} = 0.32$).

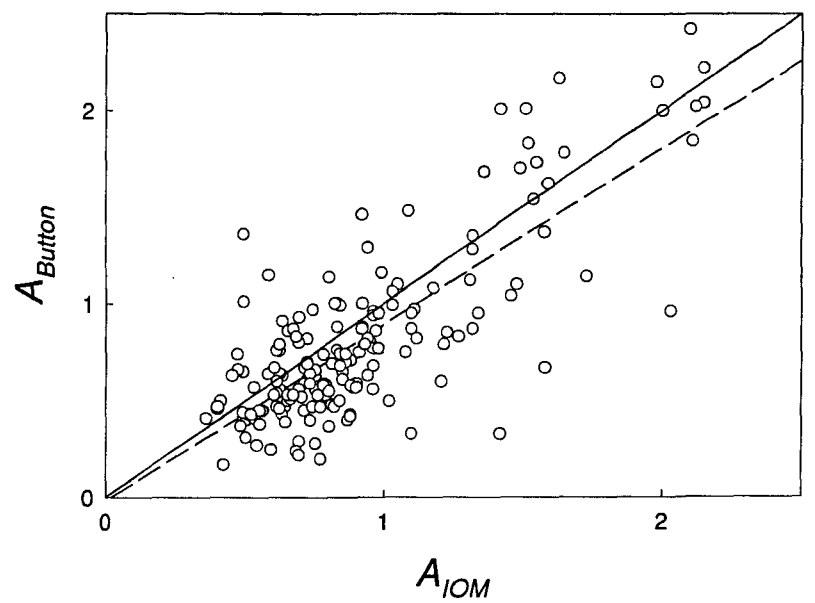

Figure 5.10: Comparison of the sampling efficiency for the Button sampler (A_{Button}) relative to the IOM sampler (A_{IOM}), for all concurrent experiments. The solid line shows perfect agreement and the dashed line is the actual relationship ($r^2_{adj} = 0.62$).

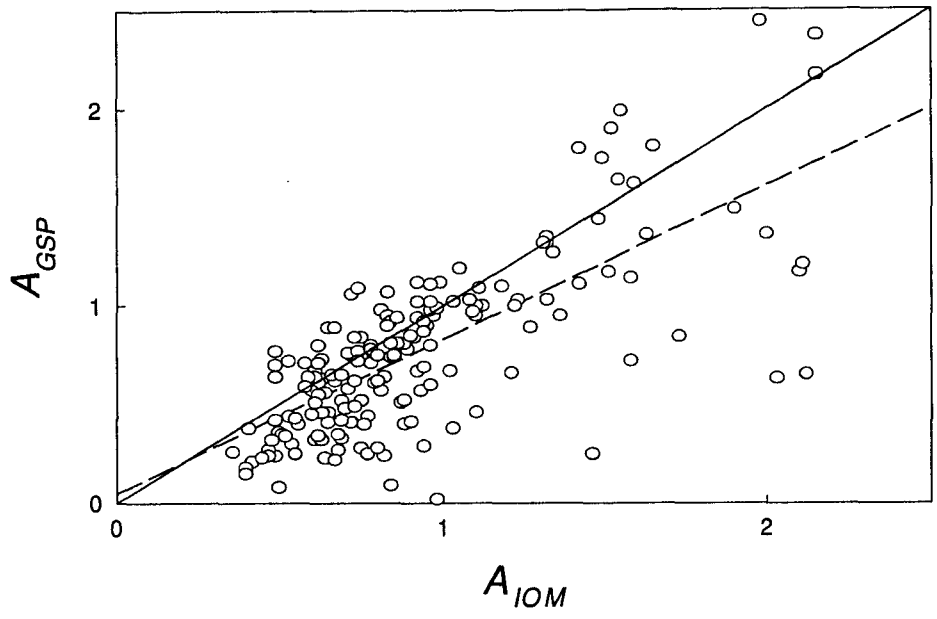

Figure 5.11: Comparison of the sampling efficiency for the GSP sampler (A_{GSP}) relative to the IOM sampler (A_{IOM}), for all concurrent experiments. The solid line shows perfect agreement and the dashed line is the actual relationship ($r^2_{adj} = 0.53$).

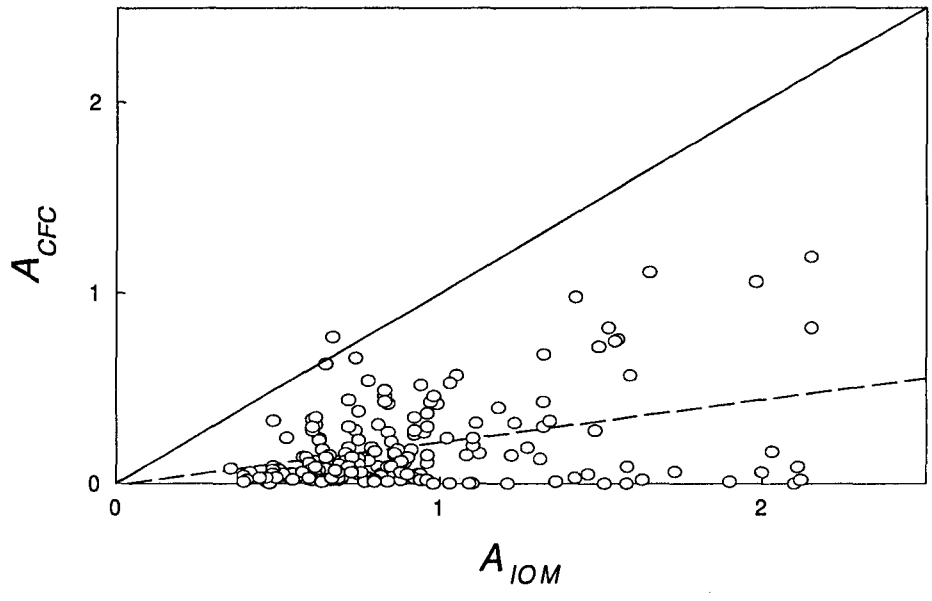

Figure 5.12: Comparison of the sampling efficiency for the CFC sampler (A_{CFC}) relative to the IOM sampler (A_{IOM}), for all concurrent experiments. The solid line shows perfect agreement and the dashed line is the actual relationship ($r^2_{adj} = 0.15$).

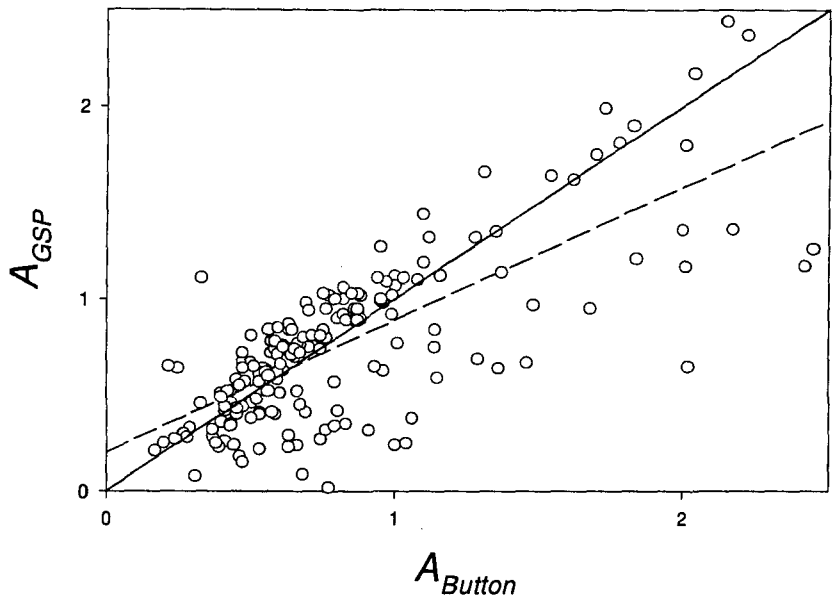

Figure 5.13: Comparison of the sampling efficiency for the GSP sampler (A_{GSP}) relative to the Button sampler (A_{Button}), for all concurrent experiments. The solid line shows perfect agreement and the dashed line is the actual relationship (r^2_{adj} = 0.56).

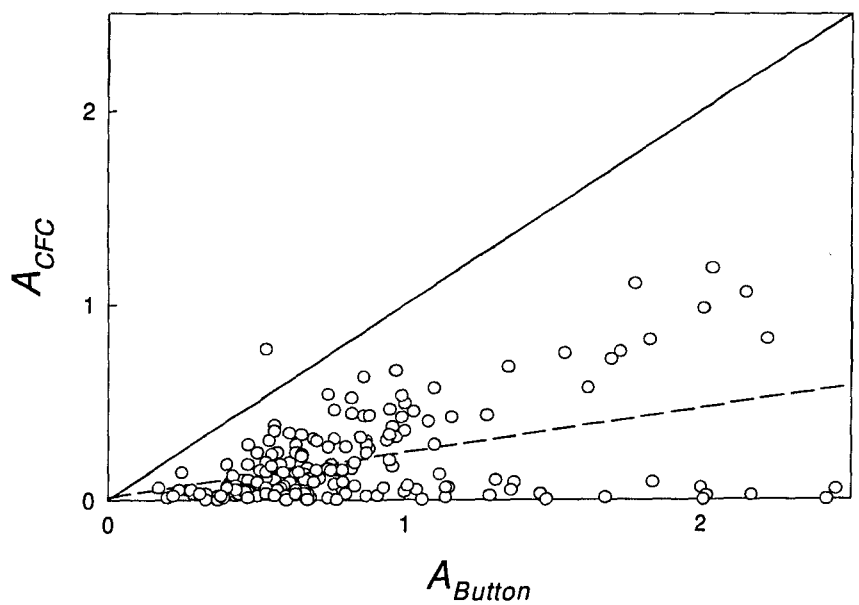

Figure 5.14: Comparison of the sampling efficiency for the CFC sampler (A_{CFC}) relative to the Button sampler (A_{Button}), for all concurrent experiments. The solid line shows perfect agreement and the dashed line is the actual relationship (r^2_{adj} = 0.21).

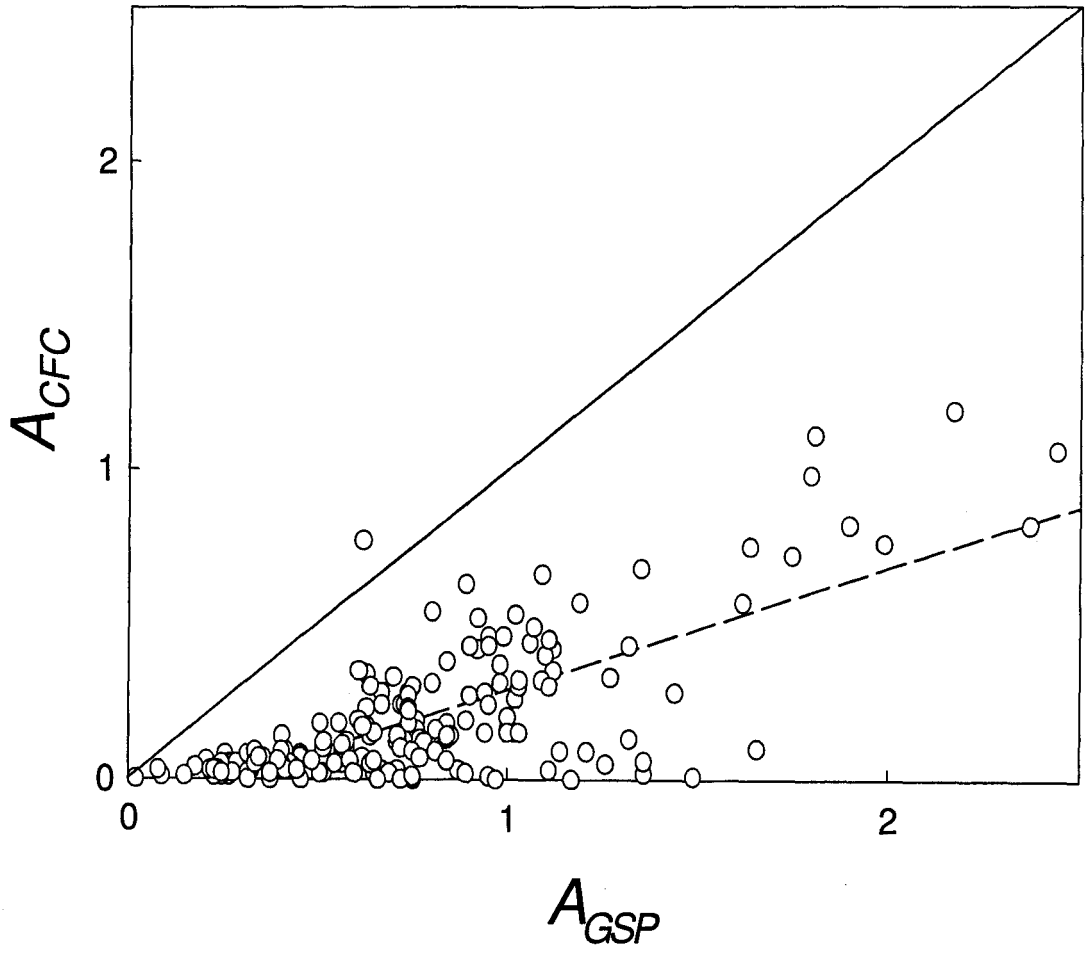

Figure 5.15: Comparison of the sampling efficiency for the CFC sampler (A_{CFC}) relative to the GSP sampler (A_{GSP}), for all concurrent experiments. The solid line shows perfect agreement and the dashed line is the actual relationship (r^2_{adj} = 0.53).

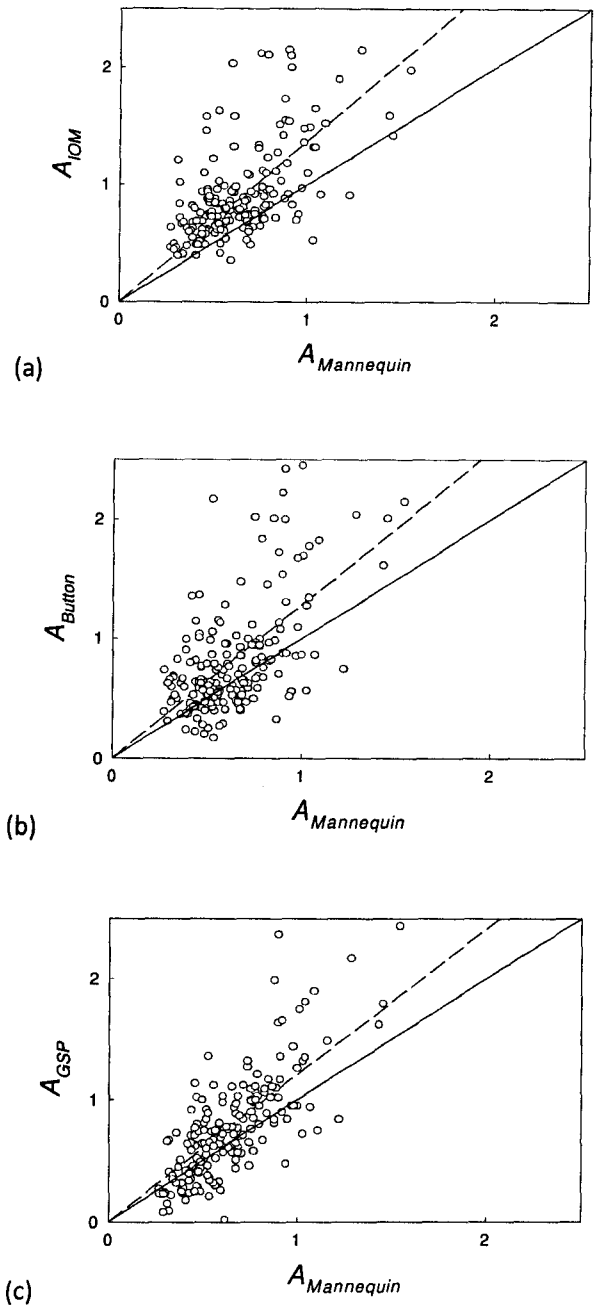

Figure 5.16: Relationship of sampling efficiency to mannequin aspiration efficiency ($A_{Mannequin}$), for the purposes of calculating a correction factor, for inhalable aerosol samplers: (a) IOM, (b) Button and (c) GSP.

6. Integration and implications

From the outset, one important objective of this research was to determine whether current particle size-selective standards – which are currently based on data that had been collected at windspeeds above about 0.5 m/s – are still appropriate at the ultra-low windspeeds characteristic of most workplaces. The first part of this part of the Report will therefore examine the results presented thus far relative to existing criteria. In light of the fact that a smaller body of similar work carried out elsewhere in calm air showed higher inhalability than that for moving air in the range previously studied, a modified criterion recently proposed for calm air will be suggested. As an extension of those discussions, the personal samplers that were tested will also be examined against the suggested new criterion. Finally, the practical implications of modifying the current convention to include the new knowledge of what happens at ultra-low range of windspeeds will be addressed.

Relation of ultra-low windspeed data to current inhalability criteria

It is recalled that the current widely-accepted inhalability convention is described by

$$I(d_{ae}) = 0.5[1 + \exp(-0.06 d_{ae})] \qquad (6.1)$$

As discussed, this expression was based on the consistent trends observed in a significant number of previous studies of human inhalability carried out at windspeeds between 0.5 and 4 m/s, going back as far as the late 1970s. In the present work, however, it has been shown that aspiration efficiency at the lowest windspeed tested (0.10 m/s) lay consistently above the curve for the convention embodied in Equation (6.1). Meanwhile, the results for the higher end of the range of windspeeds examined (0.42 m/s), aspiration efficiency appeared to fall consistently below the curve. In order to understand the relative magnitude of these differences, a paired t-test was used here comparing the data at each windspeed to the target provided by the current standard at the same particle size. The results of those comparisons did, in fact, show significant dependences on windspeed, and in the directions indicated. By way of illustration of these points, Figure 6.1 shows graphically the relationship between aspiration efficiency measured by the mannequin to that given by the inhalability convention for each of the three windspeeds tested.

Taken as a whole, our new results for inhalability at ultra-low windspeeds provide a useful basis for considering how we should treat the existing definition for the inhalable aerosol fraction, including whether a change might be suggested. Firstly, it should be noted that the entire set of ultra-low windspeed data obtained in the present research were broadly within the general range of the current convention as defined by the various standards-setting bodies. However it important also to note that significant systematic dependencies were observed, most notably relating to changing windspeed, and especially at the very lowest windspeeds. Such dependencies, although suggested by some of the experiments conducted in calm air, had not been previously observed.

Bearing the preceding in mind, it is safe to conclude that the existing inhalability criterion continues to be appropriate for windspeeds down to about 0.25 m/s (notwithstanding the

windspeed dependency for much higher windspeeds reported by Vincent *et al.*, 1990 and as incorporated into the ISO version of the standard). However, for windspeeds below about 0.25 m/s, it is now clear that the existing criterion is not representative. So a modification is called for, and this will be discussed below.

Integration of personal sampling data to current criteria

It is an important extension of the discussion about the continued applicability of the current inhalability convention at ultra-low windspeeds that personal sampler performance under these same conditions should also be considered. In fact, it is recalled, the primary application of any such criterion is to provide a benchmark against which personal samplers may be examined, with respect to how representatively they collect the inhalable aerosol fraction. Therefore, before discussion of a modified criterion can begin, integration of the results from the personal samplers relative to the existing convention is needed.

From the previous section of the Report, it is reiterated that all of the personal samplers tested showed the same basic dependences on windspeed, all indicating higher sampling efficiencies at lower windspeeds. With respect to mannequin aspiration efficiency, all three of the nominally-inhalable aerosol samplers – the IOM, Button and GSP samplers – showed greater sampling efficiencies relative to the mannequin at the lowest windspeed. Therefore, they too would each be expected to indicate performance above the current inhalability curve. What this suggests is that a personal sampler designed to match the current inhalability curve at higher windspeeds (i.e., above about 0.5 m/s) might well provide a good match with a new inhalability curve based on the present human head aspiration efficiency results for ultra-low windspeeds.

As discussed previously, the IOM sampler was originally developed specifically to match the current inhalability curve. Therefore, it is interesting to recall from the previous section of the Report that, while the IOM consistently provided a greater sampling efficiency than the mannequin, increases in mannequin aspiration efficiency were directly matched by the IOM. That 1:1 relationship implied that a simple correction factor might be appropriate to enable use of the IOM at ultra-low windspeeds. Considering those findings, it was of special interest to compare the IOM directly to the current convention. Figure 6.2 shows the IOM sampling efficiency relative to the inhalability convention for each of the three windspeeds tested. It can be observed in those graphs that the IOM consistently had greater sampling efficiency than the current convention sets as a target, with increased agreement as windspeed increased. Paired t-tests confirmed that, for each windspeed (0.10, 0.24 and 0.42 m/s), the IOM sampler indicated significantly greater values for sampling efficiency in relation to the convention (*p-values:* <0.0001, <0.0001 and 0.0147, respectively). This is not surprising considering the relationship between the IOM and the mannequin that was discussed previously, and it lends additional support for the use of an IOM correction factor at ultra-low windspeeds.

Figure 6.3 shows the relationship between the Button sampling efficiency and the inhalability convention. Here, agreement between this sampler and the current convention is similar to that for the IOM, except that agreement with the standard improved significantly at the highest windspeed. Although the two lower windspeeds revealed significant differences (*p-values:* <0.0001 and 0.0021, respectively), at the highest windspeed the Button was not statistically

different from the existing inhalability convention (*p-value* = 0.1308). This is not surprising considering that the Button sampler matched mannequin aspiration efficiency relatively well at that windspeed.

Next, Figure 6.4 shows the relationship between the GSP sampling efficiency and the inhalability convention. In this case, the GSP was significantly different from the current convention for each windspeed (*p-values:* <0.0001, 0.0029. <0.0001). Here it can be observed that at the highest windspeed (0.42 m/s), the GSP actually under-sampled relative to the convention. This is especially interesting in light of the finding that the GSP sampler matched mannequin aspiration at that windspeed.

Finally, Figure 6.5 shows the relationship between the CFC sampling efficiency and the inhalability convention. As expected, based on all previous experience with this sampler, it significantly under-estimated the inhalable fraction of aerosols at all three ultra-low windspeeds (all *p-values* < 0.0001). In this case, inspection of that figure suggests that sampling at the lowest windspeed agreed better with the existing criterion relative to the highest windspeed. This again supports the general finding that lower windspeeds were associated with higher sampling efficiency.

From this collection of results, it appears that, at the ultra-low range of windspeeds of interest, these commonly used personal samplers are not always appropriate for estimating the inhalability convention as defined by the currently-accepted criteria. On the one hand, at the highest windspeed tested here the Button and GSP samplers do appear adequate for those purposes. However, at 0.10 m/s and 0.24 m/s, adoption of an alternative inhalability criterion may be advisable.

Relation of ultra-low windspeed data to proposed calm air criteria

Although previous work at ultra-low windspeeds at the level of detail described in this Report is non-existent, there is however a sizeable body of work that has looked at inhalability and personal sampler performance in the very low air-movement conditions in calm air aerosol chambers. In what is perhaps the best previously-reported calm air study, Aitken *et al.* (1999) used their results to suggest a modified model for aerosol inhalability as a function of particle aerodynamic diameter under calm air conditions. As discussed in more detail previously, those data revealed higher values for inhalability under approximately zero windspeed conditions. Based on these, Aitken *et al.* suggested a new convention, applicable to calm air conditions, having the form

$$I(d_{ae}) = 1 - 0.0038 d_{ae} \qquad (6.2)$$

This is currently on the table for discussion by the aforementioned standards setting organizations.

As for the new results described in this Report, it is recalled that the aspiration efficiency of the mannequin at the lowest windspeed (0.10 m/s) was seen to be consistently and significantly greater than that for the higher windspeeds tested. Furthermore, it was also consistently higher

than the existing inhalability convention across the range of particle size tested. On the other hand, at the higher windspeeds (0.24 and 0.42 m/s), aspiration efficiency was shown to be either similar to – or even slightly below – the *current* inhalability convention. That said, it is reasonable for practical purposes to interpret those results as reflecting that inhalability at those higher windspeeds is sufficiently consistent with the existing standard as to suggest maintaining that standard. It then comes down to a question of how the results at the lowest windspeed of 0.10 m/s compares with the modified convention suggested by Aitken *et al.*

To help in this discussion, Figure 6.6 shows the inhalability data obtained at 0.10 m/s in the current study relative to both criteria currently on the table – the original inhalability criterion as it appears in current standards and the suggested calm air version. Here, it is clearly evident that, for this lowest windspeed, inhalability is best represented by the new one suggested by Aitken *et al.* We went further to carry out linear regression of our new data in relation to a form similar to that suggested by Aitken *et al.*, and obtained a good fit with the expression

$$I(d_{ae}) = 1 - 0.0047 d_{ae} \qquad (6.3)$$

This translates into a low windspeed model that has a somewhat steeper slope than the suggested calm air model, thus situating it between the original (and existing) convention for inhalability and the suggested new one. This is intuitively consistent since the ultra-low windspeeds of our experiments represent conditions that were intermediate between calm and faster-moving air. However, following the philosophy we have adopted for the faster- moving air situation, we concede that, for practical purposes, the convention already suggested by Aitken *et al.*, is sufficiently close as to be acceptable for very slowly-moving air situations. To support this view, Figure 6.7 shows our data and those of Aitken *et al.* summarized together on the same graph. Further, recalling the data for workplace windspeeds reported by Baldwin and Maynard (1998) that show a preponderance of windspeeds typically in the ultra-low range of what we have been discussing, there is a considerable proportion that do fall within the lowest range, thus deserving possible application of the modified criterion described by Equation (6.2). In individual practical situations the choice of whether to apply the existing convention, or some new version along the lines discussed here, will depend on the expert judgment of a well-educated industrial hygienist.

Integration of personal sampling data to proposed criteria

As stated above, examination of the personal sampling data relative to the current inhalability convention suggests a similar shift between calm and moving air somewhere in the same range of windspeed. It is therefore instructive to compare the personal sampler data at both of these windspeeds to the suggested calm air criterion. With this in mind, Figure 6.8 shows that relationship for 0.10 m/s, while Figure 6.9 shows the same relationship for 0.24 m/s. For 0.10 m/s, it is seen that all of the designated inhalable aerosol samplers indicated greater sampling efficiency relative to the proposed calm air criterion, with the exception of the CFC sampler, which indicated lower relative sampling efficiency across the board. At this lowest windspeed, all the samplers performed significantly differently from the target calm air convention (IOM, GSP and CFC: *p-values* < 0.0001, Button: *p-value* = 0.0002). That indicates that, although the calm air criterion provided a better definition of true human inhalability at 0.10 m/s, the personal samplers currently recommended for collecting the inhalable fraction do not in fact match that

criterion particularly well. Therefore, as discussed previously, the use of a correction factor to better correlate the sampler results to mannequin inhalability again emerges as a possible option.

For 0.24 m/s, agreement with the suggested new convention improved for all of the inhalable aerosol samplers, but was poorer for the CFC sampler. Although the GSP and Button samplers appear to provide moderately good fits to this convention, the data themselves were quite scattered. A paired t-test was therefore performed and revealed that the sampling efficiency of both those samplers was significantly different from the suggested calm air convention (*p-values* < 0.0001 and 0.0035, respectively). Of particular interest is the IOM sampler, however, whose aspiration efficiency did in fact match reasonably well to the proposed new convention at this windspeed (*p-value* = 0.7488), despite the fact that it over-estimated exposures directly relative to the mannequin at that windspeed.

Ultimately, considering that Kenny *et al.* (1999) had found that the IOM sampler also tracked mannequin aspiration efficiency relatively well under calm air conditions, the IOM appears to be the most appropriate sampler for measuring the inhalable fraction at ultra-low windspeeds. However, as suggested earlier, a correction factor of 0.73 would provide the best estimates of the true inhalable aerosol fraction under these conditions.

Implications for including ultra-low windspeeds in standards

From an overview of the collective results just discussed, it is suggested that an alternative definition of inhalability is appropriate for workplaces where there are windspeeds which are generally less than about 0.25 m/s. That alternative may take the form of the convention that has already been suggested by Aitken *et al.* However, the decision to provide separate criteria for inhalability based on different workplace windspeeds – effectively a 'dual' standard – presents several additional considerations. In the first instance, having different definitions for the inhalable fraction based on windspeed means that additional workplace assessments may be required to appropriately apply the standard. It was shown here that, by employing a correction factor, the IOM sampler may effectively be used in both higher and lower windspeed environments. However, in order to know whether or not that factor must be applied, a thorough assessment of the windspeed in a given working environment should be conducted. Expert judgment on the part of the industrial hygienist is another option, as already noted. On the other hand, such changes to accepted sampling methodologies might well be met with resistance from the industrial hygiene community, even beyond that provoked several years ago when the original inhalability criterion was introduced to replace the old 'total aerosol' approach..

In a similar vein, although the idea of a dual standard now appears – on the basis of the work of Aitken *et al.* and now ourselves – to be scientifically sustainable, previous experience suggests that obtaining the consensus of a standards group or committee to adopt such a standard is more difficult. The existing inhalability convention has been widely accepted throughout the world – in some cases, even written into national policy – as the primary functional definition of human inhalability. But only after many years of discussion and debate! Modifying such a standard has the potential to trigger further such debate, even to the extent of becoming a further 'political' issue in which the scientific issues become secondary. Such discussions, however, belong elsewhere, outside the scope of this Report.

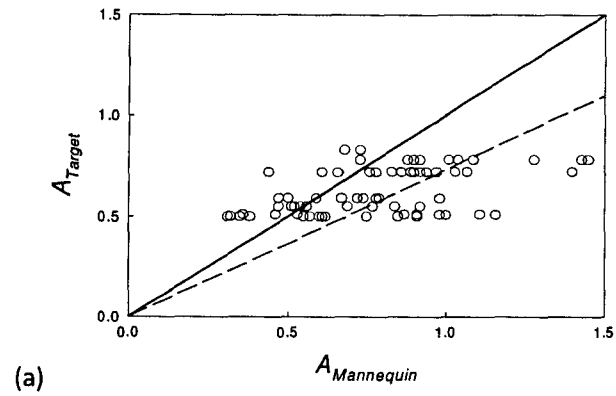

(a)

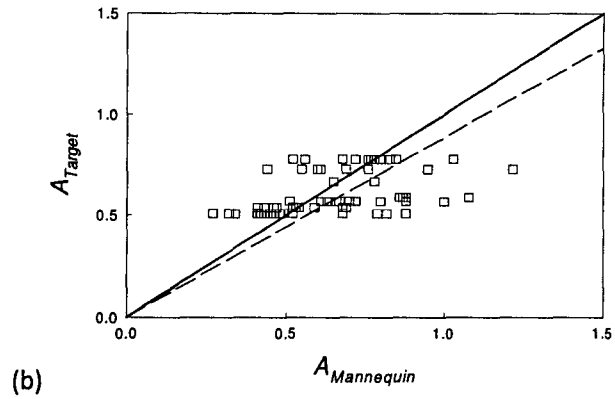

(b)

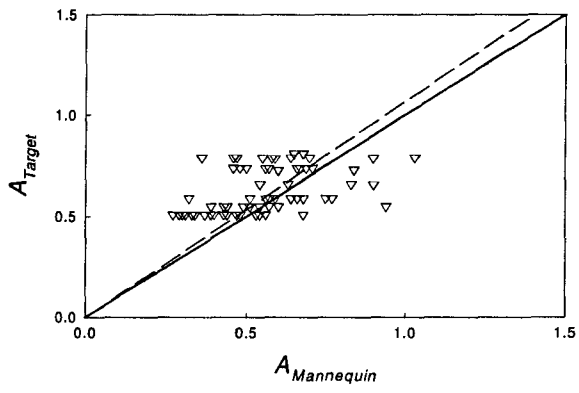

(c)

Figure 6.1: Relationship between the aspiration efficiency measured by the mannequin ($A_{Mannequin}$) to the target aspiration efficiency indicated by the current inhalability convention (A_{Target}) for windspeeds of (a) 0.10 m/s, (b) 0.24 m/s and (c) 42 m/s. The solid line represents perfect agreement and the dashed line represents a linear regression.

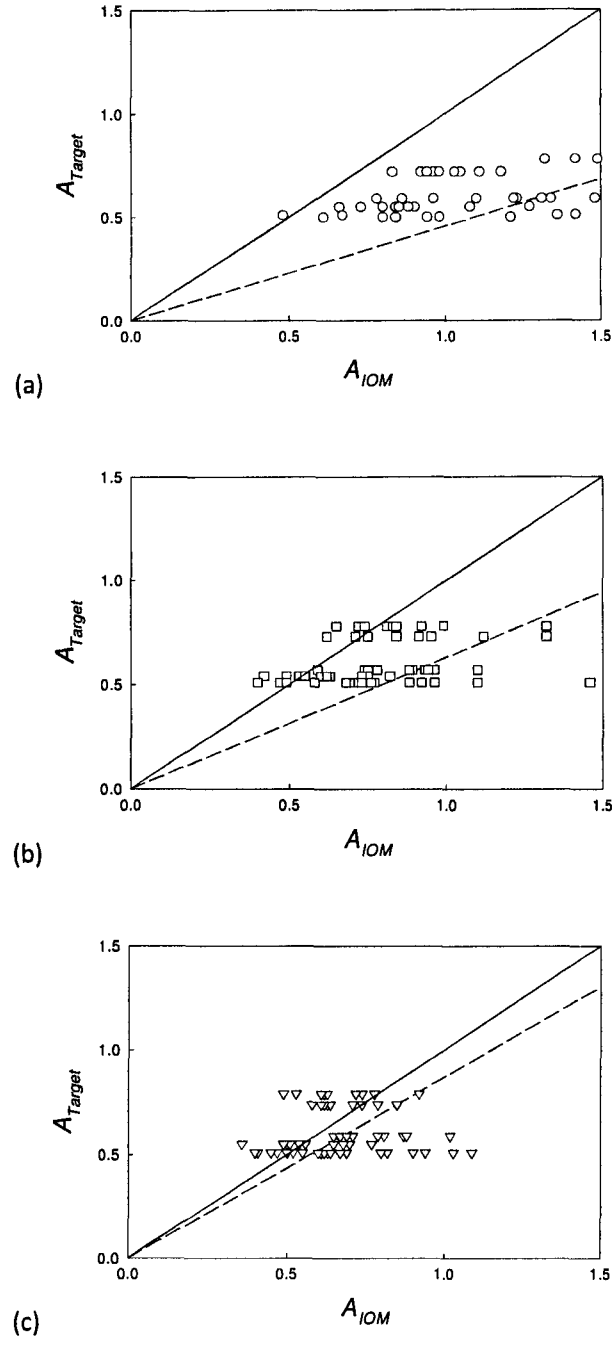

Figure 6.2: Relationship between the IOM sampling efficiency (A_{IOM}) to the aspiration efficiency suggested by the current inhalability convention (A_{Target}) for windspeeds of (a) 0.10 m/s, (b) 0.24 m/s and (c) 42 m/s. The solid line represents perfect agreement and the dashed line represents a linear regression.

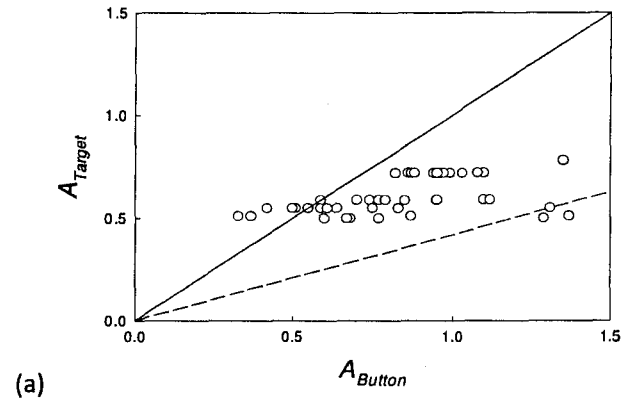

(a)

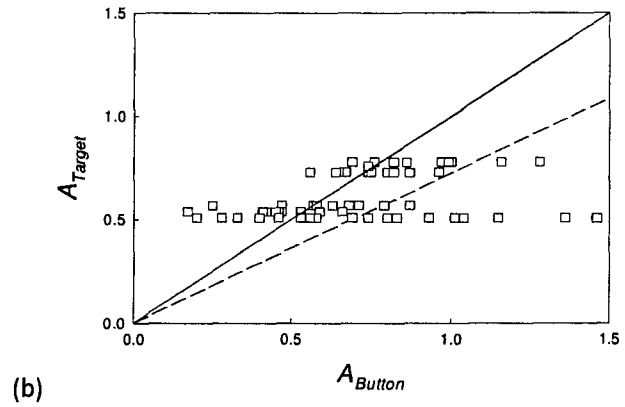

(b)

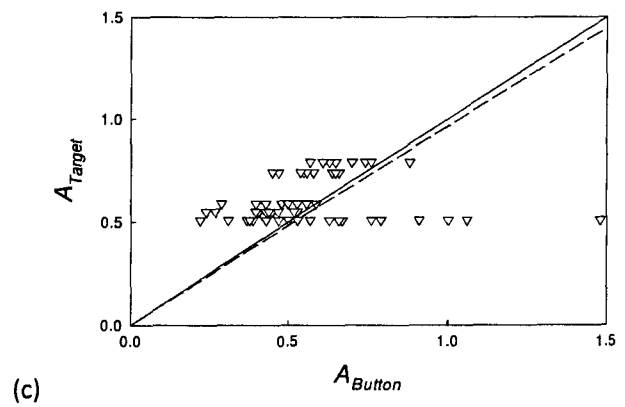

(c)

Figure 6.3: Relationship between the Button sampling efficiency (A_{Button}) to the aspiration efficiency suggested by the current inhalability convention (A_{Target}) for windspeeds of (a) 0.10 m/s, (b) 0.24 m/s and (c) 42 m/s. The solid line represents perfect agreement and the dashed line represents a linear regression.

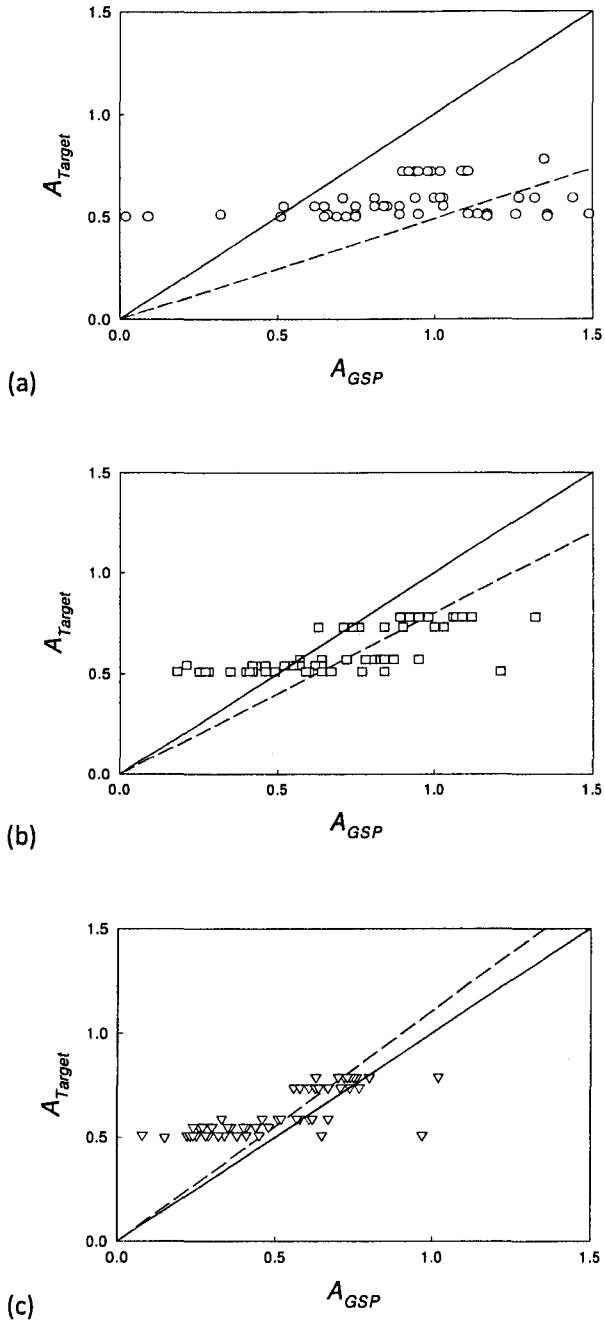

Figure 6.4: Relationship between the GSP sampling efficiency (A_{GSP}) to the aspiration efficiency suggested by the current inhalability convention (A_{Target}) for windspeeds of (a) 0.10 m/s, (b) 0.24 m/s and (c) 42 m/s. The solid line represents perfect agreement and the dashed line represents a linear regression.

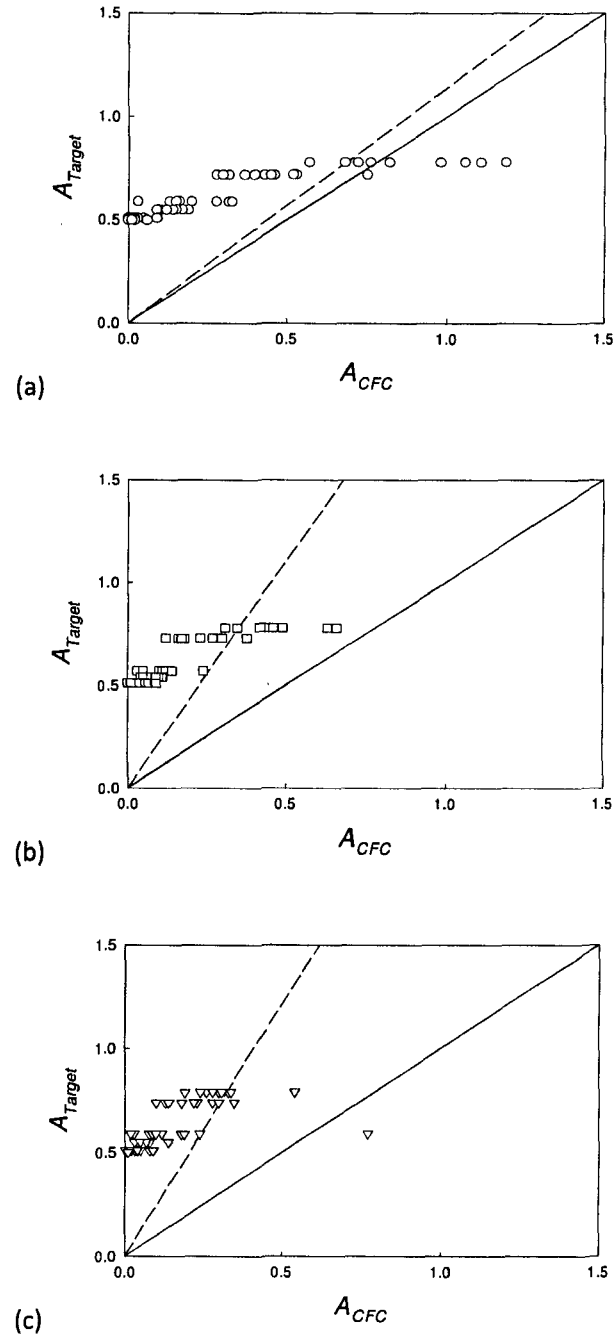

Figure 6.5: Relationship between the CFC sampling efficiency (A_{CFC}) to the aspiration efficiency suggested by the current inhalability convention (A_{Target}) for windspeeds of (a) 0.10 m/s, (b) 0.24 m/s and (c) 42 m/s. The solid line represents perfect agreement and the dashed line represents a linear regression.

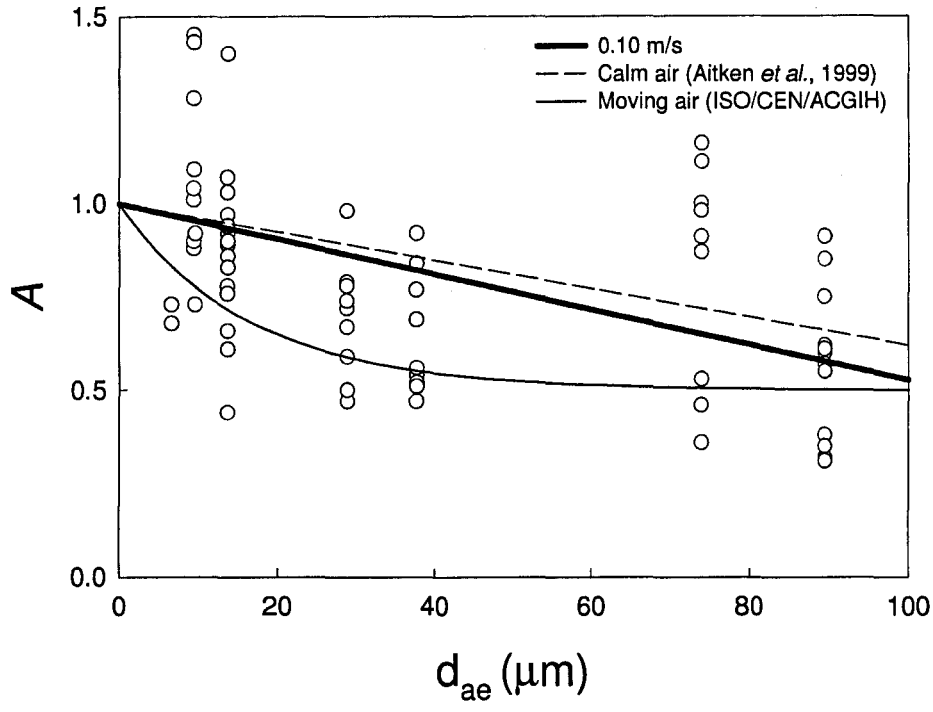

Figure 6.6: Linear regression for data at 0.10 m/s (thick solid line) compared to the existing inhalability convention (thin solid line) and the proposed calm air criteria (dashed line), shown for aspiration efficiency (A) as a function of particle aerodynamic diameter (d_{ae}). The white symbols represent each data point for aspiration efficiency obtained here at 0.10 m/s.

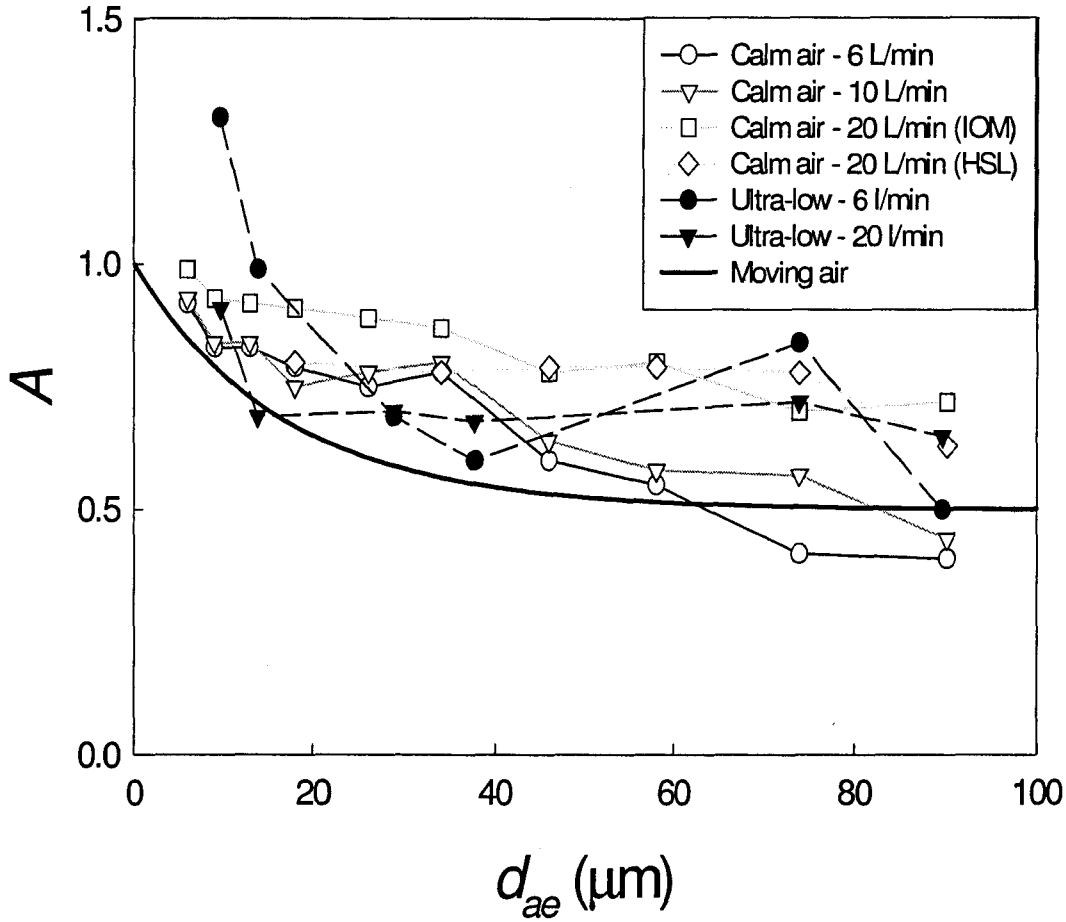

Figure 6.7: Comparison of the new data at ultra-low windspeeds (black symbols) to data obtained for calm air (Aitken et al., 1999) (white symbols), with the current inhalability convention ('moving air') also shown (thick solid line).

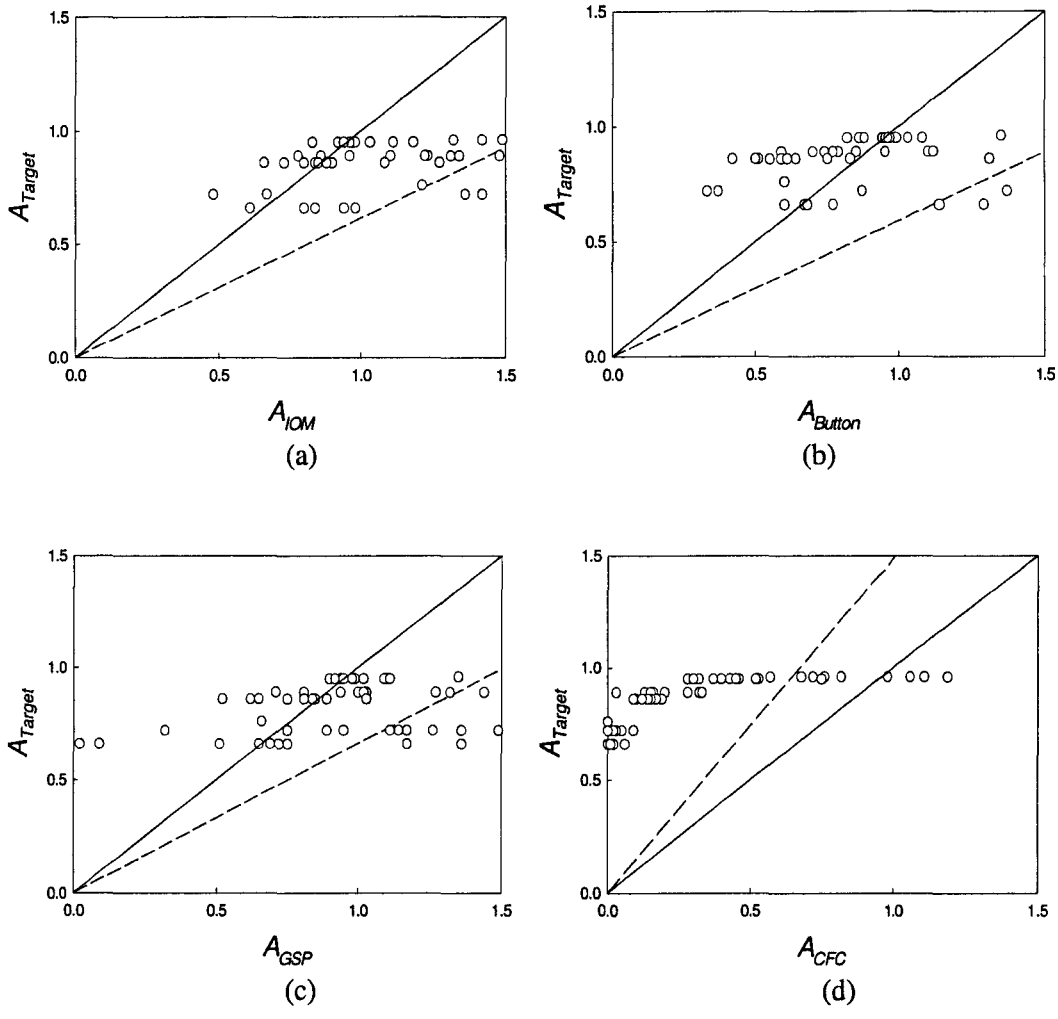

Figure 6.8: Relationship between the measured sampling efficiency to the inhalability suggested by the proposed calm air criteria (A_{Target}) at 0.10 m/s for the (a) IOM, (b) Button, (c) GSP and (d) CFC samplers. The solid line represents perfect agreement and the dashed line represents a linear regression.

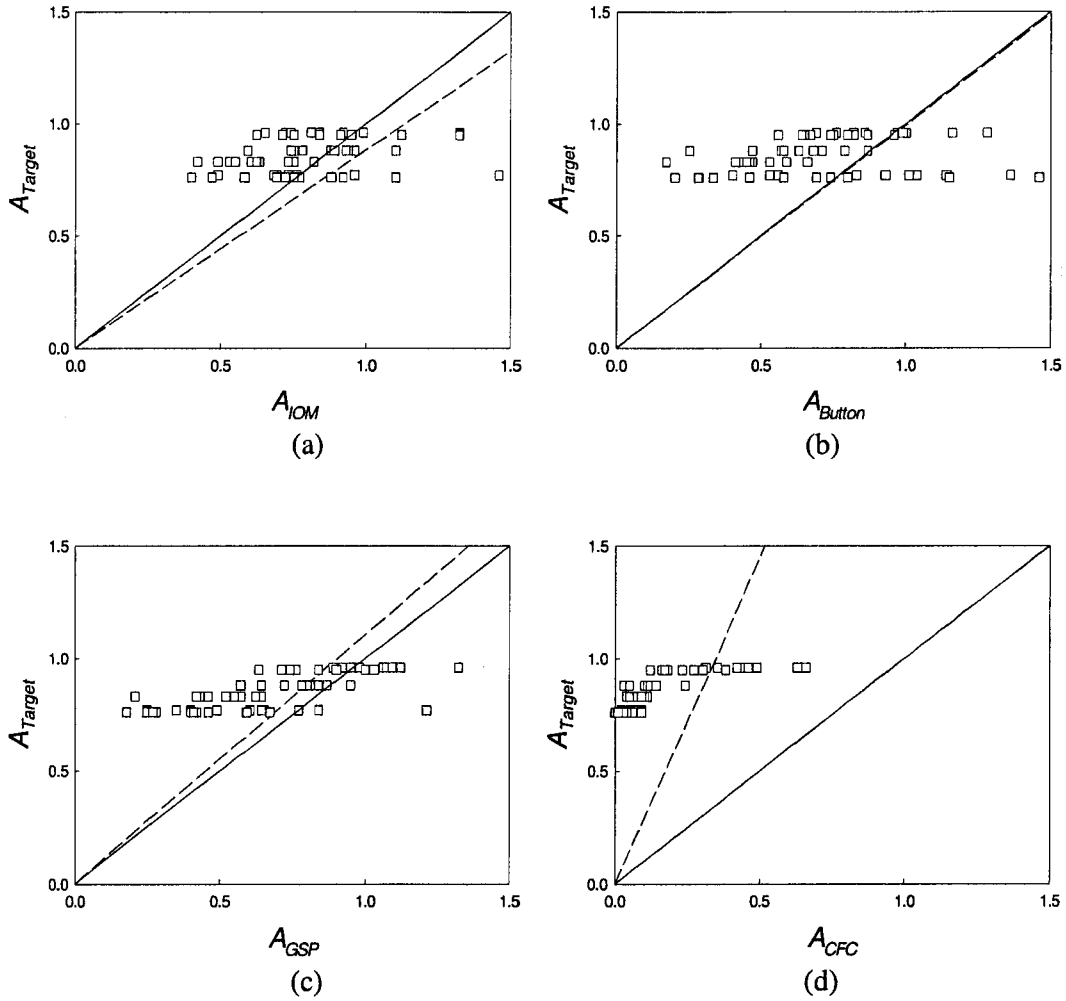

Figure 6.9: Relationship between the measured sampling efficiency to the inhalability suggested by the proposed calm air criteria (A_{Target}) at 0.24 m/s for the (a) IOM, (b) Button, (c) GSP and (d) CFC samplers. The solid line represents perfect agreement and the dashed line represents a linear regression.

7. Conclusions from the research

We have described a large body of research involving the development of facilities never previously seen and their application in the exploration of human inhalability in relation to aerosol exposures and personal samplers aimed at providing representative measures of such exposures. The experiments that have been described represent a large, cohesive body of work. All the objectives outlined at the beginning were successfully achieved. They were only slightly modified from those listed in the original proposal, based on new knowledge and awareness that emerged both before and during the work itself.

The new facility – consisting of the ultra-lowspeed wind tunnel and heated, breathing mannequin and associated auxiliary equipment – was conceptualized, built, commissioned and calibrated. It is important to emphasize the significance of the new experimental facilities, which were developed especially for this research to simulate the more relevant workplace windspeeds between 0.05 and 0.5 m/s. In order to successfully perform inhalability experiments at these ultra-low windspeeds, it was necessary to overcome severe difficulties inherent in sampling in environments characterized by very low, yet non-zero, windspeeds. With this in mind, we started by developing a theoretical basis for a novel experimental system for aerosol research in which the principles of a calm air chamber were incorporated into a traditional wind tunnel, leading to a system that may be referred to 'hybrid'. This allowed for the influence of gravitational settling to be accounted for while maintaining a spatially uniform distribution of aerosols, both in terms of aerosol concentration and particle size distribution. This part of the project represented a major achievement in itself, providing the basis of an experimental program under ultra-low windspeed conditions previously widely considered to be too difficult to achieve in the laboratory.

Following the completion of the construction of the wind tunnel and mannequin, the next major part of the project involved the commissioning of the newly-built facilities, specifically aimed at generating the desired spatial uniformity of windspeed, aerosol concentration and particle size distribution, respectively. In order to obtain the optimal spatial distribution of aerosols inside the working section of the wind tunnel, novel aerosol injection systems were designed and modifications to the wind tunnel were made as necessary as we went along. This time-consuming process involved much trial and modification. But we were ultimately able to achieve experimental conditions inside the wind tunnel that were acceptably close to what was desired across the whole range of conditions specified at the outset. We then embarked on the experimental research program, starting with flow visualizations to examine the nature of the patterns of air movement around the mannequin, particularly while it was breathing, followed by an extensive series of experiments to examine human inhalability and personal sampler performance, both employing the mannequin.

The flow visualization studies provided a large library of very informative digital flow visualization videos from which publishable-quality still pictures could also be obtained. From these it was possible to catalog air flow patterns around the heated, breathing mannequin over the whole range of experimental conditions we set out to study. Assessment of those pictorial records provided striking visual information about the roles of factors such as windspeed and breathing flowrate, as well as body heat, clothing, etc., on the nature of the flow, in turn enabling to qualitative assessment of the potential influences on human aspiration efficiency. At

combinations of low windspeed and high breathing rate, and especially for breathing through the mouth, it was seen that large and persistent disturbances in the approaching air flow were generated. It is highly likely that such disturbances will have a profound effect on aerosol transport near the mannequin, and in turn on inhalability and personal sampler performance.

Two major sets of quantitative data at ultra-low windspeeds were obtained, for both aerosol inhalability and personal sampler performance. These showed that both human inhalability and sampling efficiency were significantly dependent on windspeed, both being the highest at the lowest windspeed. In addition, it was revealed that inhalability at ultra-low windspeeds was much greater than the currently-accepted criterion based on data obtained at higher windspeeds. Taken as a whole, the results and analyses performed here supported the initial hypothesis, which stated that previous measures of inhalability at high windspeeds had under-estimated aerosol exposures at ultra-low windspeeds. This was shown to be true for both the human aspiration process – as assessed by the mannequin – as well as for the personal samplers tested. In the case of the personal samplers, rudimentary correction factors of 0.73, 0.78 and 0.83 were estimated for the IOM, Button and GSP samplers, respectively, for use at ultra-low windspeeds to better estimate the inhalable aerosol fraction. The CFC sampler, despite being one of the most commonly used devices by industrial hygienists, was confirmed as being ill suited for measuring the inhalable aerosol fraction at all ultra-low windspeeds, in addition to – as has been shown elsewhere – to higher windspeeds. In other words, it has now become clear that the CFC sampler is completely inadequate for collecting the health-related inhalable fraction.

The final objective was to examine the possibility – and practical implications – of modifying existing criteria to better estimate workplace exposures at the ultra-low windspeeds of interest. Taking into account the practical need to maintain simplicity, it was concluded that the existing standard for inhalability is still relevant to workplace environments where windspeeds exceed about 0.25 m/s. However a modified criterion is clearly needed for lower windspeeds in the ultra-low range of the order of 0.10 m/s and below. A criterion for (nominally) calm air has already been recommended by Aitken *et al.* (1999) based on their studies in a calm air chamber, and this is currently on the table for discussion by several major standards setting bodies. Our results are broadly consistent with that suggested criterion, and so we support its inclusion in revised aerosol exposure standards.

Overall, the large body of research carried out under this project has provided important new findings relevant to occupational aerosol exposure assessment, and should therefore be of interest to industrial hygienists, occupational epidemiologists and standards setting bodies. At its core, the work has focused on issues underlying the fundamental principles of aerosol science and industrial hygiene. It is fair to say that the new wind tunnel and mannequin system, along with a large array of associated new methodology, represent excellent resources for possible future exposure studies of occupational assessment at environmental windspeeds that we now know to be the most relevant.

References

Aitken, R.J., Baldwin, P.E.J., Beaumont, G.C., Kenny, L.C. and Maynard, A.D. (1999), Aerosol inhalability in low air movement environments, *Journal of Aerosol Science*, 30, 613-626.

Aizenberg, V., Choe, K., Grinshpun, S.A., Willeke, K. and Baron, P.A. (2001), Evaluation of personal aerosol samplers challenged with large particles, *Journal of Aerosol Science*, 32, 779-793.

American Conference of Governmental Industrial Hygienists (ACGIH) (1999), *Particle Size-Selective Sampling for Particulate Air Contaminants*, (Ed. J.H. Vincent), ACGIH, Cincinnati, OH, U.S.A.

American Conference of Governmental Industrial Hygienists (ACGIH) (2004), Threshold limit values for chemical substances and physical agents, and biological exposure indices (2004-2005), ACGIH, Cincinnati, OH, U.S.A.

Baldwin, P.E. and Maynard, A.D. (1998), A survey of wind speeds in indoor workplaces, *Annals of Occupational Hygiene*, 42, 303-313.

Bartley, D.L. (1998), Inhalable aerosol samplers, *Applied Occupational and Environmental Hygiene*, 13, 274-278.

Berry, R.D. and Froude, S. (1989), An investigation of wind conditions in the workplace to assess their effect on the quantity of dust inhaled, U.K. Health and Safety Executive Report IR/L/DS/89/3, Health and Safety Executive, London, U.K.

Comité Européen de Normalisation (CEN) (1992), Workplace atmospheres: Size fraction definitions for measurement of airborne particles in the workplace, European Standard EN 481, CEN, Brussels, Belgium.

Dunnett, S.J. and Ingham, D.B. (1986), A mathematical theory to two-dimensional blunt body sampling, *Journal of Aerosol Science*, 17, 839-853.

Erdal, S. and Esmen, N.A. (1995), Human head model as an aerosol sampler: calculations of aspiration efficiencies for coarse particles using an idealised human head model, *Journal of Aerosol Science*, 26, 253-272.

Fuchs, N.A., and Sutugin, A.G. (1966), In: *Aerosol Science* (Ed. C.N. Davies), Academic Press, London, 1-30.

Gilmutdinov, A. and Zivilskii, I. (2008), Three dimensional modeling of air flow, aerosol distribution and aerosols samplers for unsteady conditions, *Journal of Environmental Monitoring*, 10, 1417-1425.

Grinshpun, S.A., Willeke, K. and Kalatoor, S. (1993), General equation for aerosol aspiration by thin-walled sampling probes from calm and moving air, *Atmospheric Environment*, 27A, 1459-1470; and 28A, 375.

Hinds, W.C. and Kuo, T.-L. (1995), A low velocity wind tunnel to evaluate inhalability and sampler performance for large dust particles, *Applied Occupational and Environmental Hygiene*, 10, 549-556.

International Standards Organisation (ISO) (1992), *Air quality-particle size fraction definitions for health-related sampling*, Technical Report ISO/TR/7708-1983 (E), Revised version, ISO, Geneva, Switzerland.

Kenny, L.C., Aitken, R.J., Baldwin, P.E.J., Beaumont, G.C. and Maynard, A.D. (1999), The sampling efficiency of personal inhalable aerosol samplers in low air movement environments, *Journal of Aerosol Science*, 30, 627-638.

Kerho, M.B. and Bragg, M.F. (1994), Neutrally buoyant bubbles used as flow tracers in air, *Experiments in Fluids*, 16, 393-400.

Mark, D., Vincent, J.H., Gibson, H. and Witherspoon, W.A. (1985), Applications of closely-graded powders of fused alumina as test dusts for aerosol studies, *Journal of Aerosol Science*, 16, 125-131.

Mueller, T.J. (1996), Flow visualization by direct injection, In: *Fluid Mechanics Measurement*, (Ed. R. J. Goldstein), Taylor and Francis, Washington D.C., U.S.A., 367-450.

Ogden, T.L. and Birkett, J.L. (1978), An inhalable dust sampler for measuring the hazard from total airborne particulate, *Annals of Occupational Hygiene*, 21, 41-50.

Paik, S. and Vincent, J.H. (2002), Aspiration efficiency for thin-walled nozzles facing the wind and for very high velocity ratios, *Journal of Aerosol Science*, 33, 705-720.

Saibene, F., Mognoni, P., Lafortuna, C.L., and Mostardi R. (1978), Oronasal breathing during exercise, *Pflugers Archives: European Jouranl of Physiology*, 378, 65-69.

Sreenath, A., Ramachandran, G. and Vincent, J.H. (1997), Experimental investigations into the nature of airflows near bluff bodies with aspiration, with implications to aerosol sampling, *Atmospheric Environment*, 31, 2349-2359.

Su, W.C. and Vincent, J.H. (2004), Towards a general semi-empirical model for the aspiration efficiencies of aerosol samplers in perfectly calm air, *Journal of Aerosol Science*, 35, 1119-1134.

Vincent, J.H. (2007), *Aerosol Sampling: Science, Standards, Instrumentation and Applications*, Wiley & Sons, Chichester, England, U.K.

Vincent, J.H., Mark, D., Miller, B.G., Armbruster, L. and Ogden, T.L. (1990), Aerosol inhalability at higher windspeeds, *Journal of Aerosol Science*, 21, 577-586.

Vincent, J.H., Stevens, D. C., Mark, D., Marshall, M. and Smith, T. A. (1986), On the aspiration characteristics of large-diameter, thin-walled aerosol sampling probes at yaw orientations with respect to the wind, *Journal of Aerosol Science*, 17, 211-224.

Werner, M.A., Spear, T.M. and Vincent, J.H. (1996), Investigation into the impact of introducing workplace aerosol standards based on the inhalable fraction, *Analyst*, 121, 1207-1214.

Wood, J.D. and Birkett, J.L. (1979), External airflow effects on personal sampling, *Annals of Occupational Hygiene*, 22, 299-310.

Wu, Y.-H. (2005), *Application of particle size distribution measurement to the characterization of workplace aerosols*, Ph.D. Dissertation, University of Michigan, Ann Arbor, MI, U.S.A.

Wu, Y.-H. and Vincent, J.H (2007), A modified Marple-type cascade impactor for assessing aerosol particle size distributions in workplaces, *Journal of Occupational and Environmental Hygiene*, 4, 798-807.